Dynamic Loadability of cables in grids connected to offshore windfarms

Akshaj Srivastava
Student number: 5626897

In partial fulfillment for the degree of
Master of Science

Electrical Engineering,Mathematics and Computer Science
Delft University Of Technology
Netherlands
29-01-2024

Dynamic Loadability of cables in grids connected to offshore windfarms

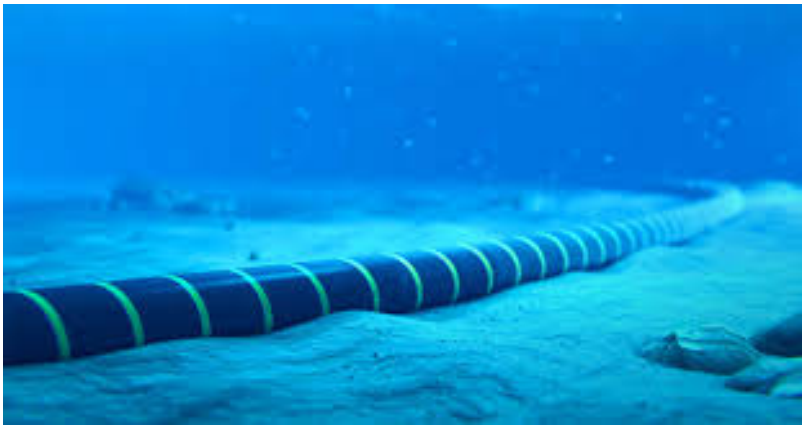

Akshaj Srivastava
Student number: 5626897

In partial fulfillment for the degree of
Master of Science

Electrical Engineering,Mathematics and Computer Science
Delft University Of Technology
Netherlands
29-01-2024

Abstract

As grids become more and more saturated due to addition of more renewable energy sources in the system, the power demand keeps on increasing. This puts a pressure on the electrical utilities especially the power cables transferring power from one voltage level to another. Therefore, prior investigation into the effect of dynamic loading of such power cables is required before implementing the system in the physical grid.

One such saturated system is the implementation of offshore wind farm cables and the utilities connected to it. The objective of this study was to check the effect of the dynamic nature of power flow through the connected cable system. In order to get a quantified result the degradation of the cable is measured in terms of the lifetime consumption of the cables under different loading schemes.

The offshore grid connection from Ijmuiden ver area in the North sea operated by Tennet has been identified as a case study for explaining the results. The offshore platforms are connected to the converter station with the help of 3-core 66kV HVAC cables. The connection from the converter station to the onshore grid is with the help of 2 525kV 1-core HVDC cables. The setup has been modelled with the help of two separate models for both the AC and DC cable sross-sections respectively. The models were developed in MATLAB (analytical) and Comsol Multiphysics 5.0 (numerical) to check the effect of dynamic loading of the cables with the help of different current vs. time profiles. The temperature variation with time was checked for the two cable systems.The parameters of soil thermal resistivity and the burial depth were varied from (0.2[W/mK],1200[mm]) to (0.36[W/mK],1500[mm]).

For the AC cable, it was observed that the lifetime consumption increases on changing the soil thermal conductivity and burial depth from 0.36[W/mK],1500[mm] to 0.2[W/mK],1200[mm]. The percentage lifetime consumption is dependent on the time duration for which the cable has been overloaded with a current value greater than the steady state value of 310[A] corresponding to 90°C. The worst case change between the two cases was observed as going from 0.4439% to 0.5295% per year.Thus, showing that prior investigation is needed before loading the cable with a certain current profile under a given scenario.

For the AC case, on overloading the cable with a current value about 1.2 times the normal value, the maximum percentage lifetime consumption observed was 0.6208%. For the DC cable, the lifetime consumption was measured in terms of the time to failure of the insulation. This parameter is a function of the radial thickness of the insulation from the conductor screen to the insulation. The time to failure increases as one moves away from the conductor screen. Greater insulation deterioration was found to happen with the burial depth and soil thermal conductivity being (1200[mm],0.2[W/mK]) as compared to the case (1500[mm],0.36[W/mK]).A reversal in the trend of time to failure was observed when the cable was overloaded with a current value of 1.2 times the normal current.The worst case mean value of time to failure observed was 39.68[y] for the normal case.

Acknowledgement

I am thankful to my supervisor and Professor Dr. Mohamad Ghaffarian Niasar for guiding me throughout the process and helping me with useful insights while building the analytical and numerical models.Also, I am grateful to my parents for supporting me through the whole duration of work.

Introduction

With increasing power load on electrical grids due to increasing demand, it is necessary to implement a method which can lead us to increased transmission capacity without overheating the power cables. Dynamic cable rating is such a method which is used to predict the temperature rise with a prospective current rating value and then limit the current rating to a particular value so that the temperature rise can be contained. Current research on this work points out two major advantages of this scheme- 1. Increased availability of the power cable for power transfer during off-peak hours and 2. Increased total lifetime of the cable, thus reducing project investment costs. Currently, for the offshore high voltage system following procedure is in use-([1]) This procedure uses both static and dynamic line ratings for calculations-

- The cable system will be designed based on a continuous maximum load profile for sections with short thermal constants (which can heat up fast)
- For the section with a (initial or future) soil coverage of more than 5 m, a dynamic load profile shall be taken into account for current rating. This option is suitable for the sections with longer thermal time constants, which heat up slow (e.g. in deeper parts of HDD's, deep installation in sand dunes, etc.).
- The Dynamic current rating is based on the following principle:Pre-load condition of the cable shall be a partial steady-state average load (Average Load*full load current)for 87,600 hours (10 years equivalent) to reach a steady state temperature. From t=0, a continuous load condition shall be used at full load current; The time shall be calculated between t=0 and the time that the conductor temperature reaches the maximum allowed temperature. Hence, a list of time taken to heat up the cable upto the maximum limit at different current values will be made. The current corresponding to the shortest possible time will be the rating of the cable system.

As compared to this model of rating cables, the same routine operation can be done in a different way computationally. The objective of this research is to propose a method of using the dynamic cable rating model. This model aims to integrate continuous current vs. time profile, thus enabling the dynamic calculation of the cable temperature variation. Finally the total lifetime consumption of the cable under the given current profile can be used for further analysis. The conclusions of this work will address the following questions, offering comprehensive insights-

- How can the power transfer in the cable be increased with the help of dynamic cable rating?
- How will variations in soil thermal conductivity and burial depth change the operation of the cable?
- What can be said about the change in lifetime consumption of the cable under changing soil thermal conductivity and burial depth. What can be suggested to mitigate this effect in the future?

To answer these questions, the work has been divided into chapters. Detailed review of the workflow can be found in chapter 1. Chapter 1 starts with the literature study about the current research on Dynamic cable rating and its implications. Chapter 2 explains about the procedure of work. Chapter 3 explains about the different load profiles which need to be implemented for operation. Chapter 4 explains about the model structure for HVAC cables used in the analysis. Chapter 5 explains about the model structure for HVDC cables used in the operation. Chapter 6 explains the results from different lifetime consumption models which are used to estimate the lifetime consumption under different possible scenarios. Chapter 7 talks about the results and highlights the future scope for research.

List of Abbreviations

T_{11}	TR between one insulation and sheath
T_1	TR for one cable core
T_2	TR for cable filler
T_3	TR for cable armor bedding, armor and outer protection
T_4	TR for soil thermal resistance
T_A, T_B	TR of equivalent 2 step ladder network
Q_c	TC of conductor
Q_{ins}	TC of insulation
Q_f	TC of filler material
Q_s	TC of sheath
Q_{ab}	TC of armor bedding
Q_a	TC of armor
Q_{se}	TC of external serving
Q_A	TC of equivalent 2 step ladder network
Q_B	TC for equivalent 2 step ladder network
c	Specific heat capacity for conductor
c_i	Specific heat capacity for insulation
c_f	Specific heat capacity for filler material
c_{sh}	Specific heat capacity for sheath
c_{ab}	Specific heat capacity for armor bedding
c_a	Specific heat capacity for armor
c_{se}	Specific heat capacity for external serving
θ_{se}	Temperature for sheath
I	Current per bay
W_d	Total Dielectric losses
R_s	Electrical resistance of the sheath
α_{20}	Heat coefficient at 20 deg$C$
θ_c	Conductor temperature
R	Electrical resistance of Conductor
R_{so}	Electrical resistance of sheath at 20 deg$C$
X	Reactance of sheath

[1] TR: Thermal resistance
TC : Thermal Capacitance

$\lambda_1^{'}$	Loss factor of sheath
$\Delta\theta$	Temperature difference between conductor and ambient environment
$\theta_c(t)$	Conductor temperature as a function of time
$\theta_e(t)$	Transient temperature variation of surrounding
$\theta_{pk}(t)$	Transient temperature due to kth cable on the surface of pth cable
$\alpha(t)$	Attainment factor
D_e^*	Diameter of cable cross section
L^*	Burial depth of cable
d_{pk}^*	Centre to centre distance between adjacent cables
$d_{pk}^{'*}$	distance between centre of one cable and image of other cable
ω	Angular frequency
TC	Thermal Conductivity
HVAC	High voltage AC
HVDC	High voltage DC
FEM	Finite element modelling
FEA	Finite element analysis
LCC	Line commutated converter
VSC	Voltage source converter
LC	Load cycle
HL	High load
IEC	International Electrotechnical Commission
CIGRE	Conseil International des Grands Réseaux Electriques
XLPE	Cross-linked Polyethylene
EPR	Ethylene polypropylene

Contents

List of Figures

List of Tables

Chapter 1

Methodology

The work is divided primarily into three parts. Development of test profiles(current vs. time variations) for ampacity study, development of models for both 66kV HVAC and 525 kV HVDC lines and the study of lifetime consumption for both the cables. This chapter explains the detailed workflow in which the work has progressed with the description of each chapter.

The work has been done taking the following setup as a use case:

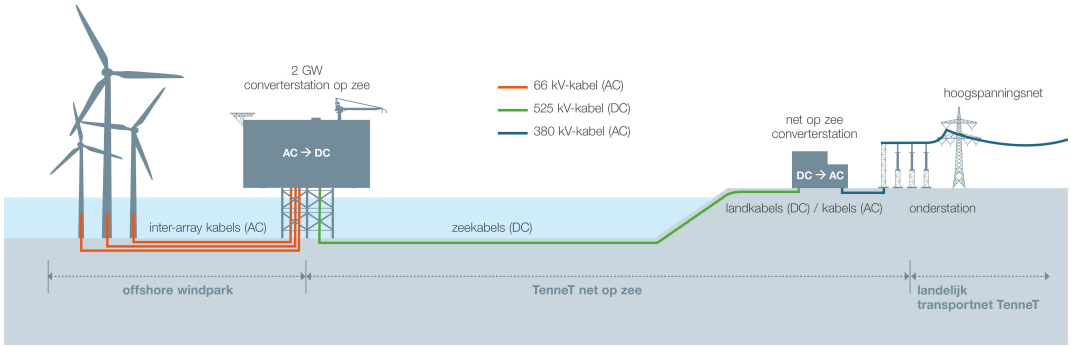

Figure 1.1: Offshore connection as to be used in the Tennet offshore grid: Source(`https://www.tennet.eu/projects/offshore-projects-netherlands`)

The work has been presented in form of chapters.

- Chapter 1: Literature Study- All the aspects related to research on dynamic cable rating which are relevant for high voltage cable studies have been mentioned in this chapter. Significant research on the use of dynamic cable rating has been underlined in this case. Significant study on the different factors contributing to the long term ageing of cables, recorded in research work was also done in this case.
- Chapter 2: Methodology - This chapter explains the flow in which the study has progressed.
- Chapter 3: Development of Load profiles - This chapter explains the different current vs. time profiles which are used for HVDC and HVAC simulations in this work.
- Chapter 4: Modelling of HVAC cable system - This chapter explains the procedure in which the model(both analytical and numerical based) for studying the 66kV setup has been developed. The model has been implemented on the 66kV setup and ends with a comparison of results for changing burial depth and soil thermal conductivity.

- Chapter 5: Modelling of HVDC cable system-This chapter explains the development of the model(both analytical and numerical). In this case, the changing electrical conductivity plays a major role in the development of the model and thus the final lifetime analysis of the cable.
- Chapter 6: Lifetime consumption of cables-This chapter explains the theory behind the consumption of life both for HVAC and HVDC cables. Results for the lifetime consumption have been summarised for different scenarios. This chapter ends with the conclusions for the given results.
- Chapter 7: Results and Conclusions- This chapter answers the basic questions which have been raised in the introduction.

Following figure provides the reader an insight into the process in which the work progressed throughout the duration-

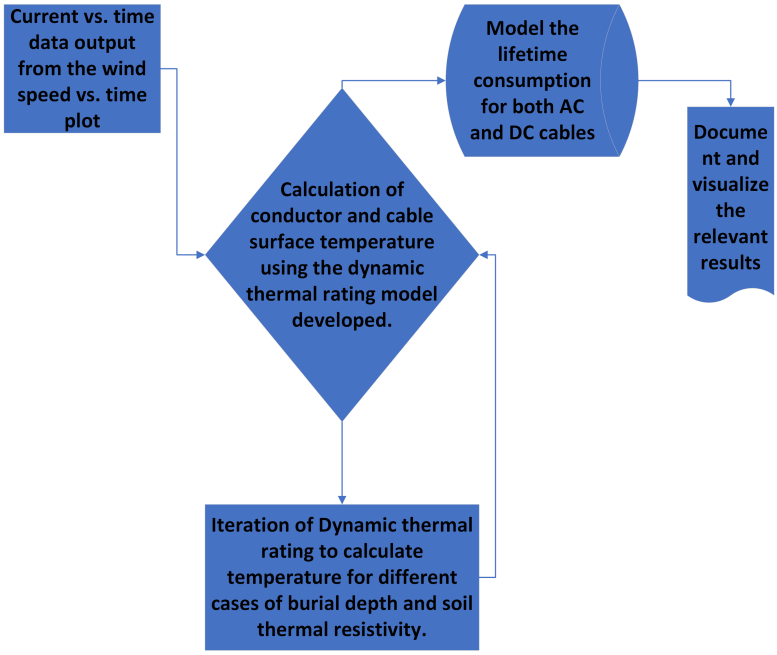

Figure 1.2: Workflow of the research undertaken

Keeping the nature of changing parameters in mind, a sensitivity analysis has been performed as part of this study to get suitable lifetime consumption results. In this case, the soil thermal resistivity is made to vary from 5 $K.m/W$ to 2.77 $K.m/W$ and the burial depth of the cable setup is made to vary from 1.2[m] to 1.5[m]. Throughout the work, results for two different cases have been worked out-

- Case 1: $L = 1200[mm], TC = 0.2[W/mK]$
- Case 2: $L = 1500[mm], TC = 0.5[W/mK]$

Chapter 2

Literature Study

Expansion of the existing power system by adding more sources of renewable energy in the grid puts thermal stress on the cable system. This makes it necessary to improve the power utilization capacity of the cables. At the same time, it is necessary to offset the financial limitations of future planning of a power grid by predicting the effect of load flow through the grid.A suitable dynamic cable rating monitoring system with an effective life-cycle prediction system needs to be placed in the existing infrastructure to mitigate the possibilities of intermittent failure in the system ([2]). Typically, offshore wind power system is being proposed as a power source in addition to other sources of energy. (for example hydrogen and natural gas based sources). But, the intermittent nature of wind output and the availability of substantial wind power has made it important to analyse the ageing patterns of the dielectric material under variable output([3]). The dynamic nature of load results in frequent cable temperature variations which result in accelerated ageing of cables. Keeping this goal in mind, substantiative research on dynamic rating systems for overhead lines and cables has been done. A theoretical background on the existing model systems has been mentioned to underline the steady-state and the transient nature of any cable system. The study aims to list out the key research areas for dynamic rating of cable systems and point out the limitations in the existing work from different perspectives. Further, the feasibility of dynamic cable rating in offshore wind farm cable connections has been explored.

Offshore wind farm connections have been usually coupled with HVDC connections to improve the power capability of transmission. Wind farms are generally used as a secondary voltage source to provide stability to grid connections. Offshore connections are generally used to provide wide area voltage control and secondary voltage control. Therefore, it becomes important to study the feasibility of operation for a HVAC cable connection connected to the grid.([3]). In such a case, the thermal rating of the cable under dynamic loading becomes an important part of the study, as offshore wind farms are connected to the converter station through HVAC cables.

2.1 Key takeaways from existing research

There are a number of factors which affect the rating of overhead cables and buried cables. Studying the effect of such factors underlines the points to be considered for research on the dynamic cable rating calculations for any cable.The major factors which effect the ampacity of a cable are mentioned below([4])-

Overhead cables	Underground cables
Conductor Size	Surrounding soil temperature
Solar radiation	Soil thermal resistivity
Time of day	Depth of burial
Ambient air temperature	Conductor material
Enclosed/dis-enclosed in conduit Groups of cables	Spacing between phases
Wind speed effects	Varying cable size with soil dry out

[1] In case of overhead cables, the surrounding air temperature was found to be the major dominating factor for affecting the ampacity of the cable. On the other hand the size of conductor and material used has considerable impact on the cable ampacity ratings in addition to the sheath bonding arrangements. In this work, the cables connected to offshore wind farms(both AC and DC) have been explored in this work. The effect of changing soil thermal resistivity and changing burial depth have been explored in detail.

The standard method of calculating cable ampacity has already been derived in the Neher-Mcgrath approach and has been modified further in the IEC60287 approach([5].

The steady state current for a given temperature difference is [6]-

$$I_{calc} = (\frac{T_c - (T_a + \Delta T_d)}{R_{ac}.(1+Y_c).R_{ca}})^{0.5} \tag{2.1}$$

The symbols are defined as

- I_{calc} : Calculated steady state current value.
- Tc : Calculated conductor temperature
- Ta : Ambient temperature
- Td : Calculated temperature rise due to dielectric loss
- Rdc : DC resistance of the conductor
- Yc : Skin effect coefficient
- Rca : Effective thermal resistance between the conductor and the ambient.

The above mentioned rule is used along with a few relevant modifications in case of AC cables and DC cables as mentioned in chapter 4 and chapter 5 respectively. Apart from the basic calculation, various parameters like cable installation conditions, existing load profile variations in ambient conditions , cable design factors and cable failure modes influence the ampacity calculation of cable systems. IEC 60287([5]) is widely used to calculate the thermal rating of the cable system. However, since the formula mentioned in it is used for the steady state, this formula can not be used to accurately calculate the temperature variations under varying cable load. Dynamic cable rating is needed to increase the power flow of the cable while still maintaining a security margin.([7]) The use of optical fibre based (DTS) system as a form of measurement system for measuring the cable temperature profile is increasingly being implemented to improve the accuracy of cable thermal measurements. According to [8], the (DTS) system when implemented properly is effective for utilizing the unused capacity of underground cables. Dynamic thermal rating of cable systems provide more line capacity than static rating. Line ampacity depends strongly on the changing power level through the cable which depends on changing wind speed. Therefore, the

[1] Underground cables- A term for cables which are installed in the ground
Overhead cables- a term for cables installed above the ground with air as the surrounding medium([4])

power cable will transport more energy compared to static line rating,with the help of a suitable dynamic cable rating system in place.([9]).

In the following figure, we can see the effect of dynamic cable rating in form of wasted production as compared to static cable rating as a function of number of wind turbines.

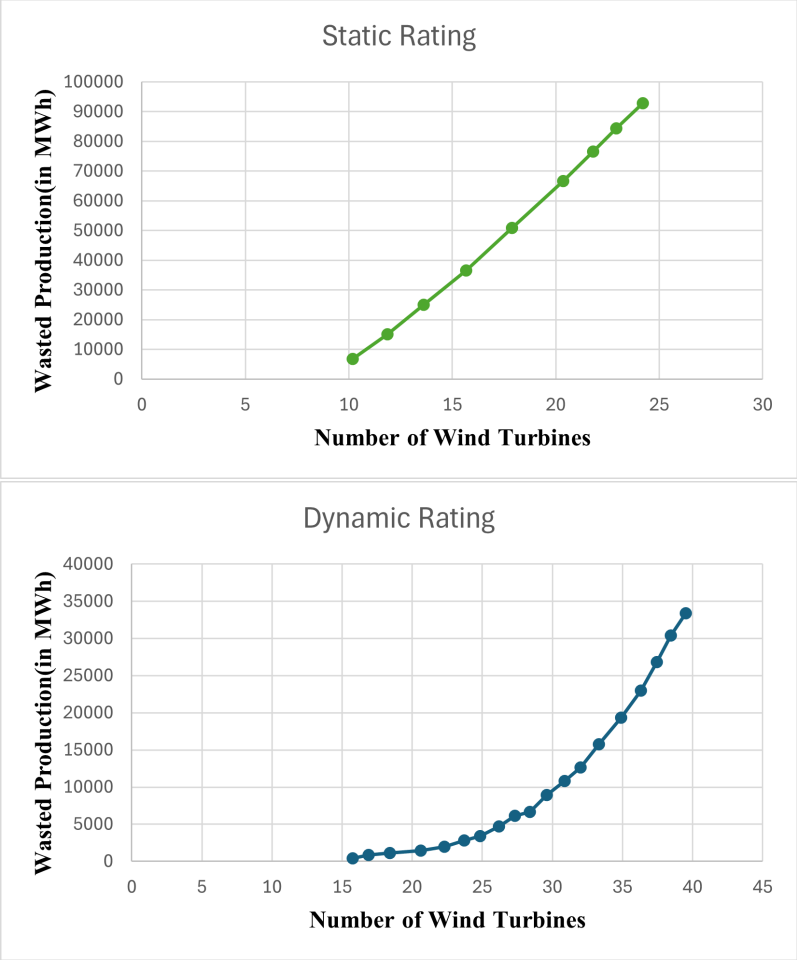

Figure 2.1: Amount of energy wasted as a function of the number of wind turbines-both for static and transient rating(Figure 5-[9])

It can be seen from figure 2.1 that the amount of power wasted increases exponentially with the number of wind turbines included when the cables are rated dynamically. But,the static variation has a much greater rate of increase in wasted energy production when compared with the dynamic case. Thus, it can be inferred from figure 2.1 that dynamic cable rating can be used to increase the total power output from the system. The thermal models of the cable generally used can be found in the next section 2.2.

Following the literature available on the implementation of dynamic cable rating systems for high voltage underground cables ([10],[11],[12],[13],[14]), an appropriate cable rating measurement system has been implemented in the work. To improve the method of cable rating in the long run, it is necessary to use predictive methods for circuit loading and use ambient temperature sensing integrated in the system. This will help in predicting the load flow curve and then using the data to calculate accurate emergency ratings of the system. ([2]).

2.2 Theoretical background behind the existing model

The existing thermal model of the underground cable system forms the basis of the dynamic cable rating of different cable systems. This section presents the heat equation and the numerical derivations which lead to the development of the existing model. The basic thermal equation is derived from the given equation for cables in different kinds of environments.

$$W_{int} + W_{ent} = W_{out} + \Delta W_{st} \tag{2.2}$$

W_{int} is the rate of heat generated in the cable by joule or dielectric losses. W_{ent} is the rate of heat entering the cable. W_{out} corresponds to the rate at which energy is dissipated by conduction,convection or radiation. ΔW_{st} is the rate of energy stored within the cable.

To describe the process of heat transfer through the cable, the heat equation is used. The physical form of the heat equation is made in the form of a thermo-electrical equivalent model shown in figure 2.2 and figure 2.3 respectively.

The differential equation describing heat transfer in soil has the following form-

$$\frac{\partial A}{\partial x} + \frac{\partial B}{\partial y} + W_{int} = c.\frac{\partial \theta}{\partial t} \tag{2.3}$$

Here, A is defined as $\frac{1}{\rho}\frac{\partial \theta}{\partial x}$ and B is defined as $\frac{1}{\rho}\frac{\partial \theta}{\partial y}$.
This is a two dimensional approximation of the heat equation which is used to formulate the numerical model for both HVAC and HVDC cable cross section. ρ is the thermal resistivity of the material in Km/W. C is the volumetric thermal capacity of the material. x, y are the two dimensional coordinates for heat transfer. θ is the temperature of the particular material in °C. Therefore, the final expression of heat transfer used is the one shown in equation 1.3. The most common way of representing the cable thermal model is in form of of an analog of an electrical circuit.

The heat sources are modelled as current sources. The thermal resistances are modelled as electrical resistances. The heat storing capacities of different elements of a cable are modelled in form of capacitances which are analogous to electrical capacitances. The different thermal resistances and capacitances of a cable depend on the number of cores, number of external heat sources around the cable, the construction (sheath,type of insulation,type of jacket and serving) of the cable , the external soil conditions (moisture migration,temperature etc).[4] The layout of the thermal model is represented in the following figure-

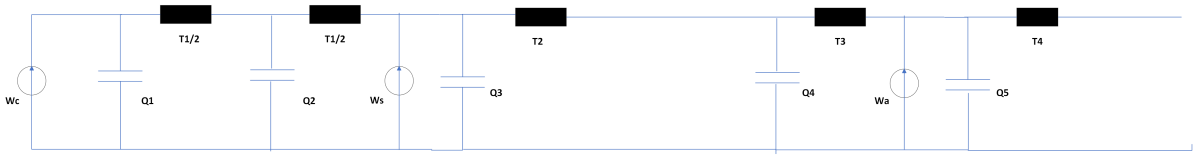

Figure 2.2: Thermal model for steady state and transient analysis of a single conductor cable,[15]

The model shown in figure 2.2 has been used in chapter 4 for further calculations. The description of the losses, thermal resistance and thermal capacitance parameters can be found in List of Abbreviations and Appendix B.

For calculating the ampacity of the HVDC connection used, a suitable thermal model for the single core extruded XLPE based cable is used. Following this, research on the analytical model for the HVDC cable suggests

that the model which is used for static circuit calculations under this case can be used to calculate the effect of dynamic current variations, as the final results do not indicate an error in both the solutions([16]). The coupled electro-thermal model for an extruded XLPE cable upto 275 kV has been used earlier. Since numerical results provided similar results for the steady state and transient variation of current, the effect of thermal capacitances is neglected in this case. A modified version of this model has been used for DC cables rated upto 500kV([17],[16])

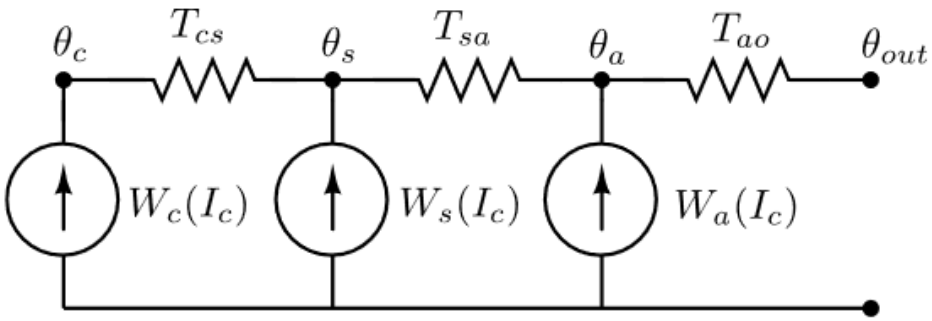

Figure 2.3: Electro Thermal model for 275kV cable(page 8,[17])

An interpolation of this model with suitable modifications is used in this work (Chapter 5).

2.3 Disadvantages of existing model in an offshore wind farm setup

As has been mentioned in 2.1, the literature indicates errors in results for complex cable system computations when comparing the FEA simulations and the analytical model. It has been pointed out in [18] that the existing method of calculating the dynamic rating of the system neglects the intermittent nature of output from wind farms and thus is not economically suitable unless a risk based approach is used to evaluate the effectiveness of the model. The uncertainties in transient model computations can be improved by adapting a weather forecasting framework to predict the emergency rating of the buried cable analytically [2]. This prediction does not include the accurate variations in characteristic parameters of the surrounding soil and other ambient parameters. As these changes are not only dependent on the environment but also on the existing load profile of the system, a better alternative is to predict the ageing of a cable based on the ampacity ratings. This will help the cable-system operators in deciding the economic compatibility of the Thermal rating model.

These existing thermal models show inaccuracy when compared to corresponding finite element based simulations in case of cables systems with heat sources crossing their paths, and presence of duct banks.But the models show close accuracy when they are used on cable systems alone(minimal errors between analytical and FEM results achieved in case of single core cable systems [19],[13]). As Dubitsky[19] suggests, an experimental validation with a proper (DTS) based system is necessary to modify the existing steady state model from IEC-60287.

Extensive literature indicates that the ampacity of a HVDC cable heavily depends on the effect of soil thermal resistivity and ambient temperature variations on the electric field of the insulation and the conductor.([20]). Apart from this the laying conditions of the sub-sea cable also influence the change in cable ampacity. To offset the geographical effects, different types of cable designs have been explored and implemented worldwide. However, the extruded XLPE(cross linked polyethylene) cable design has been explored so far in detail.

The HVDC insulation also shows variation in electrical conductivity with the application of short term transients and transient overvoltages.([21])

2.4 Ageing of underground cables and effect of different factors

It becomes imperative to see the effect of ageing on a cable system with changing parameters. Although literature suggests that ageing and degradation of cables are different terms, in most cases, both of these words are used interchangeably. Ageing (long term deterioration) of an underground cable is dependent on various factors. Degradation refers to the medium term mechanism of cable deterioration where different factors come into play. For the purpose of this study, ageing and degradation are used to refer to the deterioration of the cable with suitable explanations. The analysis of the ageing of the submarine cable system becomes important whenever the cable is to be operated near its maximum operating limit. Since, the time duration of such an event is difficult to predict beforehand, the results from dynamic cable rating of cable system (temperature vs. time duration) can be used to predict the ageing of the cable system. Though, a lot of factors responsible for the ageing of cable systems act simultaneausly([22],[23]), results from the modelling can be compared with the experimental results to get an accurate estimate. This work shows the effect of thermal stress (on AC cables) and thermal and electrical stress (on DC cable) under changing external parameters.

Densley([23]) suggests different ageing mechanisms for different insulation systems of cables-Paper/oil or fluid filled cable systems and extruded cable systems(XLPE) and ethylene propylene rubber(EPR). The effect of electrical ageing factors like electrical treeing, water treeing and partial discharges is significant. Under abnormal conditions, thermal ageing also plays an important role.([24]). The effect of ageing, namely occurrences of contaminants, defects ,protrusions and voids make the accessories like joints and terminations more vulnerable. It is observed that a hard impact on the cable insulation can lead to a rupture in the insulation which can lead to breakdown. Usually electrical faults lead to degradation of the cable systems in the long run which can cause water treeing, onset of partial discharge and electrical degradation. If the faults are not detected, then this can eventually lead to a breakdown of the cable system. ([25]).

Earlier work on Dynamic rating on medium voltage power cables by Jensen ([26]) shows that the capacity of power transfer is dependent on these external factors which need to be taken into picture. Although the causes of degradation can be many, chemical degradation and water treeing are two major factors which play an important role in reduction of lifetime of operational lifetime.

Following table shows the different ageing factors which are responsible for cable ageing-

Thermal	**Electrical**	**Environmental**	**Mechanical**
Maximum Temperature (T)	Voltage (ac,dc,Impulse)	Gases (air,oxygen,etc.)	Bending
Low, High ambient T	Frequency	Lubricants	Tension
Temperature gradient	Current	Water /humidity	Compression
Temperature cycling		Corrosive chemicals	Torsion
		Radiation	Vibration

Table 2.1: Ageing factors that affect cable insulation systems

Out of all the factors, thermal ageing has been the most important aspect as shown in research conducted upto now.([27],[28],[29]). Rapid ageing of the cable usually leads to cable reaching its end of life soon. As Jensen mentions in his work([26]), The end of life is usually estimated with the help of -

- 50% breakdown voltage
- 50% elongation in the insulation
- 0.5% weight loss
- 50% tensile stress at 100% extension.

A combination of one of these factors is used to get to the end of life for a cable system. The effect of ageing is not limited only to the insulation. This effect is spread over to the insulation sheath as well as the semi-conductive shield between the conductor and the insulation material. But experimental validation is necessary to properly measure this effect in the long run. Following figure shows the effect of ageing with temperature for different classes of XLPE material on which electrical stress tests have been run-

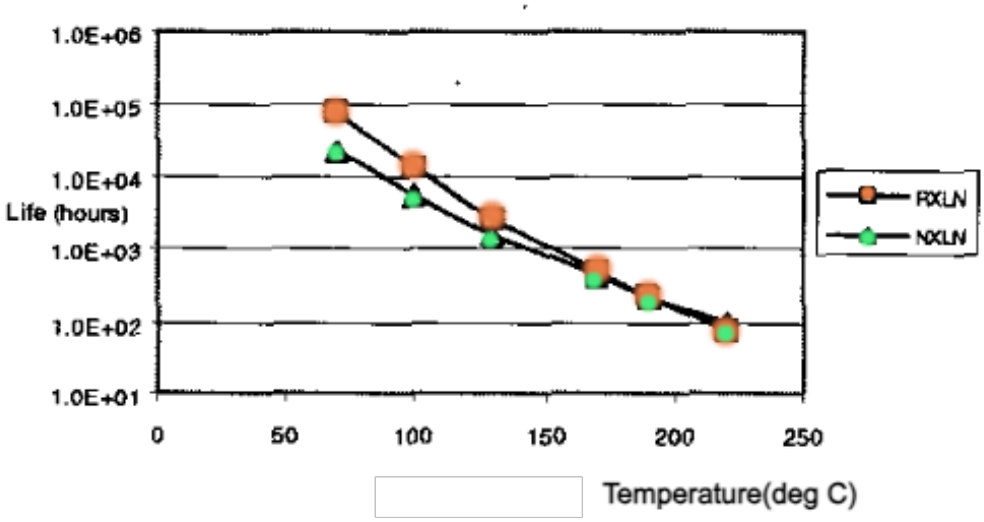

Figure 2.4: Ageing variation with temperature(2 types of XLPE materials [28])

Montanari explains that results similar to the one shown in figure 2.4 are fit on suitable lifetime models for evaluation of numerical parameters. With progressing time, the computing power has increased, making it easier to model the defects (particularly electrical treeing) and presence of space charges in microvoids using complex rules such as the one mentioned in equation 6.9. ([30]). The effect of ageing of the complete cable system is dependent on the effect of different thermo-mechanical effects on the cable accessories as well. Also, the process of manufacturing also affects the ageing process of XLPE insulation.([31]). Therefore, experimental validation along with the theoretical computations shown here should be used to arrive at any conclusive result in practical cases. The starting point of any such analysis is to fit the time to failure data to a suitable weibull distribution. The scope of this work is to provide the time to failure data from analytical and numerical simulations. The time to failure data can be then used to figure out suitable weibull distributions. The metrics of such statistical models need to be calculated experimentally.

2.5 Problem Statement

In order to get a prior understanding of the deterioration of the high voltage cables under different loading conditions, it is necessary to understand the effect of varying thermal and electrical stress on the different layers of the cable system (particularly the insulation layer). Since the rate of cable degradation is dependent on the external conditions of the environment under which it is operating, it becomes important to study the results before a physical implementation is done.

2.6 Summary

In accordance with the literature, the purpose of this work was to consider the effect of changing soil thermal conductivity and burial depth on extruded XLPE insulation based cable systems (generally used in Dutch offshore grids) under dynamic loading conditions.The HVDC cables have a voltage level of 525kV and HVAC connection have a voltage level of 66kV. The cable systems are modelled both analytically and numerically. The results for both are compared.The results for the temperature vs. time curves from the models are used to further calculate the ageing of particular cable systems. Further details regarding each topic can be found in detail in chapter 1.

Chapter 3

Development of Load Profiles

As mentioned in 1.2, continuous current vs. time profiles [1] are needed to test the performance parameters of the cable systems which are eventually translated into suitable thermal models for the cables. Both HVAC and HVDC systems need different type of current profiles to work with. This chapter explains the process in which the different current vs. time profiles needed for numerical and analytical simulation have been developed. The relevant data and the code needed to develop them has been explained in further detail in Appendix C.

3.1 Development of Current vs. time load profile for 66kV HVAC cables

For this case, research on the existing 66kV HVAC cable setup in the Ijmuiden ver area operated by Tennet has been studied. As mentioned in [1], the proposed system has a total real power capacity of 2GW. Following this, 4 platforms(500 MW each) have been developed in total. Further research indicates that each 500MW AC platform is supposed to collect power from a wind farm housing 80 wind turbines of 6MW capacity each[32]. Details regarding the electrical connection of the cables to the wind turbines are not known. The cable connection from the coupling point on each platform to the converter station has been used for this study (refer figure 1.1).For this case, data for a Vestas 6MW wind turbine has been used to build the model[33].

Each 500MW block has capacity to connect 7 66kV bays. Only 6 bays will be used in the operation, with one being used as a universal bay[34].

3.1.1 Process workflow for the load profile

Following figure explains the development process of load profile for the HVAC system.

[1] **Test profiles**: Term used for the current vs. time profiles developed according to the documentation.
Load profiles: Actual current vs. time profiles

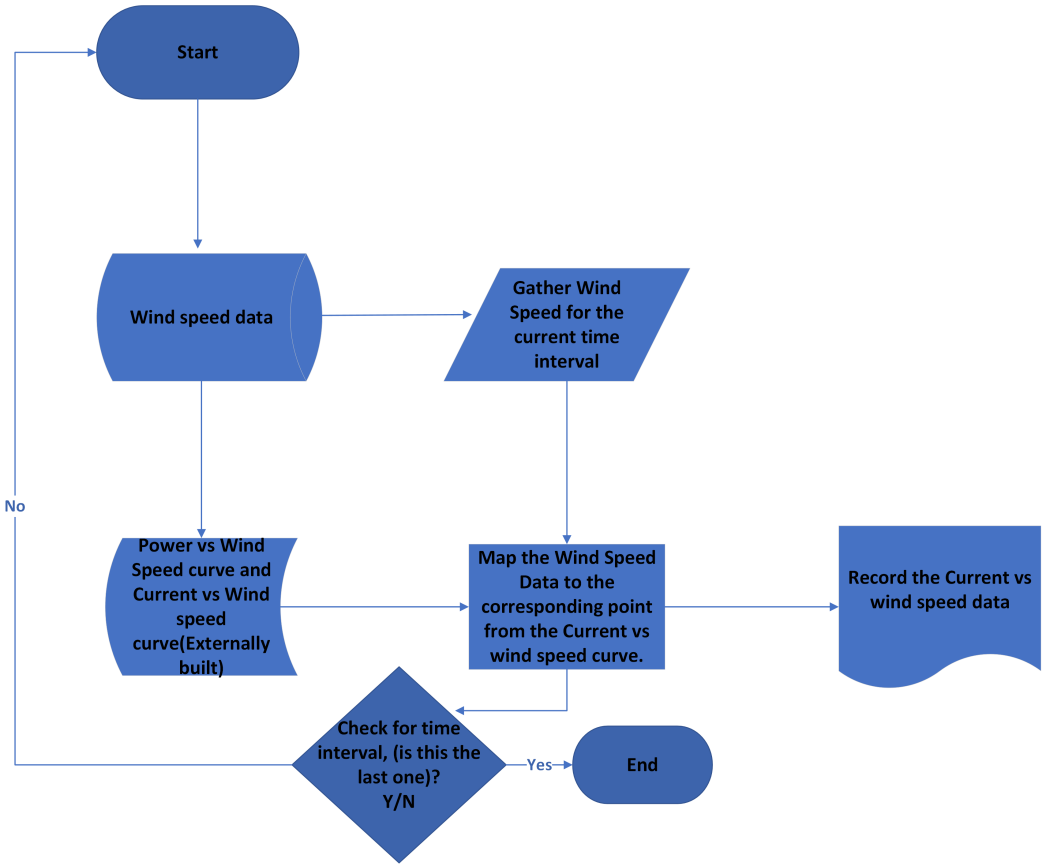

Figure 3.1: Load profile for 66kV system

Some assumptions have been made in the process which are listed as below-

- All the wind turbines are assumed to be operating at a nominal power coefficient value of 0.5(figure 2- [35]). In practice, this value varies depending on the tip speed ratio and the wake effects due to the wind on the blades of the turbine.
- To take the worst case picture, all turbines are assumed to be operating throughout the year.
- To take the variability of wind power over a wide area, an aggregated capacity factor of 27% has been taken here to calculate the total power output from the wind turbines in form of electricity generation(Figure 8,Page 35-[36]).

The wind speed data has been taken from the knmi data platform for the previous year (2021-22). The wind speed data is updated at every 10 min interval on the data platform([37]). The wind speed data is fit on the power-wind speed curve developed for the 500MW offshore wind farm. The resulting power curve is then translated to the intended current vs time-index curve. The current values are then used as input in the model explained in chapter 4.

3.1.2 Development of the power-wind speed curve and resulting load profile

The power wind speed curve is developed following these steps.

- The formula to be used for power output is $P = 0.5 * \rho * c_p * (\pi * (r^2)) * (v^3) * 80 * (1e-6)$. Here P is the power in MW, ρ is the density of air, c_p is the coefficient of power transfer from air to electrical form, v is the speed of wind in m/s and r is the radius of the rotor blade.

- The minimum wind speed(cut-in value) is taken to be 3 m/s and the maximum value(cut-out) value is taken to be 25 m/s.
- The power curve is then fit based on the wind speed limit to get the power vs wind speed curve.

Following figure shows the total current vs. time distribution for all platforms of 500[MW]. This current distribution is further translated to the current per bay.

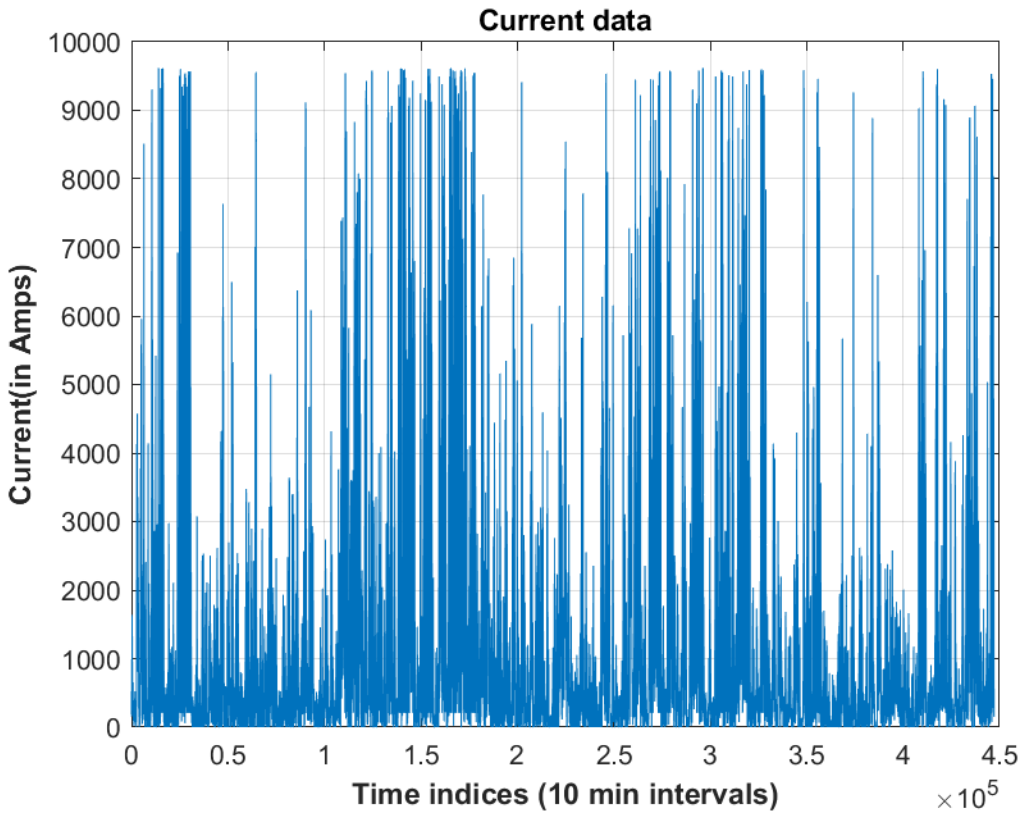

Figure 3.2: Current vs. time(in s) corresponding to the wind speed data for 8.5[years]

After building the power vs wind speed curve, the current value for each 66kV bay is calculated as follows-

$$P1 = \frac{P}{7} = \sqrt{3} * 66kV * 0.8 * I$$

The total power $P1$ is divided by 7 here to get the power transferred through each 66kV power cable connected to the offshore platform. The term 0.8 here refers to the power factor of operation.
This value is assumed to be constant for the sake of approximation. Theoretically, this value fluctuates with the changing power output from the wind turbines. The term I represents the current of operation which we need to calculate.

In the following figures, the accumulated current vs time load profile can be found.

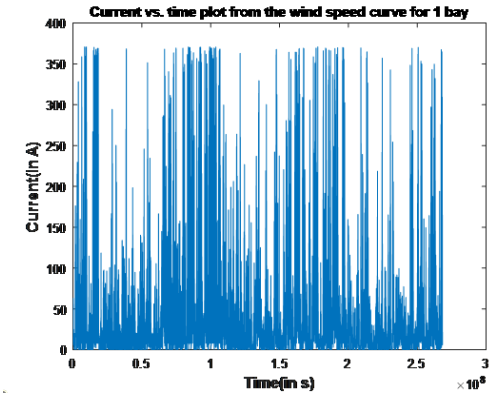

(a) Current vs. time profile from the wind speed data (for 8.5 years)

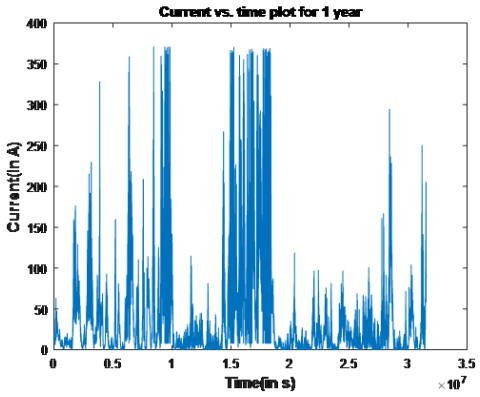

(b) Current vs. time profile from the wind speed data (for 1st year)

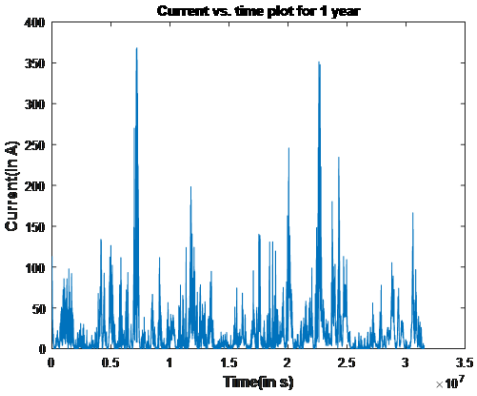

(c) Current vs. time profile from the wind speed data (for 2nd year)

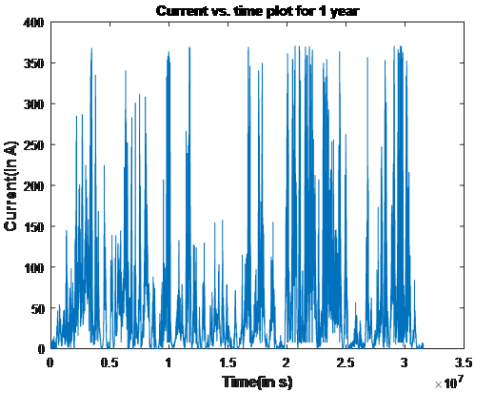

(d) Current vs. time profile from the wind speed data (for 3rd year)

Figure 3.3: Time series plots for the current vs. 10-min time interval load profiles.

Figure 3.3 shows the accumulated current vs. time load profile for 1 bay containing the 66kV power cable. Figures 3.3b, 3.3c and 3.3d represent the yearly current variation data. These portions of the load profile have been used for further analysis of the HVAC cable in chapter 4.

3.2 Development of current vs. time profiles for HVDC cable setup

The HVDC cable setup has been used to model the results from the actual load profile as well as the measurement current vs. time profiles to check the suitability of the analytical and the numerical model under different cases. The load profile used here is the scaled up version of the load profile mentioned in figure 3.3. Since the total power transferred is the same throughout the HVAC and the HVDC cables, the HVDC cable has been applied with a total power of P*4 to take the total power transferred through all the offshore platforms into account. This total power transfer is then divided by a gross value of 525 kV to account for the actual current vs. time profile in this case. The total current variation is distributed in hours and the hourly current variation is used to simulate results for the HVDC cable in chapter 5. The actual implementation of the resultant current vs. time profiles are shown here-

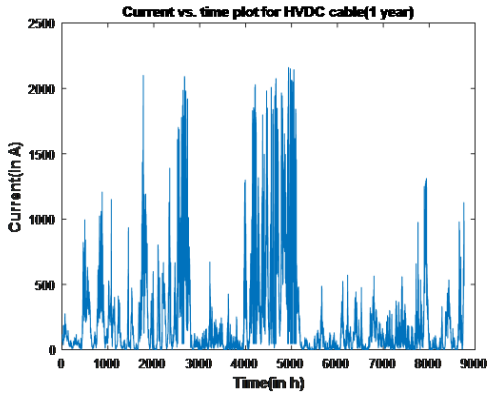

(a) DC case profile 1

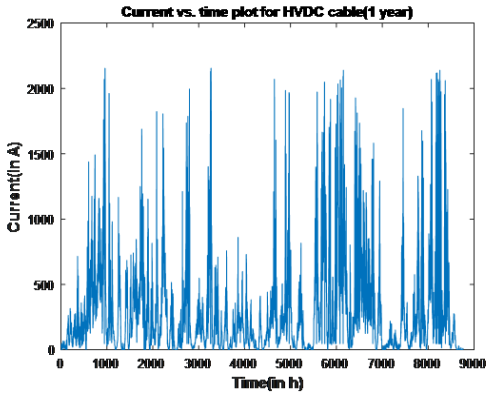

(b) DC case profile 2

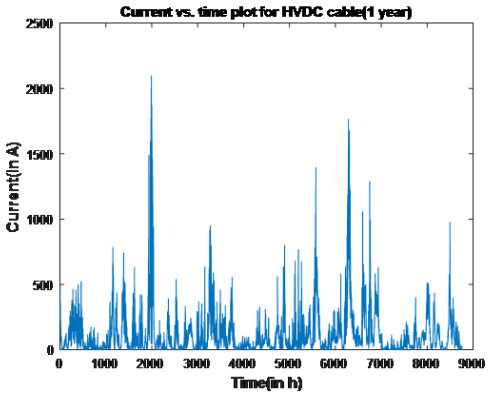

(c) DC case profile 3

Figure 3.4: HVDC load profiles

Figure 3.4 shows the portions of the actual load profile which has been derived from the wind speed data. The assumptions which have been mentioned in subsection 3.1.2 limit the maximum DC current operation to 2300[A]. Based on the converter setup and the information mentioned in [38], the HVDC setup can be operated in 3 modes-

- Symmetrical monopole
- Rigid bipole
- Bipole with dedicated metallic return

For this case, only the operation in symmetrical monopole has been considered.

Chapter 4

Modelling of HVAC cable system

In this chapter, the 66kV HVAC setup has been modelled for one offshore wind platform of 500MW capacity. Each such 500MW feeder has 6 feeders of 66kV capacity each. In reality, multiple such feeders are used in form of underground cables. For ease, the effect of two such feeders has been considered in this case. To support the findings from the numerical model method, an analytical code has been developed in Matlab to analyse the results of a varying load profile on the 66kV setup. After the analysis,the temperature vs. time results obtained for the cable surface have been used to calculate the lifetime consumption of the particular setup in consideration in Chapter 6.

This chapter starts with a basic theoretical understanding of the cable system used. A description of the relevant characteristics of the cable used has been mentioned. After this, an explanation of the analytical and the numerical model has been mentioned. Finally, the results from the analytical and the numerical model for the different current vs. time profiles have been examined under separate cases. Lastly, a section on conclusions sums up the relevant points from the simulation results.

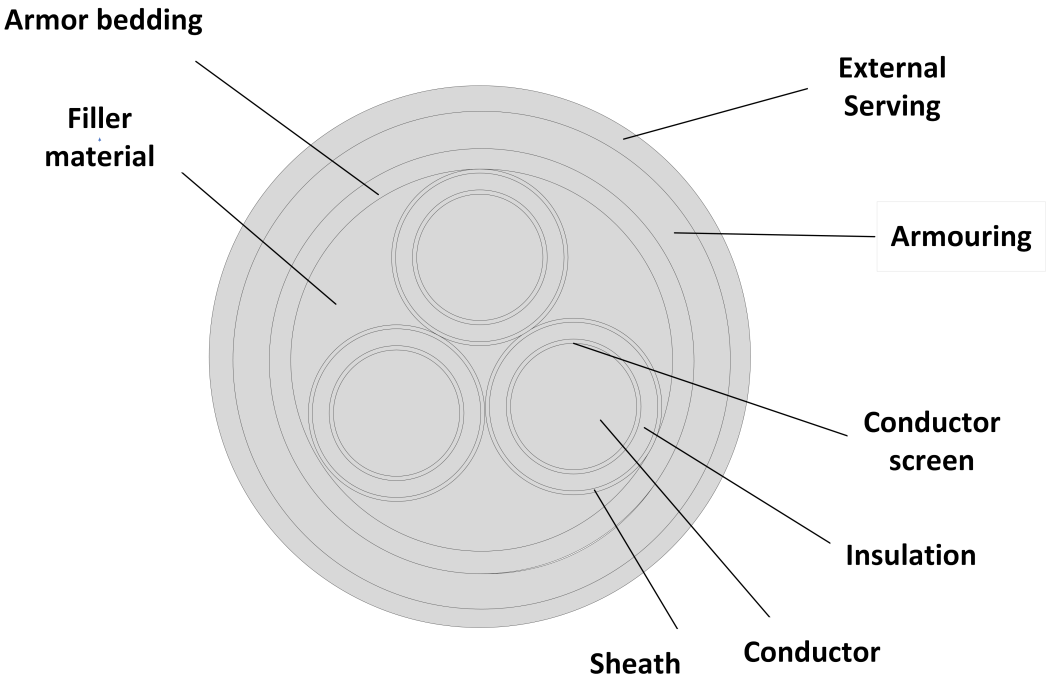

Figure 4.1: Cross section of 66kV cable used

Figure 4.1 shows the cross section of the HVAC cable used.

The details of the cross section are given as follows- [1]

S.no	Name	Dimensions	Material type
1	Conductor	15.95[mm]	Copper
2	Conductor screen	1[mm]	Copper(with semiconductive compound)
3	Insulation	10[mm]	Ethylene Polypropylene
4	Screen	5[mm]	Copper
5	Filler	45.81[mm] approx.	XLPE
6	Armor bedding	5[mm]	Polypropylene
7	Armor	12.6[mm]	Galvanized steel
8	External serving	5[mm]	Polypropylene

Table 4.1: Description of the 66kV cable cross section for the base model

4.1 Cable description for the 66kV cable system

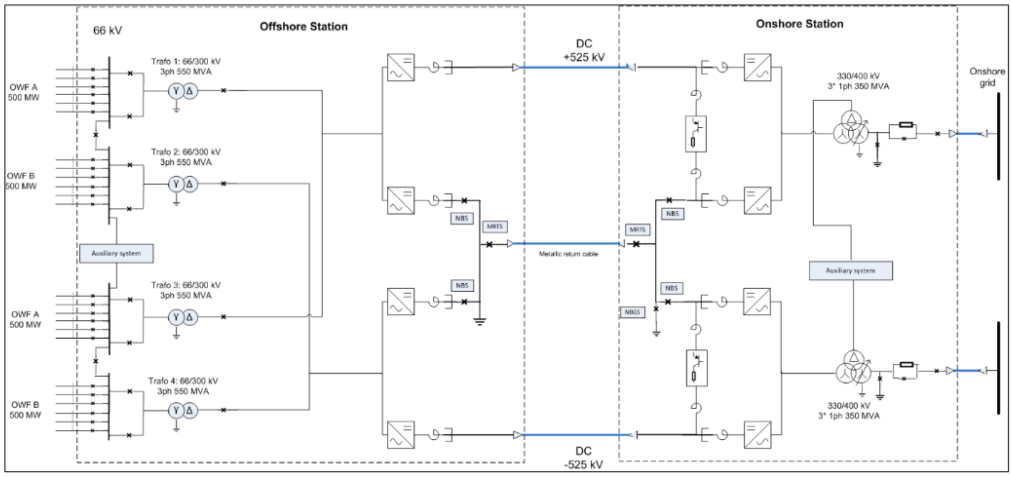

Figure 4.2: SLD for the complete layout of system-([1])

The existing setup of Tennet is designed as shown in figure 4.2. From the figure it can be seen that the offshore platform is connected to 4 500MW blocks through 6 66kV bays. Therefore further course of analysis is done for one 500MW block with 6 66kV bays connected together. The design separation between each bay is taken to be 30[m]([32]).

The structure of the cable system has been modelled as a trefoil formation.

[1] The first row in table 4.1 shows the radius of the conductor, rest of them show the thickness of the specified part

Typical 66 kV cable design for offshore wind

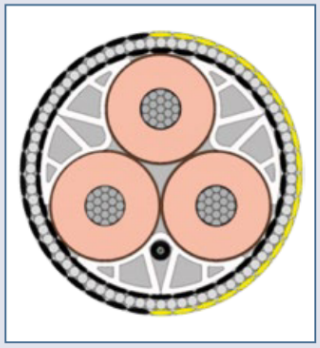

Conductor	Copper or aluminum conductors longitudinally water blocked
Conductor screen	Extruded semi conductive compound
Insulation	EPR
Insulation screen	Extruded semi conductive compound
Screen	Individual Cu-tape screen on each phase
Fibre optic unit	Up to 3 FO units with metal tube
Lay up	Three power cores laid up with extruded fillers
Armour Bedding	Polypropylene yarns
Armouring	One layer of galvanized steel wires, flushed with bitumen
Outer protection	Polypropylene yarns in customisable colours

Figure 4.3: Cable schematics for single phase of three phase 66kV cable([39]

1 cable of the type mentioned in figure 4.3 representing three phases has been placed under the ground level. 2 such cables have been modelled in parallel with separation between them being 30[m].

4.2 Theoretical description of the model

The model used in this analysis is similar in structure to the one shown in figure 2.2. The model parameters have been calculated first keeping the steady state ampacity in picture. This model is then converted to a two step ladder network model. A description of the code for this can be found in Appendix 7.3. The equivalent parameters for the thermal resistances and thermal capacitances can be found in table 4.2.

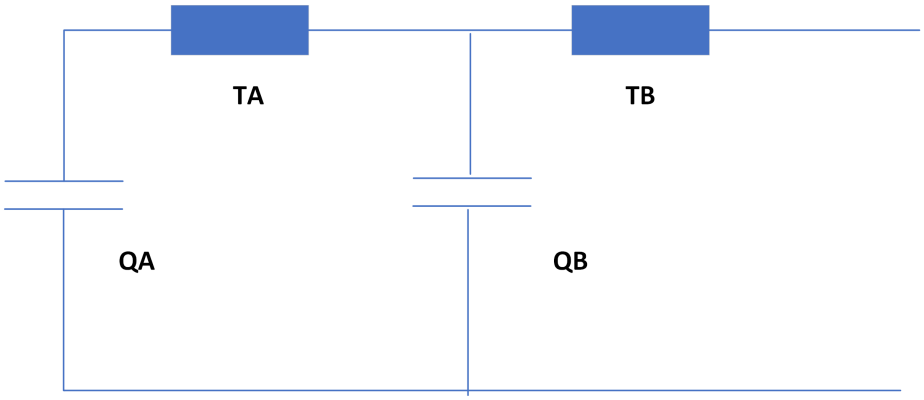

Figure 4.4: Representation of 2 Step ladder network

Values for the thermal resistances and the thermal capacitances are taken from [40] and [41]. After calculating the resultant two step ladder network, and the various losses, equations for transient temperature variation are used here to calculate the temperature profile over a given loading period.

[2] The thermal resistances are defined as follows-

$$T_{11} = \frac{\rho_{epr}}{2\pi} \ln(1 + \frac{2t_{ins}}{d_c}) \tag{4.1}$$

$$T_1 = T_{11}/3 \tag{4.2}$$

$$T_2 = \frac{\rho_f}{2\pi} G \tag{4.3}$$

$$T_3 = \frac{\rho_{pp}}{2\pi} \ln(1 + \frac{2t_{ab}}{D_f}) + \frac{\rho_{st}}{2\pi} \ln(1 + \frac{2t_a}{D_f + (2t_{ab})}) + \frac{\rho_{pp}}{2\pi} \ln(1 + \frac{2t_{op}}{D_f + (2t_{ab}) + 2t_a}) \tag{4.4}$$

$$T_4 = \frac{\rho_s}{2\pi} \ln(\frac{4L}{D_e}) \tag{4.5}$$

The capacitances are defined as given-

$$Q_c = S.c \tag{4.6}$$

$$Q_{ins} = \frac{\pi}{4}(D_i^2 - d_c^2)c_i \tag{4.7}$$

$$Q_f = \frac{\pi}{4}(D_f^2 - (D_f - 2t_f)^2)c_f \tag{4.8}$$

$$Q_s = \frac{\pi}{4}((D_i + 2t_s h)^2 - D_i^2)c_s h \tag{4.9}$$

$$Q_{ab} = \frac{\pi}{4}((D_f + 2t_{ab})^2 - D_f^2)c_{ab} \tag{4.10}$$

$$Q_a = \frac{\pi}{4}((D_f + 2t_{ab} + 2t_a)^2 - (D_f + t_{ab})^2)c_a \tag{4.11}$$

$$Q_{se} = \frac{\pi}{4}((D_f + 2t_{ab} + 2t_a + 2t_o p)^2 - (D_f + 2t_{ab} + 2t_a)^2)c_{se} \tag{4.12}$$

The thermal capacitances are clubbed for representation using the van wormer coefficients as mentioned in [15] .

$$p = \frac{1}{2\ln\frac{D_i}{d_c}} - \frac{1}{(\frac{D_i}{d_c})^2 - 1} \tag{4.13}$$

$$p_f = \frac{1}{2\ln\frac{D_f}{46.18}} - \frac{1}{(\frac{D_f}{46.18})^2 - 1} \tag{4.14}$$

$$p_{ab} = \frac{1}{2\ln\frac{(D_f + 2t_{ab})}{D_f}} - \frac{1}{(\frac{(D_f + 2t_{ab})}{D_f})^2 - 1} \tag{4.15}$$

$$p_2 = \frac{1}{2\ln\frac{D_e}{(D_e - 2t_{op})}} - \frac{1}{(\frac{D_e}{(D_e - 2t_{op})})^2 - 1} \tag{4.16}$$

[2]The description of the formulae units can be found in Appendix B.

The thermal capacitances used in the model are defined as-

$$Q_1 = 3(Q_c + pQ_{ins}) \tag{4.17}$$
$$Q_2 = (1-p)Q_{ins} + p_f Q_f + Qs(1+Lsh) \tag{4.18}$$
$$Q_3 = (1-p_f)Q_f + p_{ab}Q_{ab} \tag{4.19}$$
$$Q_4 = (1-p_{ab})Q_{ab} + Q_a(1+La) + p_2 Q_{se} \tag{4.20}$$
$$Q_5 = (1-p_2)Q_{se} \tag{4.21}$$

After modelling the different parameters of the thermal circuit in accordance with figure 2.2, the different thermal resistance and thermal capacitance values are clubbed together to get the parameter values for the two step ladder network as shown in figure 4.4.([15])

$$T_A = T_1/2 \tag{4.22}$$
$$T_B = (T_1/2) + (T_2(1+L_{sh}) + T_3(1+La) + T_4 \tag{4.23}$$
$$Q_A = Q_1 \tag{4.24}$$
$$Q_B = Q_2 + Q_3((T_2(1+L_{sh}) + T_3(1+La) + T_4/(T_B^2)) + Q_4(T_3(1+La) + T_4/(T_B^2)) + Q5(T_4/(T_B^2)) \tag{4.25}$$

The description and data for the terms used here can be found in Appendix B.

The values of thermal resistance and capacitances as simulated from the model parameters analytically are defined as follows-

S.no	Description	Value
1	T_1	0.123 KW^{-1}
2	T_2	0.3008 KW^{-1}
3	T_3	0.0462 KW^{-1}
4	T_4	1.5429 KW^{-1}
5	Q_c	0.3085 JK^{-1}
6	Q_{ins}	2.7583 JK^{-1}
7	Q_f	18.0049 JK^{-1}
8	Q_s	0.2618 JK^{-1}
9	Q_{ab}	4.3067 JK^{-1}
10	Q_a	6.9862 JK^{-1}
11	Q_{se}	2.6842 JK^{-1}
12	Q_1	4.3525 JK^{-1}
13	Q_2	11.59 JK^{-1}
14	Q_3	38.77 JK^{-1}
15	Q_4	5.9166 JK^{-1}
16	Q_5	18.6612 JK^{-1}
2 step Ladder network Parameters		
17	T_A	0.0615 KW^{-1}
18	T_B	3.1222 KW^{-1}
19	Q_A	4.3525 JK^{-1}
20	Q_B	66.0357 JK^{-1}

Table 4.2: Values for thermal resistance and thermal capacitances

4.3 Theoretical aspect for the 66kV analytical model

The model has been made in following steps.The respective formulae for calculations are mentioned in [15] ,[5] and [42].

- The model parameters are used to derive the thermal resistances and thermal capacitances of the different parts The final formula for calculation of thermal resistances and capacitances are computed from equations 4.1 - 4.25.
- The parameters for the sheath loss factor and the armor loss factor factor are calculated as follows in continuous iteration.

For screen loss-

$$\theta_{sc} = \theta_c - [I^2R + 0.5W_d]T_1 \tag{4.26}$$

$$R_s = R_{so}(1 + \alpha_2 0(\theta_{se} - 20)) \tag{4.27}$$

$$\lambda_1' = (\frac{R_s}{R})\frac{1.5}{1 + (\frac{R_s}{X})^2} \tag{4.28}$$

For armor loss factor-

$$\theta_a r = \theta_c - (I^2R + 0.5W_d)T_1 + (I^2R(1 + \lambda_1 + W_d))T_2 \tag{4.29}$$

$$R_A = R_{Ao}[1 + \alpha_2 0(\theta_{ar} - 20)] \tag{4.30}$$

$$\lambda_2 = 0.358(\frac{R_a}{R})(\frac{2r1}{d_A})^2 \frac{1}{\frac{2.77R_A(10^6)^2}{\omega} + 1} \tag{4.31}$$

$$\tag{4.32}$$

- The various losses in the cable are calculated after this calculation. The Conductor loss W_c, Dielectric loss W_d, Screen Losses $W_s = \lambda_1 * W_c$, Armor losses $W_a = \lambda_2 * W_c$. Total losses $W_I = W_c + W_s + W_a$ are computed
- All the parameters are then used to calculate the steady state current rating, the temperature difference and the transient current rating of the cable system. The equations for these are as follows([15])- For the transient computation-

$$\theta_c(t) = W_c[T_a(1 - \exp(-at)) + T_b(1 - \exp(-bt))] \tag{4.33}$$

$$\alpha(t) = \frac{\theta_c(t)}{W_c(T_A + T_B)} \tag{4.34}$$

$$\theta_e(t) = (W_I + W_d)(\frac{\rho_s}{4\pi})[-E_i(\frac{D_e*^2}{16\delta t}) + E_i(\frac{-L*^2}{\delta t})] \tag{4.35}$$

- The equation for steady state computation used is -

$$I_{ss} = [\frac{\Delta\theta - W_d[0.5T_1 + n(T_2 + T_3 + T_4)]}{RT_1 + nR(1 + \lambda_1)T_2 + nR(1 + \lambda_1 + \lambda_2)(T_3 + T_4)}]^{0.5} \tag{4.36}$$

The parameters are defined in accordance with the transient equation parameters mentioned in [15]. The values for all these parameters can be found in Appendix B.

As has been explained in chapter 3, a current-time load profile is derived from the wind speed data, different portions of the cumulated load profile have been used to simulate cases. The simulation has been performed in steps as explained below-

- First the steady state current value has been calculated corresponding to a conductor temperature of 90°C which is the rated temperature for XLPE material. Then the steady state current has been calculated for temperature values of 110°C and 130°C.The results have been calculated for a maximum temperature upto 130°C.
- A pulse current profile with current values corresponding to 90°C, 110°C and 130°C has been used to compare the results for the analytical model and the numerical model.
- After this, the current vs. time profiles are used to check the temperature variation and subsequent ageing (Chapter 6). These current vs. time profiles have been taken from the actual load profile mentioned in figure 3.3.

The simulations (both analytical and numerical have been run with 1 year of data distributed in seconds. Following figures show the current vs. time profiles.

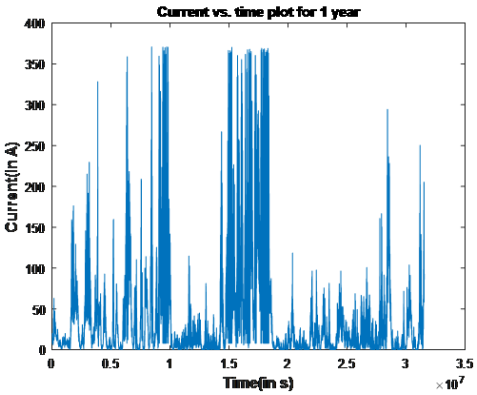

(a) Profile 1

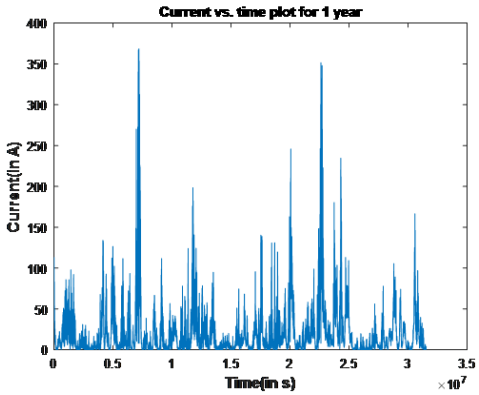

(b) Profile 2

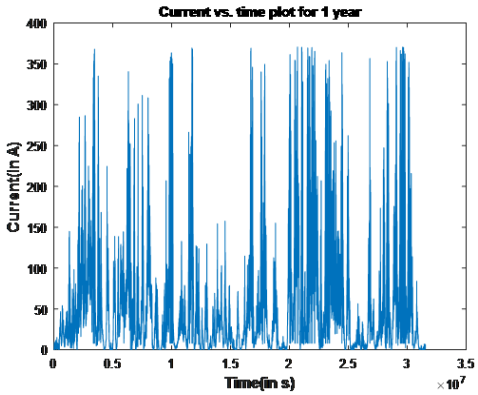

(c) Profile 3

Figure 4.5: Current vs. time(in seconds) profiles used for analysis

Figure 4.5 shows the different portions of the load profile which are to be used for the analytical and numerical simulation. The results have been compiled for two different cases of burial depth and soil thermal resistivity- $L = 1500[mm]$, $TC = 0.36[W/mK]$ and $L = 1200[mm]$,$TC = 0.2[W/mK]$.

4.4 Description of the numerical model developed-Comsol

This section explains the basic development of the numerical model which has been used along with the analytical model to validate the results. The numerical model has been developed in Comsol Multiphysics. The various current vs. time profiles as shown in figure 4.5 have been simulated in the model. While solving the results a time-dependent step solver with a time duration corresponding to the current profile has been used to get the results.

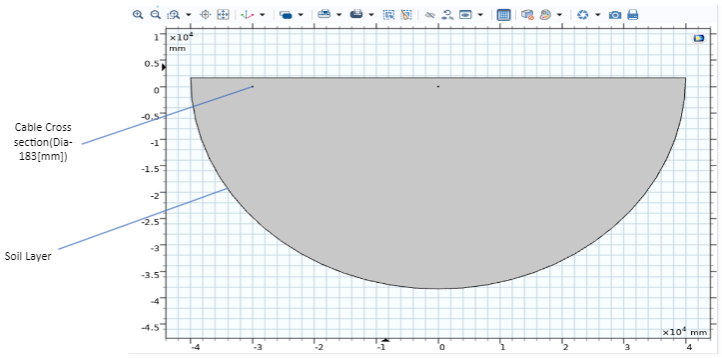

Figure 4.6: Model geometry for the cable cross section

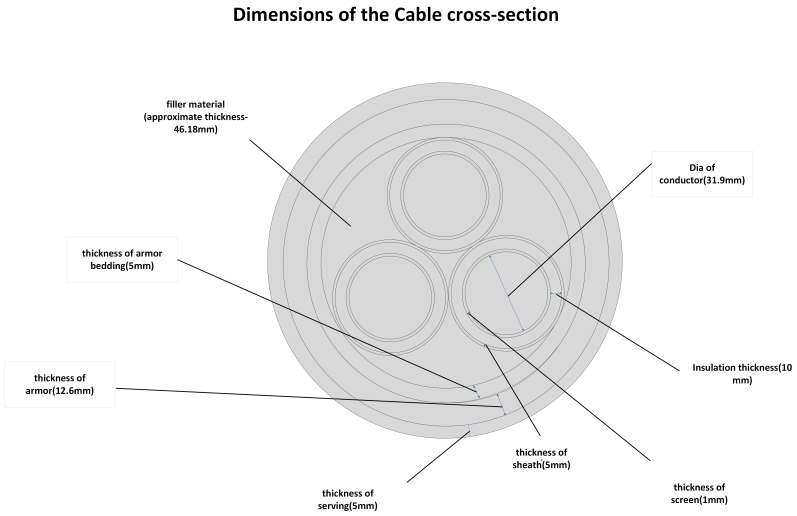

Figure 4.7: Cable geometry for the cable cross section

Figure 4.6 shows the geometry of the numerical model which has been used to simulate the numerical results. The semi-circular region is the soil layer which has a overall radius of 40[m]. This figure also shows 2 cable cross-sections each having a diameter of 183[mm]. The distance between both the cables is taken to be 30[m]. The enlarged version of this cross-section is mentioned in figure 4.7.

The model has been solved with the help of a heat transfer module with the conductors in the cable being taken as the sources of heat. The heat rate of each conductor is taken to be the ohmic losses in the conductor. The expression used for this calculation is -

$$Q = (I^2) * R_{ac} \tag{4.37}$$

Here R_{ac} is the AC resistance of the conductor.I has been replaced with the different dynamic current profiles for simulation. Following equations demonstrate the physical thermal model which has been built in Comsol-

$$d_z \rho C_p \frac{\partial T}{\partial t} + d_z \rho C_p \vec{u}.\nabla T + \nabla.q = d_z Q + q_o + d_z Q_t \tag{4.38}$$

$$q = -d_z k \nabla T \tag{4.39}$$

A description of the relevant terms can be found as-

- d_z is the elemental length of heat transfer.
- ρ is the density of the material involved.
- C_p is the specific heat of the material.
- $\vec{u}$ is the unit vector along the length d_z.
- q is the heat transferred along the length d_z.
- Q is the total amount of heat transferred.(Heat rate in Watts)
- q_o is the initial elemental heat transfer.
- Q_t is the amount of heat contributed by the heat source present(it is 0[W] if no heat source is there)

The parameters which have been used to model the different material properties along with their description can be found in Appendix B. A step solver with a step time of 3600[s] has been used to model the thermal profile in Comsol.

4.5 Results with the 66kV HVAC cable system

In this section, the implementation of the analytical model on the 66kV offshore HVAC system is discussed. The numerical results for the current vs. time profiles used here have been used to validate the analytical results. The final cable surface temperature variation from the result has been collected for 2 sets of values for burial depth(L), in [mm] and soil thermal conductivity(TC), in WmK^{-1}- (1500,0.36) and (1200,0.2). These temperature variations are then used in the lifetime analysis of the cable systems.(Chapter 6)

The steady state current calculated for a conductor temperature of 90°C was 310.04[A]. For a temperature of 110°C it was 351.55[A] and 388.66[A] for 130°C. The values for both analytical and numerical simulation are shown further.

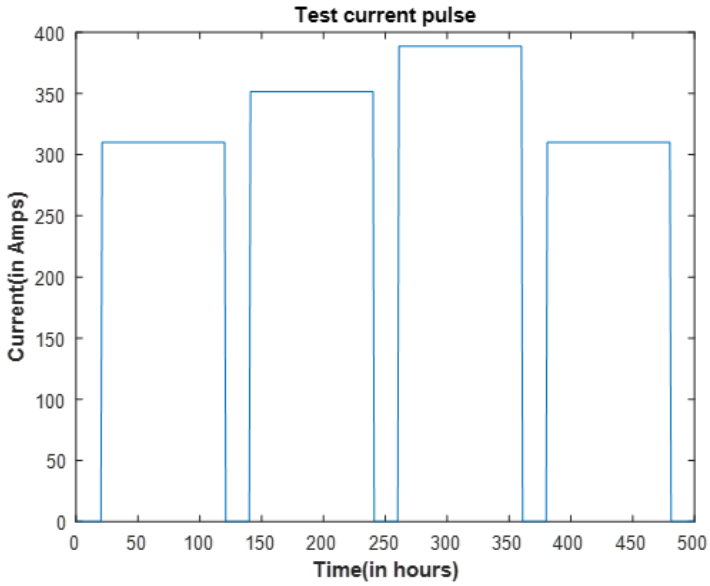

Figure 4.8: Step current waveforms for different temperature values

Figure 4.8 shows the plot for the step current waveforms which have been used for the test case. This waveform has been used to validate the results for both the analytical and the numerical models.

Following figure show the analytical and the numerical results for the cable surface temperature transient for the given test case waveforms.

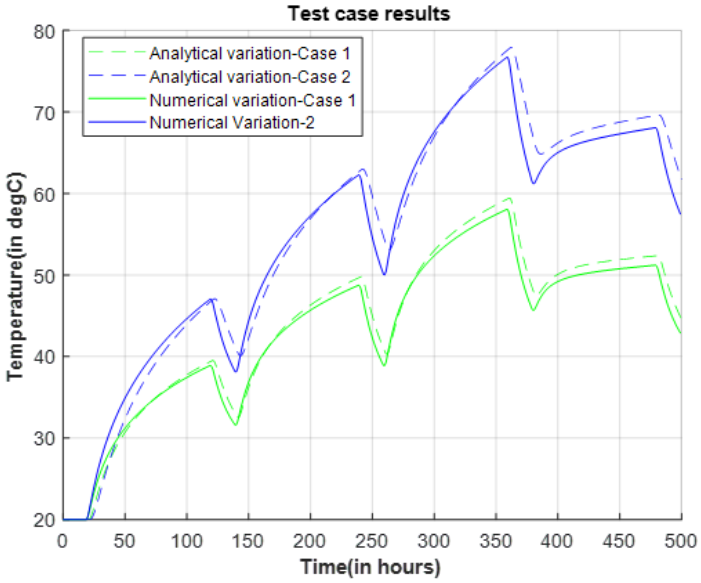

Figure 4.9: Results for the cable surface temperature transient for step current waveform(shown in figure 4.8)-(Case 1- $L = 1500[mm]$,$TC = 0.36[W/mK]$ and Case 2- $L = 1200[mm]$,$TC = 0.2[W/mK]$

This variation which is shown in 4.9 compares the results for both the analytical transient variation and the numerical transient variation. The results have been plotted for both the different cases. As can be seen, the maximum error achieved between the numerical and analytical models does not exceed 1°C.

After running the numerical validation in Comsol, the analytical model built has been used to simulate the transient temperature variation for the different current profiles (shown in figures 4.5a,4.5b and 4.5c).

4.5.1 Results from the analytical model computation

Following figures show the temperature distribution for different cases of the load profile (shown in figure 4.5). The analytical simulation was run for two different cases-Case 1: $L = 1200[mm]$ and $TC = 0.2[W/mK]$ and Case 2: $L = 1500[mm]$ and $TC = 0.36[W/mK]$. Following figures show the variation in cable surface temperature and conductor surface temperature for the two different cases. (Case 1 and Case 2 respectively).

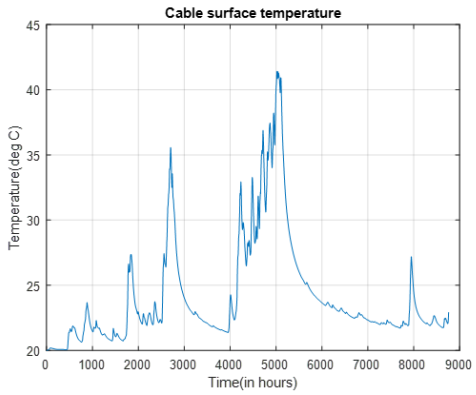

(a) Results for Case 1

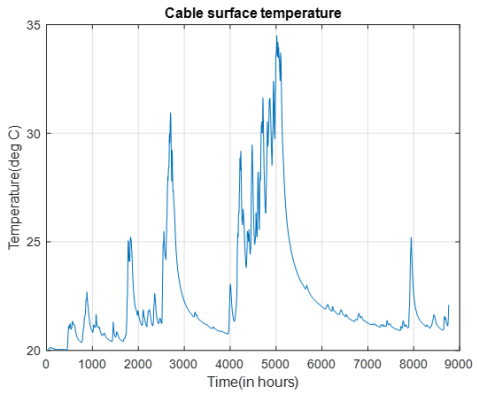

(b) Results for Case 2

Figure 4.10: Temperature result for Profile 1 (figure 4.5a)

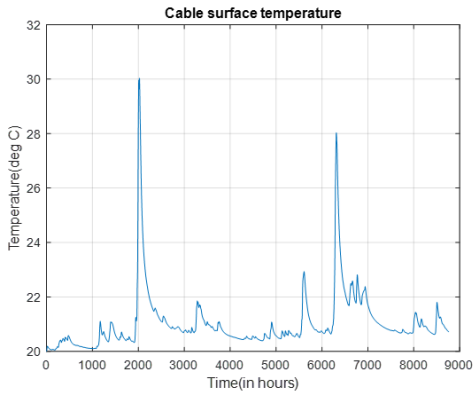

(a) Results for Case 1

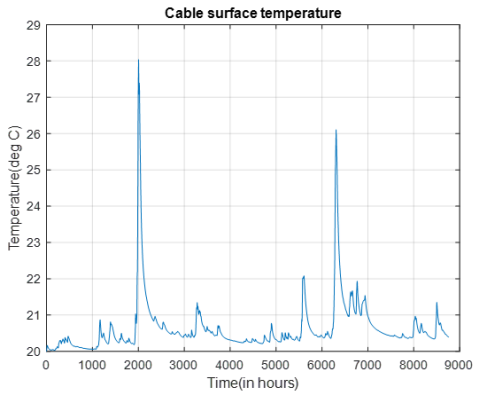

(b) Results for Case 2

Figure 4.11: Temperature result for Profile 2(figure 4.5b)

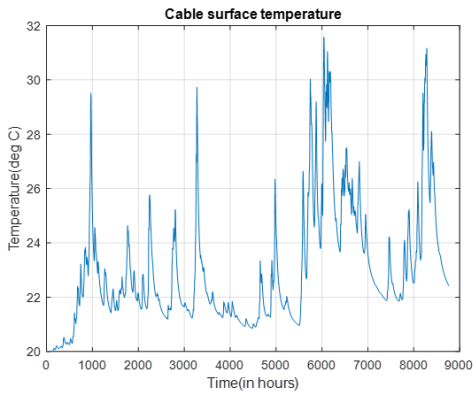

(a) Results for Case 1

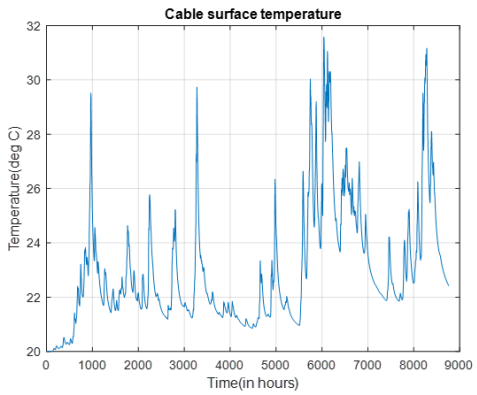

(b) Results for Case 2

Figure 4.12: Temperature result for Profile 3(figure 4.5c)

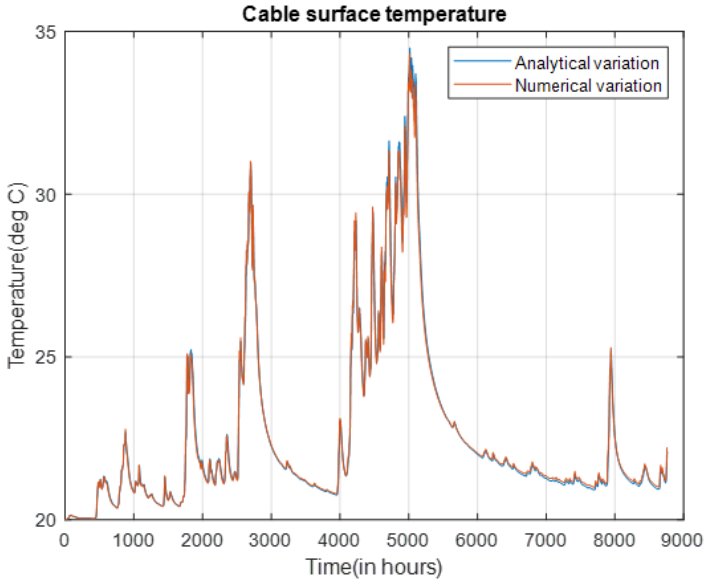

Figure 4.13: Comparision for Cable surface temperature(Case 2: $L = 1500[mm, TC = 0.36[W/mK)$

To get a numerical validation for the surface temperature, the analytical result was compared with a Comsol validation, for case 1, for the profile shown in 4.5a.- Not much variation was observed between the numerical and analytical variations. The figures 4.10, 4.11 and 4.12 show the final temperature of the cable cross section under different sections of the load profile with two different cases for burial depth and thermal conductivity. As the soil thermal conductivity increases with decreasing moisture content, it has been assumed that the moisture content decreases with increasing burial depth.

Following figures show the conductor surface temperature variation on the conductor surface.(Case 1 and Case 2) respectively

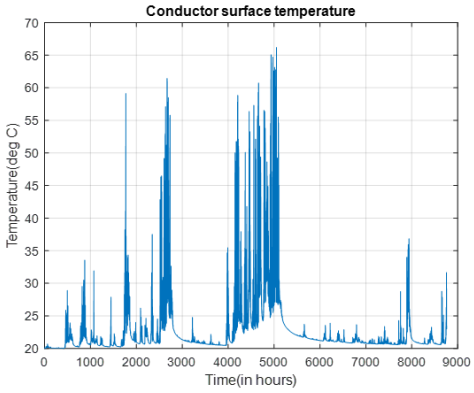

(a) Results for Case 1

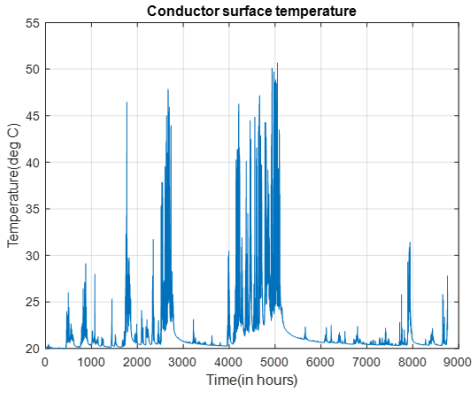

(b) Results for Case 2

Figure 4.14: Temperature result for Profile 1(figure 4.5a)

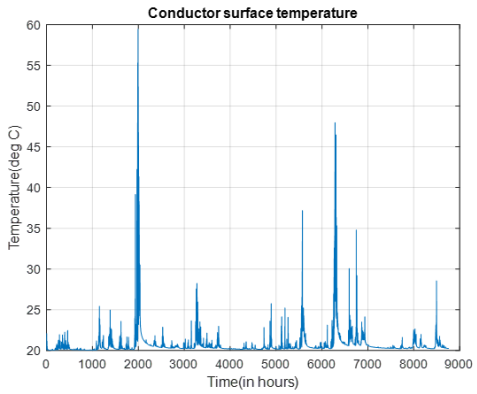

(a) Results for Case 1

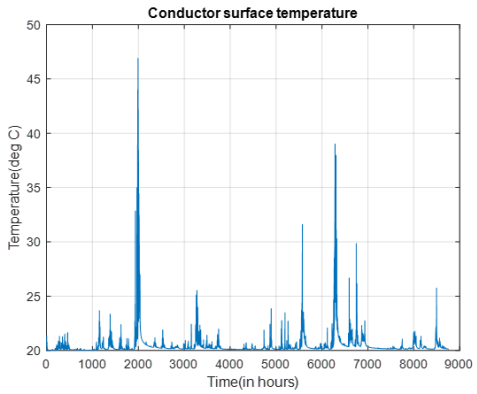

(b) Results for Case 2

Figure 4.15: Temperature result for Profile 2(figure 4.5b)

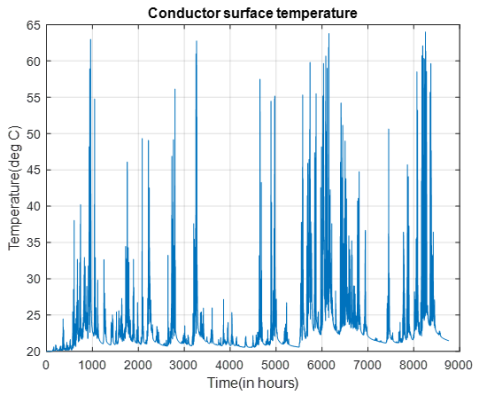

(a) Results for Case 1

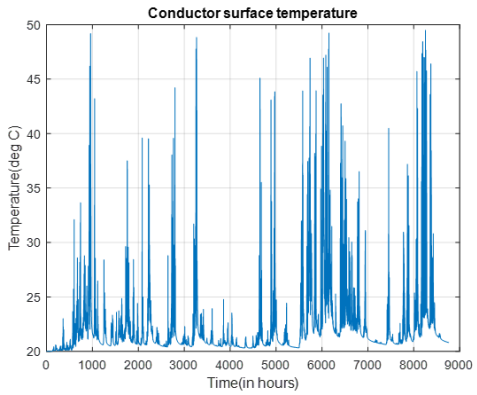

(b) Results for Case 2

Figure 4.16: Temperature result for Profile 3(figure 4.5c)

4.6 Conclusions from the results

This section discusses the results for both the numerical model and the analytical model. The numerical model was essentially used to cross-check the accuracy of the analytical model itself. As the result from the test case profile shown in figure 4.8 shows, the difference in cable surface temperature as modelled between the analytical and numerical results is less than 1°C.(figure 4.9. To cross-check the validity of the Analytical model with an actual load profile case, the simulation was performed for current profile shown in 4.5a, the result obtained has been shown in figure 4.13.

Further analytical results for the cable surface temperature under different cases have been shown in figure 4.10, figure 4.11 and figure 4.12. It is observed that the surface temperature magnitude at any time is lower for Case 2 when compared to Case 1. Further, The conductor surface temperature variation for different cases has been shown. It has been found from these figures(4.14, 4.15 and 4.16) that the conductor surface temperature does not cross the rated value of 90°C at any time. Therefore, it is concluded that the transient conductor temperature rating is lower than the steady state value. This result is similar to earlier research on this topic [9]). To compare the results between the static and dynamic thermal rating for different current vs. time profiles, the worst case scenario was taken. The results for burial depth as $1200[mm]$ and thermal conductivity as $0.2[W/mK]$ was

selected. The resultant difference between the static and the dynamic thermal rating of the conductor surface can be observed as follows-

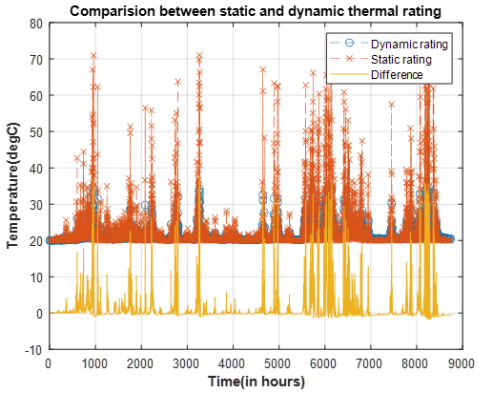

(a) Results for one conductor

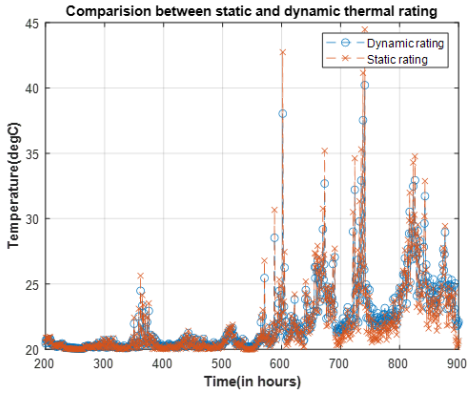

(b) Results for one cable conductor surface-enlarged portion of profile

Figure 4.17: Static and dynamic temperature result comparison for one profile(figure 4.5c-Case 1)

Figure 4.17 shows the comparison between static thermal rating and the dynamic thermal rating of the conductor surface for different current values. From figure 4.17b, it can be observed that for certain values of current,the static rating exceeds the dynamic thermal rating by more than 40°C.

From the results, it can be concluded that dynamic thermal rating is necessary to provide the maximum rating of the cable, as lesser values of temperature rise using dynamic rating have been observed. Results for the cable surface temperature will be further used to calculate the lifetime consumption of the insulation using the Arrhenious equation. These results can be found in chapter 6.

Chapter 5

Modelling of the HVDC cable system

The aim of this chapter is to explain the effects of changing parameters like current, soil thermal resistivity and transient voltages on the temperature variation and electric field variation of the 525kV extruded XLPE cable in different scenarios. As has been mentioned in section 2.3, research on the HVDC cables upto 275kV suggests variation in electrical conductivity of the insulation to be dependent on the changing electric field and changing temperature of the insulation. Similar effects have been found to be present for HVDC cables of higher voltage ratings. Here, an HVDC cable with extruded XLPE insulation upto 525kV has been chosen as this is the standard cable which is going to be installed in Netherlands offshore network.

The chapter starts with the theoretical description of the various relevant formulae for electric field and temperature variations on a cable. The second part covers the modelling aspect of the 525kV cable in use. The third part explains about the analytical model which has been built to integrate the effect of space charges along the cable cross-section. Finally, results from the numerical and analytical model for different current vs. time profiles have been compared here. The results from the actual load profile(refer figures 3.4a, 3.4b) have been shown.

5.1 Description of the model parameters used

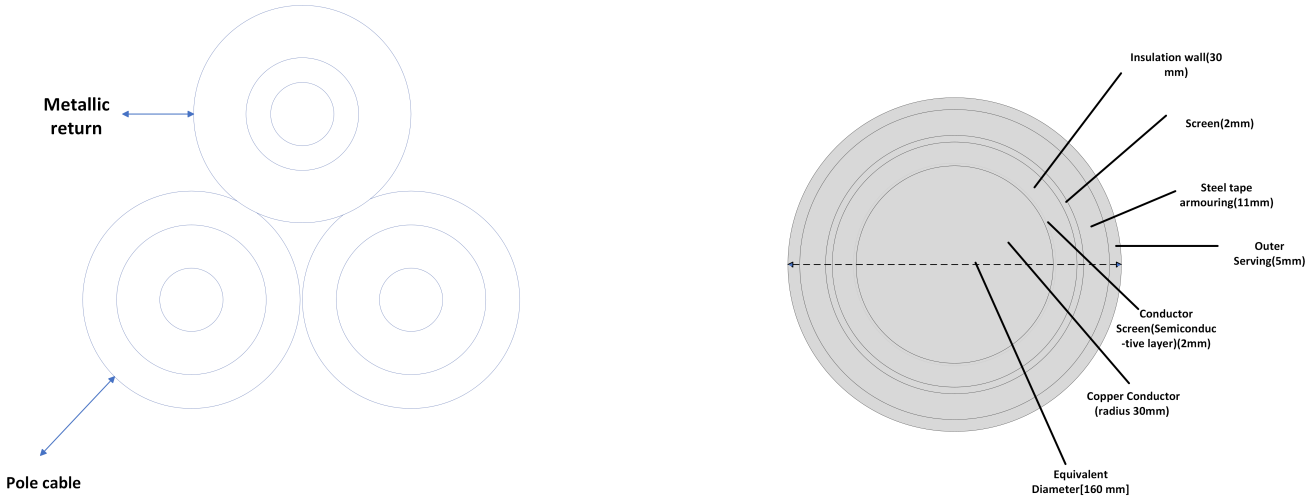

(a) Cable cross section([43]

(b) Cross-section used for modelling the cable([44])

Figure 5.1: Details of the XLPE cable used for modelling(monopolar configuration)

As shown in figure 5.1a, a bundled cable structure has been considered as the ideal choice for 525kV transmission. Therefore, this structure has been used as reference for simulating the analytical and numerical results. In addition to this, the seafloor and the cable do not heat up at a uniform rate. The characteristic thermal time constant of the seafloor is much larger than the cable itself. The seafloor temperature is assumed to be a constant here. The analytical model has to be refined to take the effect of space charges into account. Such a model variation is not possible for the numerical. However, the numerical analysis for the changing soil temperature in dynamic scenario cannot be modelled in the analytical framework due to lack of a suitable analytical equation to describe the soil dry out over time. For modelling purposes, the analytical model assumes the ambient temperature to remain constant.

The cable cross section shown in figure 5.1a shows two 525kV poles with one metallic return. As has been mentioned in chapter 3, the cable system can be operated in symmetrical monopole, rigid bipole or a bipole with dedicated metallic return (Figure 4.2). In any case, only one pole of the cable structure will be used. In order to model the worst case scenario, the symmetrical monopole configuration has been chosen for analysis. This implies continuous current flow through one pole throughout the year.

Following table describes the dimensions of the cable pole. [1]

[1]The dimension for the conductor is it's radius. For the rest of the parts, it is the thickness of the component.

S.no	Name	Dimensions	Material type
1	Conductor	30[mm]	Copper
2	Conductor screen	2[mm]	Copper (with semiconductive compound)
3	Insulation	30[mm]	Extruded XLPE
4	Screen	2[mm]	Copper
5	Armor	11[mm]	Galvanized steel
6	Serving	5[mm]	Polypropylene

Table 5.1: Description of the pole cross section components

The parameters of the cable model can be found in mentioned in Appendix B.

5.2 Theoretical description of the model formulae and parameters used

In order to model the HVDC cable, it is necessary to underline the relevant formulae for associating the changes in electrical parameters with temperature. Apart from the internal parameters, changes in the ambient soil thermal parameters and the laying conditions are also found to have a major effect on the accuracy of the model. As mentioned in [45], the effect of space charges and partial discharges in the cable cannot be accurately taken into picture with the help of an analytical model. Therefore, significant model calculations mentioned in [11] for the effects on current rating due to thermal effects have been used in the computation to approximate the results. The equations for calculating the effects of space charges have been taken from [45]. Following equations have been used to model the electrical conductivity of the different components numerically-

$$\sigma_{conductor} = \frac{1}{(1.72e-8*(1+(1.39e-3*(T_c-T_a))))} \tag{5.1}$$

$$\sigma_i = (8.15e6)*\exp\frac{(-0.78*1.6*1e-19)}{(1.38e-23*T)}*\frac{\sinh 1.4e-7*E}{E} \tag{5.2}$$

$$\sigma_{is} = \frac{-9}{670}T + \frac{877}{670} \tag{5.3}$$

Here σ_i is the electrical conductivity of the insulation. σ_{is} is the electrical conductivity of the sheath. It is important to highlight that the electrical conductivity for the sheath has been taken as a constant in the analytical model . The electrical conductivity of the external serving has been neglected as the cable is grounded at the screen.

The theoretical equations for modelling the electrical effects been used here are-

$$\begin{aligned} J &= \sigma * E \\ \nabla.J &= -\frac{\delta\rho}{\delta t} \\ \nabla.E &= \frac{\rho}{\varepsilon_o\varepsilon_r} \\ E &= -\nabla V \end{aligned} \tag{5.4}$$

To relate the effects of changes in electrical effects with the changes in real time temperature, the multiphysics environment of Comsol has been used here- Following equations couple both the effects-

$$\rho C_p \nabla T + \nabla.(-\lambda \nabla T) = Q_e \tag{5.5}$$

$$Q_e = J.E \tag{5.6}$$

The power transferred across the conductor is written as-

$$P_l = I_c^2 * R \tag{5.7}$$

Here, R is the dc resistance of the cable. It is defined as-

$$R = R_o * (1 + \alpha(\theta_c - \theta_a)) \tag{5.8}$$

This value of resistance is mentioned only for the heat produced in the conductor.
For modelling the thermal resistance of the cable in the analytical model, following equations have been used.

$$\begin{aligned} T_c &= \frac{\rho_T}{2\pi} \ln(\frac{D_o}{D_i}) \\ T_{cs} &= \frac{\rho_i}{2\pi} \ln(1 + \frac{2t_{ii}}{D_{cs}}) + \frac{\rho_{ls}}{2\pi} \ln(1 + \frac{2t_{ls}}{D_s}) \\ T_{sa} &= \frac{\rho_a}{2\pi} \ln(1 + \frac{2t_{sa}}{D_a}) + \frac{\rho_{se}}{2\pi} \ln(1 + \frac{2t_s}{D_{se}}) \\ T_{amb} &= \frac{\rho_s}{2\pi} \ln(\frac{4L}{D_e}) \end{aligned} \tag{5.9}$$

The details for the values of the thermal resistances along with the notations used can be found in Appendix B. For modelling the steady state value of the cable ampacity we use this numerical rule -

$$I = (\frac{\Delta\theta}{R * (T_c + T_{cs} + T_{sa} + T_{amb})})^{0.5} \tag{5.10}$$

However, these are the equations for the steady state temperature rise of the cable system. To check the transient variation, an analytical model has been developed which will be explained in the coming section.

5.3 Description of the analytical model

The analytical model has been built in Matlab. To build the steady state model, the equations mentioned in section 5.2 have been used with the data given in the table 5.1. Building the transient model of the cable requires the following these steps.

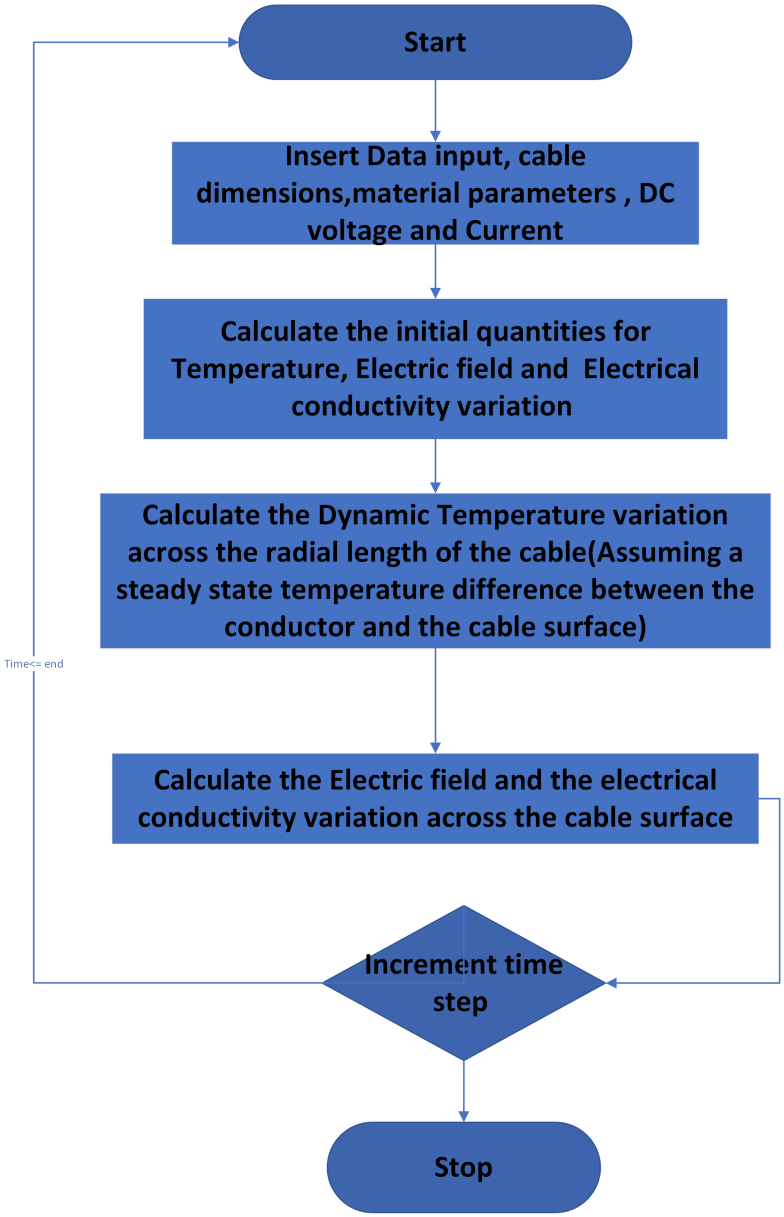

Figure 5.2: Analytical model for HVDC cable

As shown in the flowchart in figure 5.2, all the values are calculated for a single time step. For a continuously varying load profile this implies that the current values will be updated for each time step according to the load profile. To model the entire effect, the space charges are assumed to accumulate simultaneously as time passes by. The different equations solved in iteration are mentioned here. The values for different parameters used in the equations can be found in Appendix C.

For modelling the temperature distribution, the code used for calculating the cable surface temperature in case of changing current profile has been implemented to calculate the ambient soil temperature. After this calculation,

following equations are used to get the temperature gradient

$$v_c = \frac{(T_{cs} + (T_{sa} + T_{amb})\eta)I^2 + \theta_{amb}}{1 - (T_{cs} + (T_{sa} + T_{amb})\zeta)} \tag{5.11}$$

$$\Delta T_d = \frac{1}{2 * \pi * TC} * (\frac{\rho_{cu}}{\pi * (r_c^2)}) * (1 + \alpha_{cu20} * (v_c - \theta_{amb})) * I^2 * \ln\frac{r}{r_i} \tag{5.12}$$

$$T = v_c - \Delta T_d \tag{5.13}$$

$$\eta = (1 - \alpha_{cu20} * 20) * R_{20} \tag{5.14}$$

$$\zeta = R_{20} * \alpha_{cu20} \tag{5.15}$$

Here, r is the value of radial thickness of the insulation measured from the conductor. η and ζ are constants which are used to calculate the conductor surface temperature. Where, v_c is the value of conductor temperature for different current values obtained and stored in form of an array of 8760 values. ΔT_d is the value of temperature gradient calculated for different conductor temperature values. r_i is the value of radius upto the conductor screen(32[mm]). TC is the value of soil thermal conductivity calculated for different cases(1&2). T is the temperature variable storing the temperature gradient variation for different insulation thicknesses and different current values. both ΔT_d and T are mapped as (301x8761) variables, where the row number corresponds to the radial thickness of the insulation divided into 300 points with each point at 0.1[mm] of difference. The column number corresponds to the length of the duration of the current profile.

To take the effect of insulation electric field variation with the temperature and the presence of space charges, the formulae for electric field are modified([46]). Since the electric field shows a capacitive variation initially and a resistive variation afterwards, the Eoll's approximation has been used to account for the resistive field after a certain time duration([20]). After calculating the electric field, the electrical conductivity calculation is done afterwards which is then used to re-calculate the space charge distribution at a particular radial length for the next time interval. The required formulae are mentioned as follows-

$$E(r) = \frac{1}{r} * \frac{U_0}{\ln\frac{r_b}{r_a}} + \frac{1}{r} * C_a + \int_{r_a}^{r_b} \frac{\rho_a r}{\varepsilon_a} dr .. r_a < r < r_b \tag{5.16}$$

Space charges can accumulate within several locations inside the insulation ([20],[46])-

- Near the electrodes - This is usually the test case. But in this case, the electrodes are usually defined as the conductor material and the lead sheath. This form of space charge distribution can only be measured experimentally.
- Inside the insulation bulk-The presence of space charge within the insulation bulk has been modelled here. In practice, this space charge distribution is dependent on the amount of charge initially present in the insulation.
- At the dielectric interfaces - Usually, they are present in form of interfacial charges. This has not been modelled here as an experimental verification is needed to approximate this distribution.
- At the electrode insulation interface - When a DC voltage is applied at the insulation, charges are present at both electrode-insulation interfaces. These have also been left out here.

After about 3600[s], the numerical simulation shows the field distribution as resistive distribution. Therefore, after 3600[s] the first term of the electric field distribution is approximated analytically as-

$$E = \frac{I_d \rho_0}{2\pi r_0} * (E_m^B) * ((\frac{r}{r_0})^{A-1}) * \exp -((a * T(r_0)) + B) \tag{5.17}$$

$$E_m = \frac{U_0}{r_0 - r_i} \tag{5.18}$$

$$B = b * E_m \tag{5.19}$$

$$A = \frac{\Delta T_d * a}{\ln\frac{r_0}{r_i}} \tag{5.20}$$

Here, U_0 is the potential difference across the conductor and sheath layer. I_d is the current across the conductor. r_0, r_i are the outer and inner radii of the layer. a, b are constants for the XLPE insulation respectively. ρ_0, T are the electrical resistivity and the thermal distribution parameters respectively.

C_a constant is defined as follows ([46])-

$$C_a = \frac{-(\int_{r_a}^{r_b} \frac{1}{r}(\int_{r_a}^{r_b} \frac{\rho_a r}{\varepsilon} dr)dr)}{\ln \frac{r_b}{r_a}} \tag{5.21}$$

Therefore, the total electric field variation becomes $E_t = E_r + E_\rho$. Where $E_\rho)$ is the electric field due to space charge distribution in the insulation bulk and is defined as-

$$E_\rho = \frac{1}{r}(C_a + (\int_{r_a}^{r_b} \frac{\rho_a r}{\varepsilon} dr)) \tag{5.22}$$

After calculating the electric field and the temperature profile along the radial length of the cable, following equations have been used to calculate the electrical conductivity and the space charge distribution.

$$\sigma_i = (8.15e6) * \exp \frac{(-0.78 * 1.6 * 1e-19)}{(1.38e-23 * T)} * \frac{\sinh 1.4e-7 * E}{E} \tag{5.23}$$

$$\rho = \frac{-\varepsilon_0 \varepsilon_r}{\sigma} \frac{\partial \rho}{\partial t} + J.\nabla(\frac{\varepsilon_0 \varepsilon_r}{\sigma}) \tag{5.24}$$

5.4 Description of the numerical model and comparision of results from analytical and numerical model

5.4.1 Numerical model results

The numerical model has been built in Comsol for the monopolar cable configuration with the sheath grounded. The transient simulation has been simulated for a time long enough to allow the temperature difference ΔT_d to reach a specific value and then the results are compared to the analytical model results.

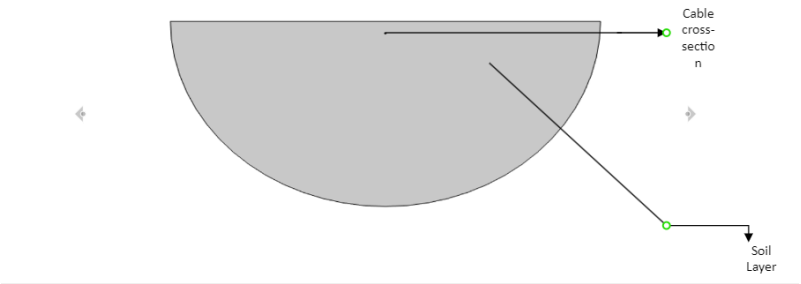

(a) HVDC cable model

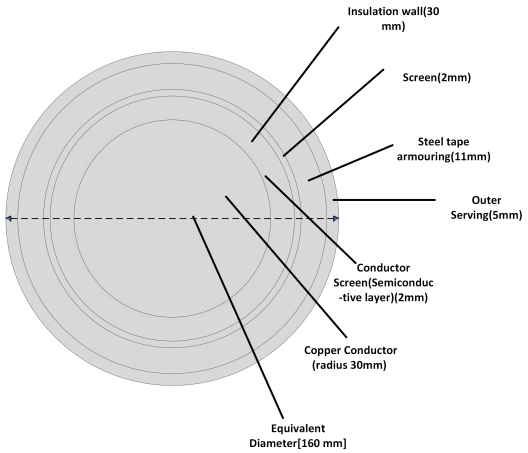

(b) HVDC cable cross section

Figure 5.3: Numerical implementation of the HVDC cable setup(single pole)

The model uses the geometry shown in figure 5.1 and the data from table 5.1 as input. The electrical conductivity formula from equation 5.1 are used as input for the electrical conductivity of the conductor, insulation, insulation screen and serving material. The heat transfer module and the electrical potential module are used to study the behaviour of the cross section.The heat transfer module is used to solve the heat equation using the conductor as the source of heat. The electric potential module is used to calculate the effect of applied potential across the insulation. The outer boundary of the conductor has been used as a heat source. The outer boundary of the insulation screen has been grounded. The FEM simulation is solved with a time dependent solver wit a linear setting for the two cases, Case 1-$L = 1200[mm]$, $TC = 0.2[W/mK]$ and Case 2: $L = 1500[mm]$ and $TC = 0.36[W/mK]$.Following figures show the important numerical figures for the temperature and electric field distribution of the load profiles.

The analytical and numerical model were tested for both the different cases with a pulse current waveform of magnitude 2100[A] as shown here.

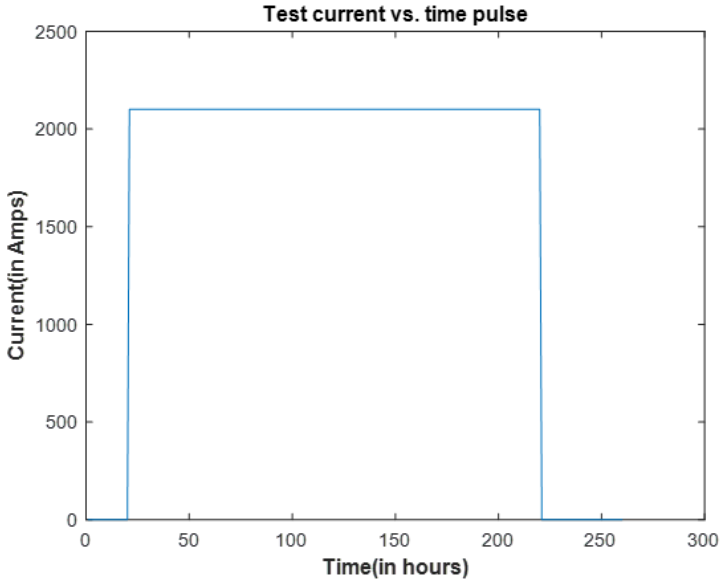

Figure 5.4: Test Current pulse

The analytical and numerical results for Case 1 was found to be as follows-

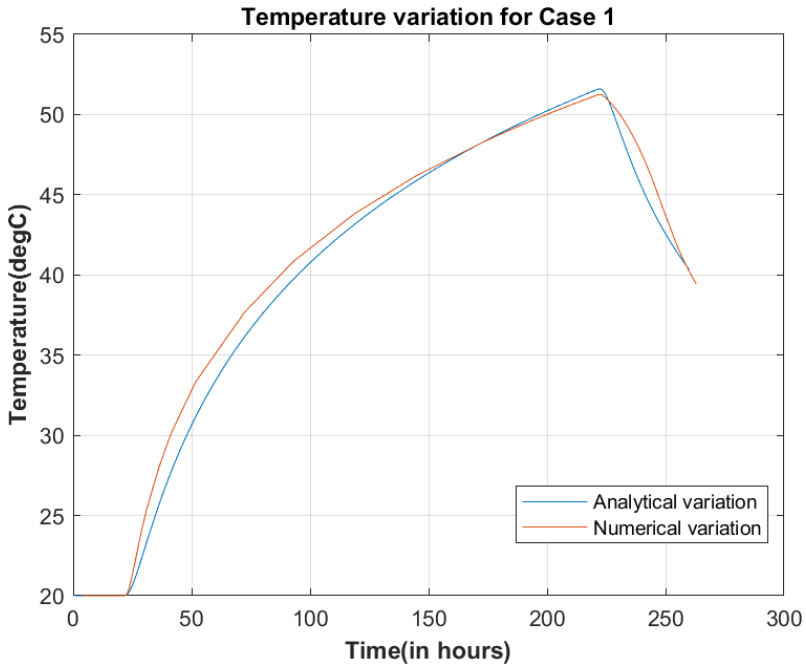

Figure 5.5: Surface temperature result for Case 1: $L = 1200[mm], TC = 0.2[W/mK]$

The electric field results for the two cases obtained are shown as follows-

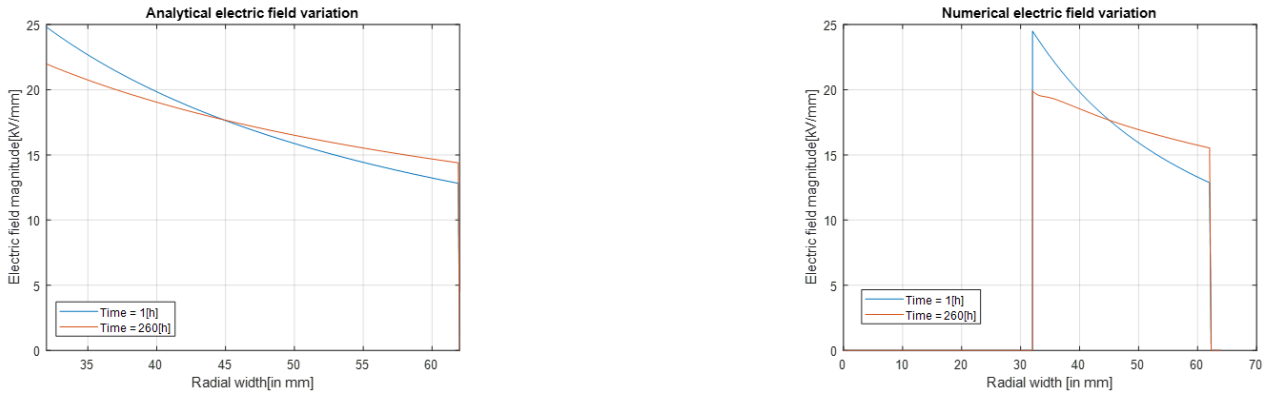

Figure 5.6: Electric field magnitude results for Case 1

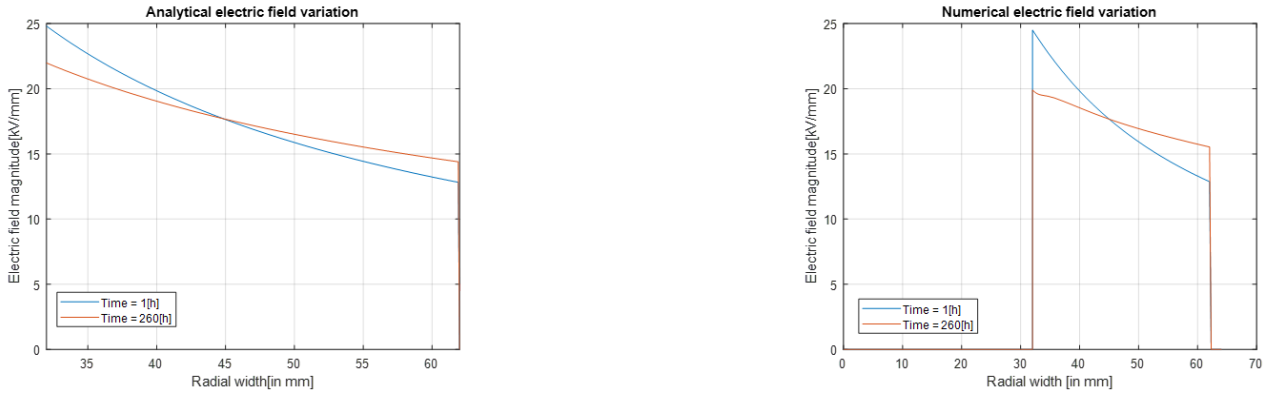

Figure 5.7: Electric field magnitude results for Case 2

With this result, the following cable analytical model has been used to compute further results for the different variations of the load profile.

5.4.2 Analytical model results

For the analytical model simulation, the resultant load profiles are simulated as Matlab variables to get the resultant electric field variations. The code for this can be found in Appendix 7.3. This sub-section shows the relevant results for different current vs. time profiles shown in chapter 3.

Results for the load profiles

In this subsection the results for the temperature and the electric field variation are explained for both the cases: Case 1-$L = 1200[mm]$ and $TC = 0.2[W/mK]$; Case 2- $L = 1500[mm]$ and $TC = 0.36[W/mK]$. The results for the Electric field and the temperature are stored in form of 2-dimensional matrices. One dimension shows the radial distribution of the insulation thickness. It is distributed equally in 300 annular regions. The other dimension represents the hourly change in the variable with change in current magnitude. The final accumulated variables have a total size of 301x8760 values for both the cases 1 and 2.

The results shown here show the surface plot and the hourly distribution across the radial length of the insulation thickness respectively. The distribution of the temperature and electric field variables has been chosen for some specific hours for visualization.
For the profile in figure 3.4a

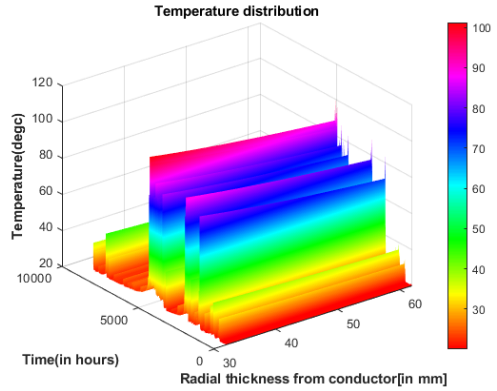

(a) Temperature surface plot

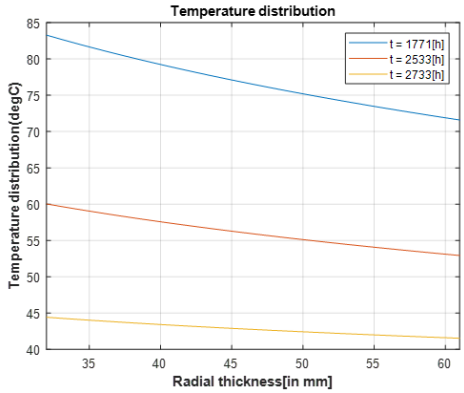

(b) Temperature hourly plot

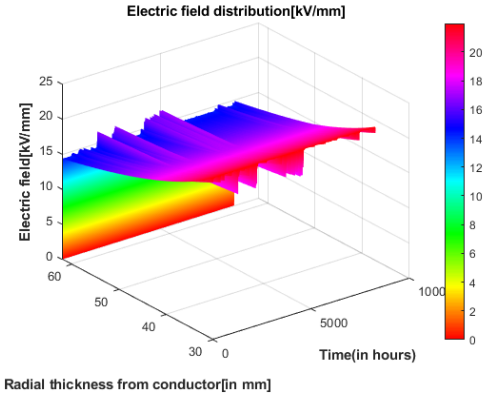

(c) Electric field surface plot

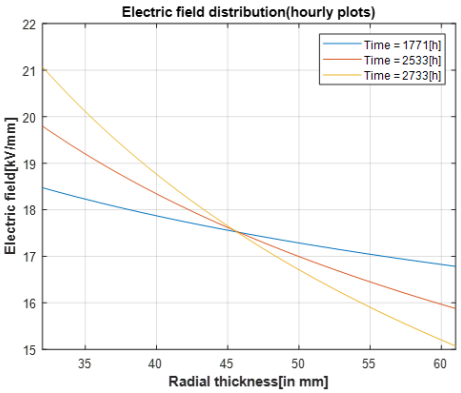

(d) Electric field hourly plot

Figure 5.8: Results for the current profile in figure 3.4a(Case 1)

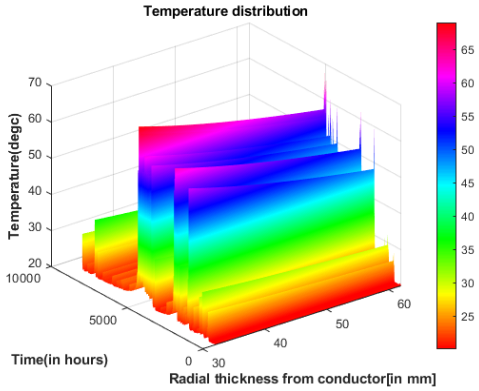

(a) Temperature surface plot

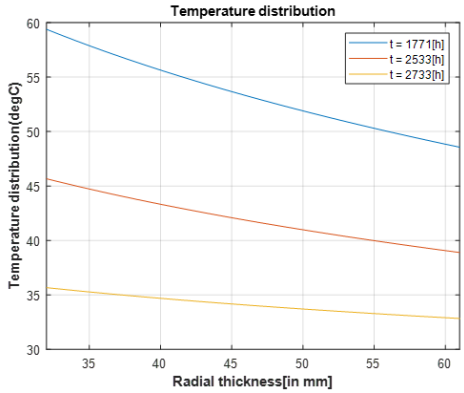

(b) Temperature hourly plot

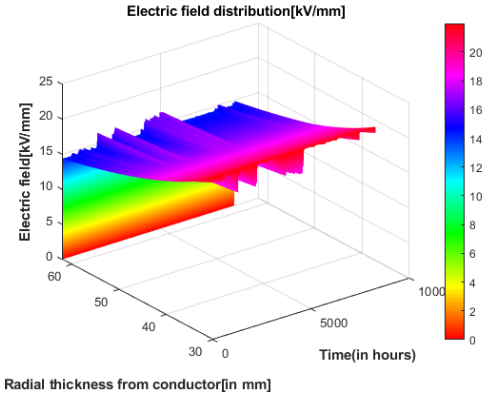

(c) Electric field surface plot

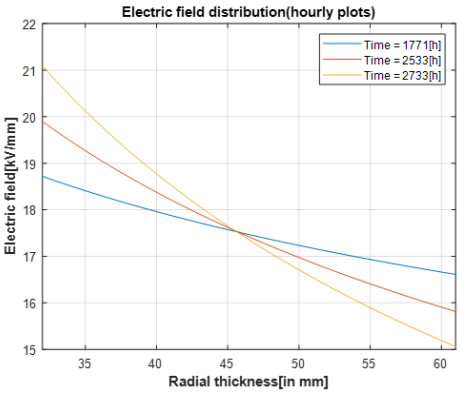

(d) Electric field hourly plot

Figure 5.9: Results for the current profile in figure 3.4a(Case 2)

The results for the profile shown in figure 3.4b are as follows.

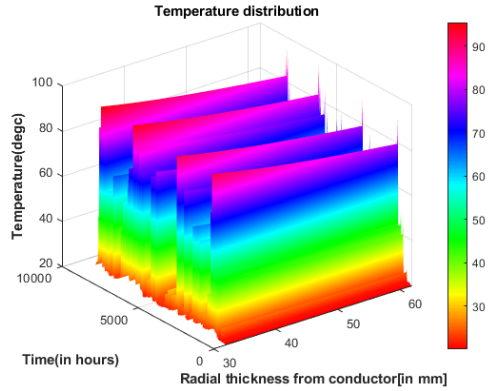

(a) Temperature surface plot

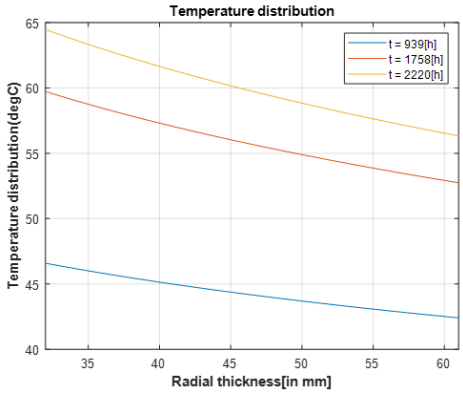

(b) Temperature hourly plot

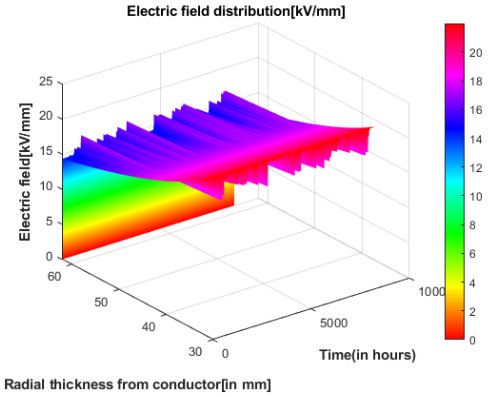

(c) Electric field surface plot

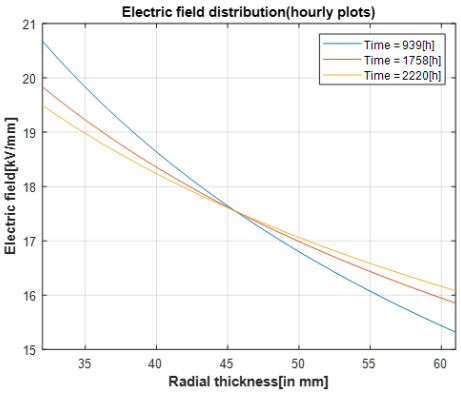

(d) Electric field hourly plot

Figure 5.10: Results for the current profile in figure 3.4b(Case 1)

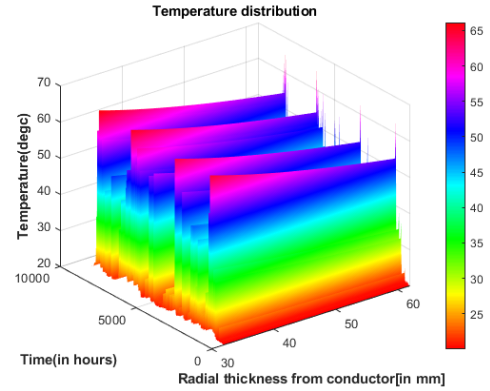

(a) Temperature surface plot

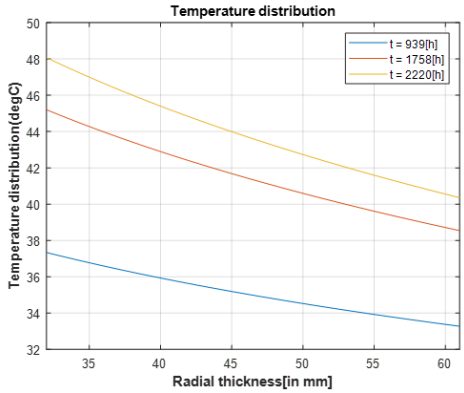

(b) Temperature hourly plot

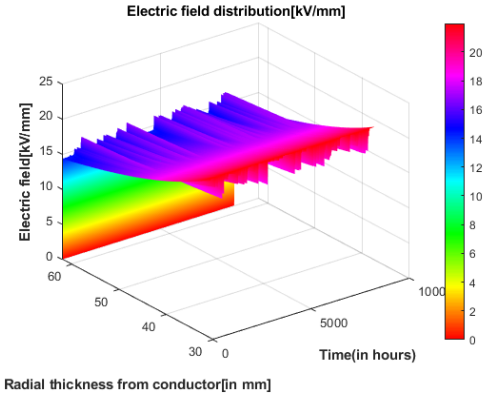

(c) Electric field surface plot

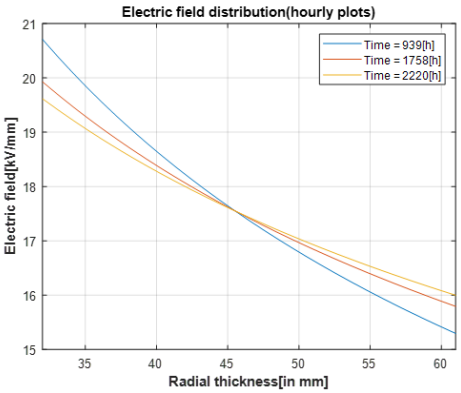

(d) Electric field hourly plot

Figure 5.11: Results for the current profile in figure 3.4b(Case 2)

The results for the profile shown in figure 3.4c are as follows.

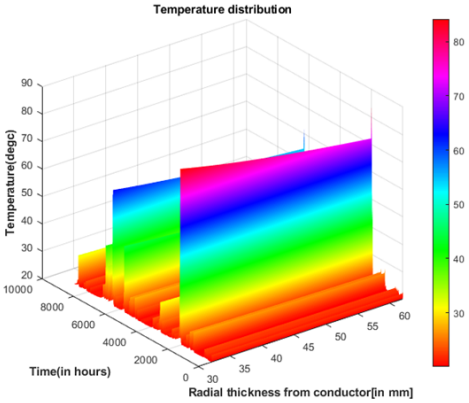

(a) Temperature surface plot

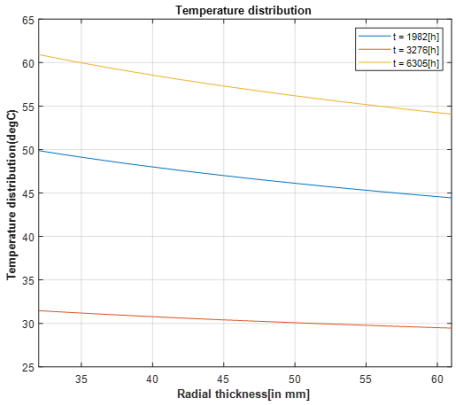

(b) Temperature hourly plot

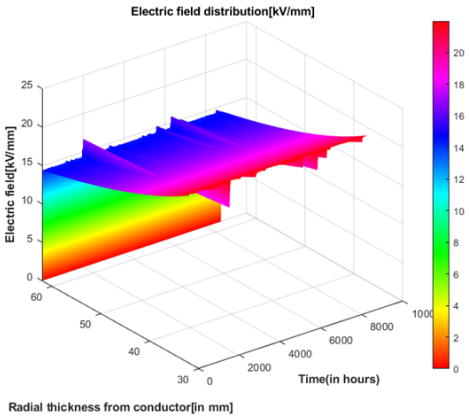

(c) Electric field surface plot

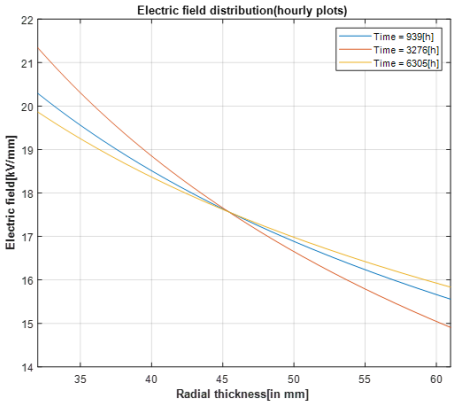

(d) Electric field hourly plot

Figure 5.12: Results for the current profile in figure 3.4c(Case 1)

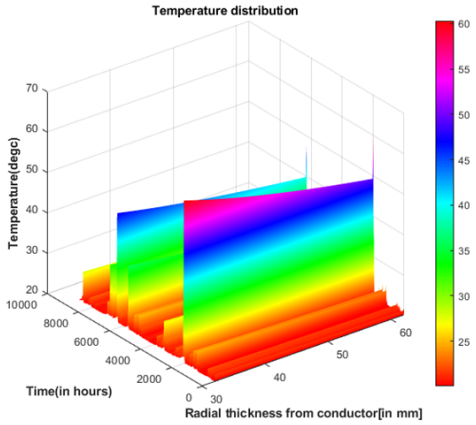

(a) Temperature surface plot

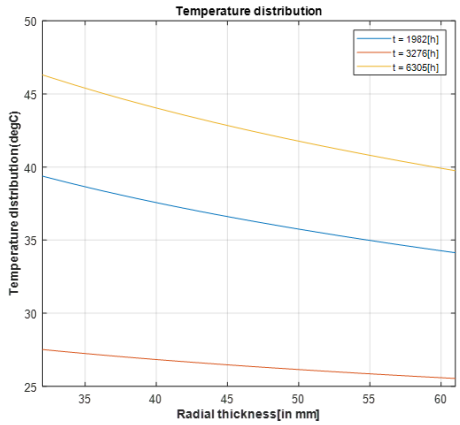

(b) Temperature hourly plot

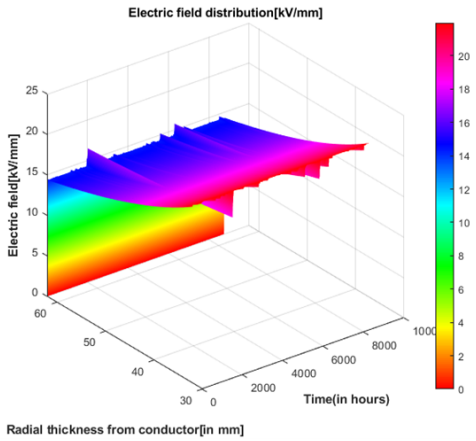

(c) Electric field surface plot

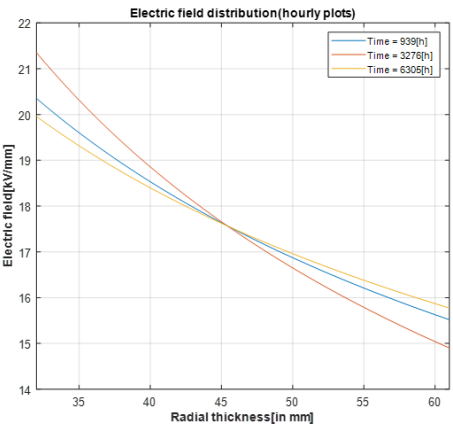

(d) Electric field hourly plot

Figure 5.13: Results for the current profile in figure 3.4c(Case 2)

To explicate the difference between the temperature results and the electric field results for the two cases, an hourly difference plot has been plotted. The plotted results show the variation of difference in temperature and electric field magnitude respectively for specific hours of the simulation. The difference has been calculated as : variable value corresponding to Case 2($L = 1500[mm] and TC = 0.36[W/mK]$) - value corresponding to Case 1($L = 1200[mm]$ and $TC = 0.2[W/mK]$).

The results for the profile shown in figure 3.4a are as follows.

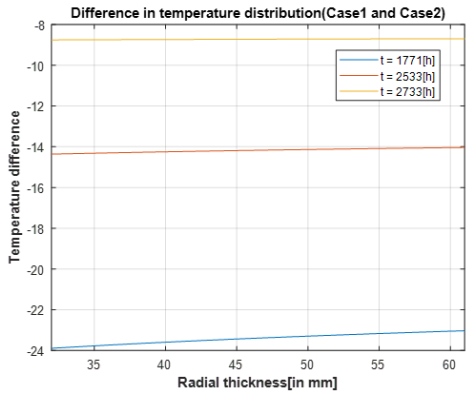

(a) Temperature difference

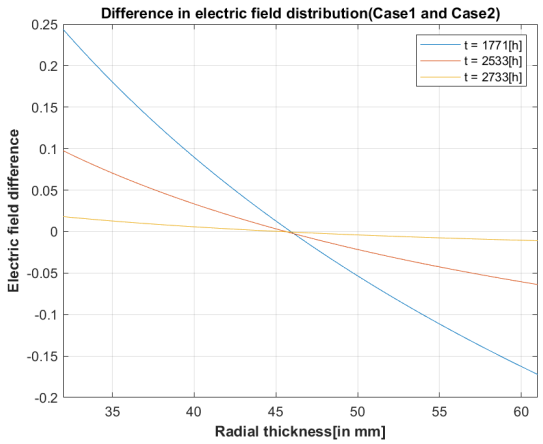

(b) Difference in electric field magnitude

Figure 5.14: Results for the current profile in figure 3.4a

The results for the profile shown in figure 3.4b are as follows.

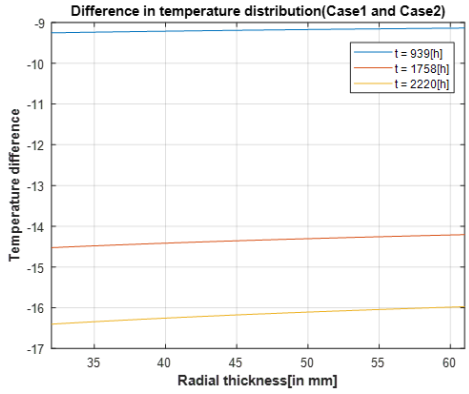

(a) Temperature difference

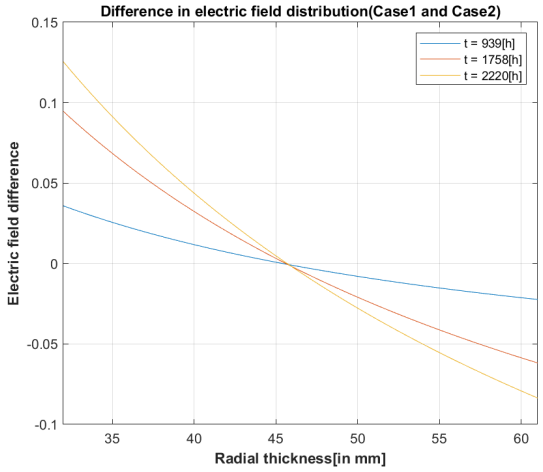

(b) Difference in electric field magnitude

Figure 5.15: Results for the current profile in figure 3.4b

The results for the profile shown in figure 3.4c are as follows.

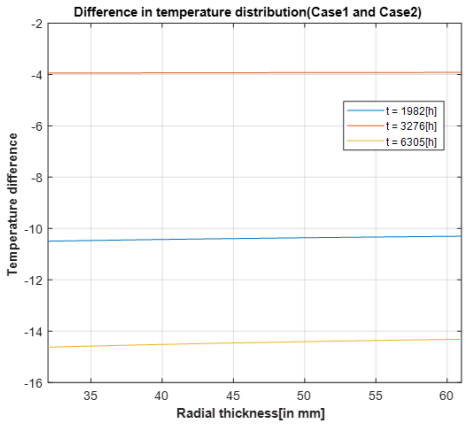

(a) Temperature difference

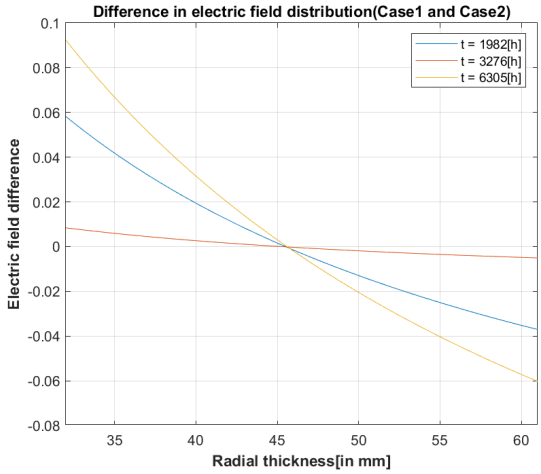

(b) Difference in electric field magnitude

Figure 5.16: Results for the current profile in figure 3.4c

5.5 Inferences from the test profiles

This section provides the general inferences from the numerical and analytical results for the different current vs. time profiles which have been used for simulations.

5.5.1 Inferences from the Test current vs. time profile

Both the numerical model and the analytical model were tested with a current pulse of value 2100[A]. The results are mentioned in figure 5.5 and **??**, corresponding to case 1 and case 2. Both of these results indicate a maximum error not more than 1.5°C between the results. Similarly the results for the electric field calculation have been shown for both the cases here. It is observed that the electric field variation for both the analytical and the numerical variation (shown in figure 5.6 and 5.7) shows similar variation for the selected hours. Since, the electric field variation remains the same for both the cases, it is concluded that change in burial depth and soil thermal resistivity results in change in temperature profile for the cable. The analytical model is then used to simulate further results.

5.5.2 Inferences from the current vs. time profiles

The results for the temperature variation have been shown here in form of a surface plot and hourly variations have been plotted for a few hours. The surface plot shows the temperature variation across the cable insulation for all the hours. With changing current per hour, it can be observed that the temperature has different magnitudes and therefore different thermal profiles are observed. To get a more accurate picture, temperature distribution for hourly plots have been plotted. The results from the hourly plots for case 1 and case 2 show that the temperature distribution across the insulation is dependent on the losses in the conductor which is indirectly dependent on the current through the conductor.When the cases 1 and 2 are compared it is observed that a burial depth of 1200[mm] results in a higher temperature across the insulation as compared to the case with a burial depth of 1500[mm]. Such a difference can be observed from figures 5.8b and 5.9b. Similar results can be observed for other current profile variations (shown in figures 3.4b and 3.4c).

The static thermal rating at each current value was compared to the dynamic current rating of the cable. To check the worst case comparison, temperature data for a burial depth of 1200$[mm]$ and thermal conductivity of 0.2$[W/mK]$ has been used for getting the results.

Following figure describes the comparision between static and dynamic thermal rating.

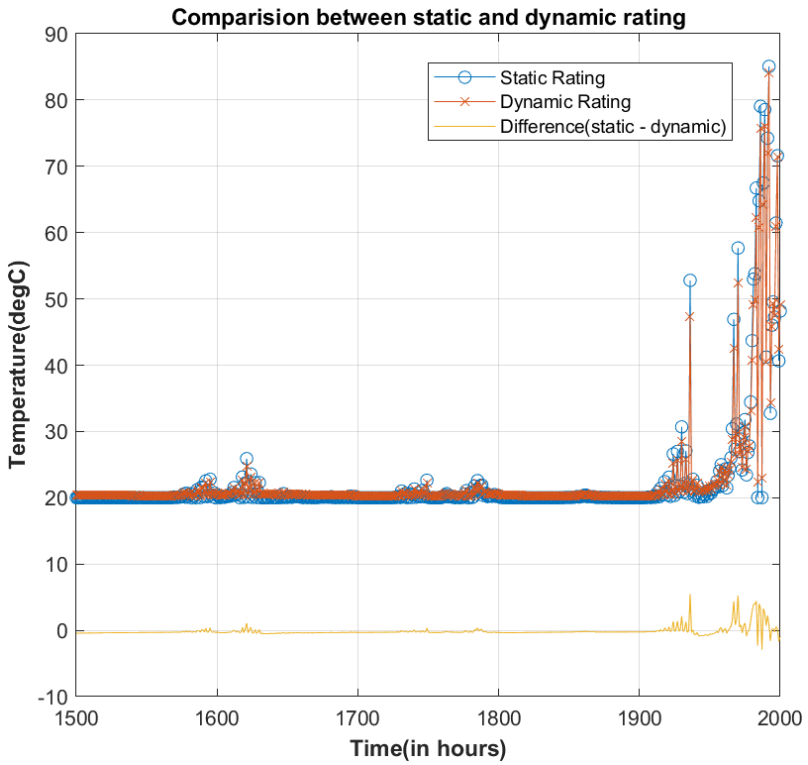

Figure 5.17: Temperature profile comparision-for profile in figure 3.4b

When the electric field variations were observed, the maximum electric field magnitude variation observed was from 21.96$[kV/mm]$ to 15.3$[kV/mm]$.With increasing time, the electric field magnitude decreases in the portion close to the conductor screen and increases from 15.3$[kV/mm]$ to higher values. This is also observed when the electric field magnitude difference plot for different current profiles were compared(Figures 5.14b, 5.15b and 5.16b).

Further results on ageing of the cable insulation are mentioned in chapter 6.

Chapter 6

Lifetime Consumption of HVAC and HVDC cables

This chapter starts with the temperature profile results from the chapters 4 and 5. The continuous current profile results are used to numerically calculate the time to failure for the particular cable systems used analytically. Thermal effect is considered to be the most relevant factor for cable ageing as compared to chemical and physical effects.([28]). Life tests are important while estimating the lifetime consumption of the given cable under different stresses. Because insulating material is bound to deteriorate with time, the thermal history of the cable becomes important when considering an estimate.([28],[29]).This chapter provides an analytical estimate to the lifetime consumption of cables under different conditions(varying burial depth and soil thermal resistivity). However, it is important to note that such results need to be backed up with experimental validation before any physical implementation of the cable system is done. The first section provides the relevant theoretical understanding of the cable system and the required formulae to compute the lifetime degradation of the cable. The second section provides the relevant results for different analytical cases of current vs. time profile.

6.1 Theoretical aspect of Lifetime degradation

This section provides a short description of the relevant formulae which are used to calculate the lifetime of the cable system. Different approaches are used to get the lifetime data for the different cable setups-HVAC and HVDC setups.

For the HVAC setup, the simulated temperature profile $\theta(t)$ has been used to calculate the lifetime usage over different time intervals across the load profile. Arrhenious equation (originally proposed by Dakin-[47]), is a well known process to model the thermally induced chemical degradation of the cable insulation material. This data is then further used to approximately calculate the ageing rates of the cable insulation.([26]). The equation is given as-

$$R = R' \exp \frac{-W}{k_B * \theta} \tag{6.1}$$

where-

- R is the ageing rate of the chemical reaction.
- R' is a constant
- W is the activation energy (in eV).

- k_B is the Boltzmann constant ($0.8617*10^{-4}[eV/K]$)
- θ is the absolute temperature.

It is assumed that the rate of reaction is a constant and is independent of the number of molecules at a given time. It is furthermore assumed that the breakdown process is a first order reaction. Following these assumptions, it can be shown that the following holds true-

$$\ln\frac{t_o}{t_a} = \frac{W}{k}(\frac{1}{\theta_o} - \frac{1}{\theta_a}) \tag{6.2}$$

Here, t_o is the time at the temperature θ_o, which results in the same number of reactions as the time t_a at the temperature θ_a. Hence, the lifetime is expressed by the equation-

$$L(\theta) = L_o \exp(\frac{-W}{k_B}(\frac{1}{\theta_o} - \frac{1}{\theta})) \tag{6.3}$$

The average ageing rate is then determined as the reciprocal lifetime, i.e.

$$R_a(\theta) = \frac{1}{L_a(\theta)} \tag{6.4}$$

$$= \frac{1}{L_o}\exp(\frac{W}{k_B}(\frac{1}{\theta_o} - \frac{1}{\theta})) \tag{6.5}$$

Under the assumption, that ageing rate is independent of the thermal history, the thermal lifetime consumption for a given temperature profile from time t_1 to t_2 is determined as-

$$\Delta L_t = \int_{t=t_1}^{t_2} R_a(\theta)dt \tag{6.6}$$

This equation will be used to approximate the thermal lifetime consumption for the temperature profiles obtained in chapters 4 and 5.

For the HVDC cable cross section, the formula for lifetime approximation will depend on both the electric field and temperature variation. The exact formula used here has been described as [20], [48]-

$$L(E,T) = L_D(\frac{E}{E_D})^{-(n_D - b_{ET}T")}(\frac{E_D}{E_o})^{b_{ET}T"}\exp -BT" \tag{6.7}$$

$$T" = \frac{1}{T_D} - \frac{1}{T} \tag{6.8}$$

The parameters and their descriptions are mentioned in a tabular form as shown-

Serial number	Name	Description
1	L	Lifetime consumption of the cable[in years]
2	L_D	Design life of the cable - 40[y]
3	E_D	Design electric stress - 21.96[kV/mm]]
4	n_D	Design VEC -10 [1]
5	T_D	Design thermal stress-363.15[K]

Table 6.1: Description of parameters used

b_{ET}, B are constants. b_{ET} is the synergism coefficient whose value is taken to be 0.5. The value of B is dependent on the material properties of the XLPE insulation tested under an applied DC voltage. Based on the test results as mentioned by Diban([21]), this value is taken to be $12430[K^{-1}]$. This formula is based on the assumption that the probability of failure of the cable insulation is equal to the design probability of failure of the insulation. This formula does not take the deterioration of the cable insulation due to the effect of space charges into account.

6.2 Lifetime consumption analytical results

The results for lifetime consumption modelling of both the cable systems have been mentioned in this section. In the end, the lifetime functions are calculated for the different variations of soil thermal resistivity and burial depth parameters.

The lifetime consumption for both HVAC and HVDC cable cross sections are calculated with the help of the analytical formulae mentioned in equation 6.5 - 6.6 for HVAC cable and equation 6.7 - 6.8 for the HVDC cable cross-section respectively. The results are mentioned in order in this section.

6.2.1 Results for HVAC temperature vs. time profiles

Following the analysis shown for HVAC cables, data for cable surface temperature for the different cases of the load profile (refer figure 4.14, 4.15 and 4.16) were collected and used in the calculation of ageing rate(equation 6.6). The final percentage lifetime ageing has been calculated using equation 6.7 and mentioned in form of a table.

Following results for the lifetime consumption of the cable were achieved-

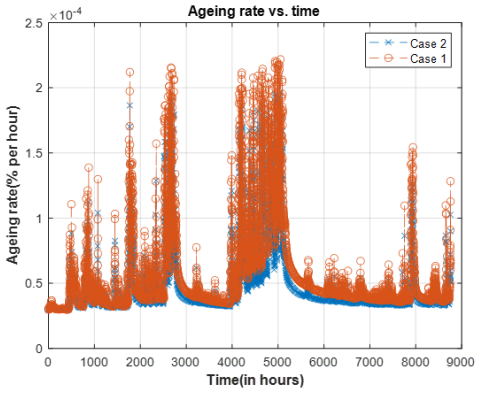

(a) Ageing rate vs. time interval for figure 4.5a

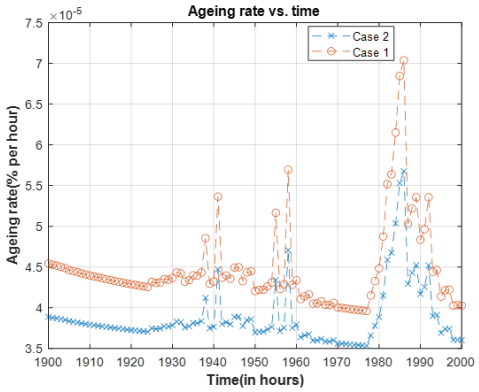

(b) Ageing rate vs. time interval (enlarged curve) for figure 4.5a

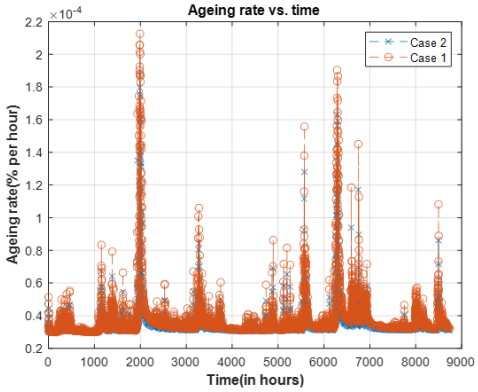

(c) Ageing rate vs. time interval for figure 4.5b

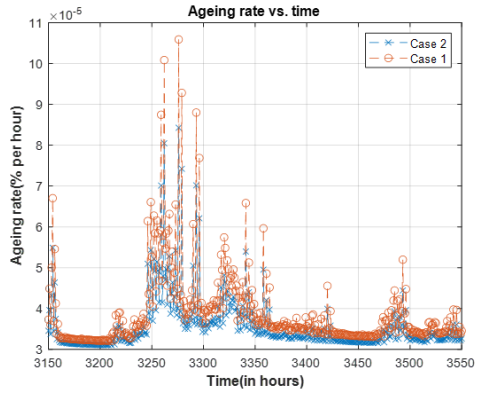

(d) Ageing rate vs. time interval (enlarged curve) for figure 4.5b

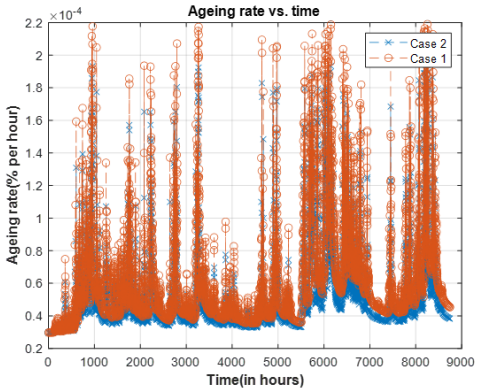

(e) Ageing rate vs. time interval for figure 4.5c

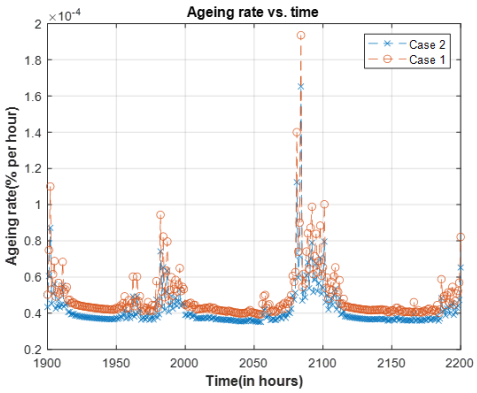

(f) Ageing rate vs. time interval (enlarged curve) for figure 4.5c

Figure 6.1: Lifetime consumption plots for changing burial depth and soil thermal conductivity

Figure 6.1 shows the ageing rates calculated for different temperature values resulting from current vs. time values for one year. Case 1 refers to a cable burial depth of 1200$[mm]$ and soil thermal conductivity 0.2$[W/mK]$. Case 2 refers to a burial depth of 1500$[mm]$ and soil thermal conductivity of 0.36$[W/mK]$. As can be seen, the normal ageing rates(% per hour) are in the order of 10^{-4}%. This suggests that continuous variation of temperature

for the cable insulation does not result in a very high ageing rate. The table following this result shows the cumulative percentage lifetime consumption for a duration of one year-

Profile	$L = 1500[mm], TC = 0.36[W/mK]$	$L = 1200[mm], TC = 0.2[W/mK]$
Profile 1 (figure 4.5a)	0.5145[%]	0.5142[%]
Profile-2 (figure 4.5b)	0.3005[%]	0.3214[%]
Profile-3 (figure 4.5c)	0.4439[%]	0.5295[%]

Table 6.2: Percentage lifetime consumption calculated under Dynamic loading

6.2.2 Results for HVDC cable temperature vs. time profiles

This sub-section summarises the results for the HVDC cable temperature vs. time profiles which have been calculated with the help of the formula given in equation 6.7. The results for the time to failure data were calculated for two cases of burial depth and soil thermal conductivity.(L= 1500[mm],TC = 0.36[W/mK]; L = 1200[mm],TC = 0.2[W/mK]). The data for the final lifetime consumption was obtained in form of a [2x2] matrix for each case. The row number represents the hourly variation of the current profile(i.e. 8760 hours). The column number represents the radial thickness of the insulation from the conductor to the insulation screen(i.e. 30[mm] of insulation divided into 300 points). Therefore. the complete lifetime matrix has dimensions of [8760x301] points. The data is obtained in form of surface plots. To represent the data, lifetime consumption for the complete insulation length has been plotted for specific hour values. Following figures show the plots for different current vs. time profiles-

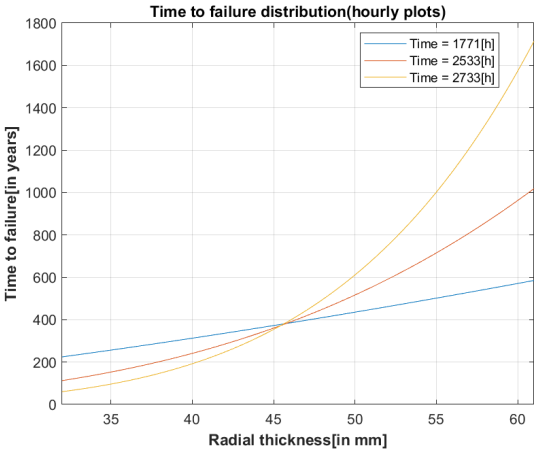

(a) Plot for time to failure of the insulation layer (Case 1)

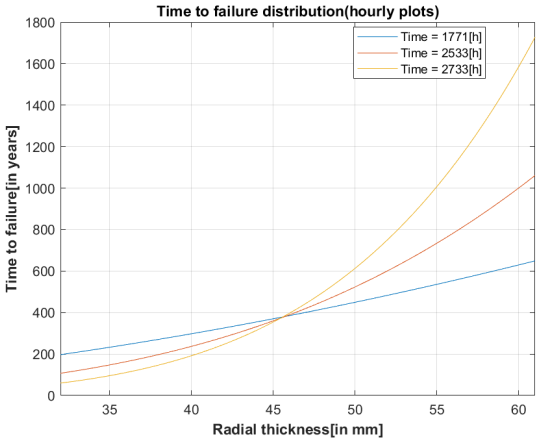

(b) Plot for time to failure data of the insulation layer (Case 2)

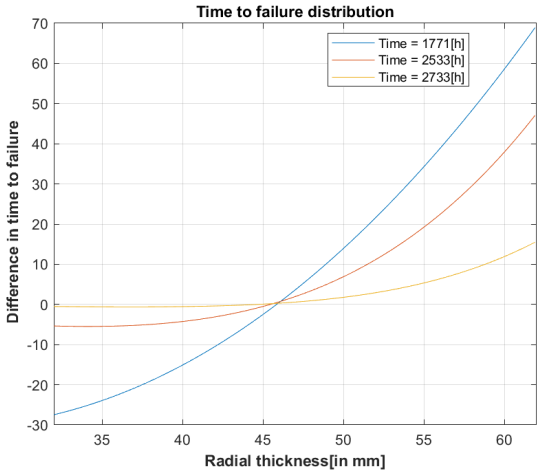

(c) Difference in time to failure for figure 3.4a

Figure 6.2: Variation of time to failure with radial distance[mm] and time interval[h]- (figure 3.4a)

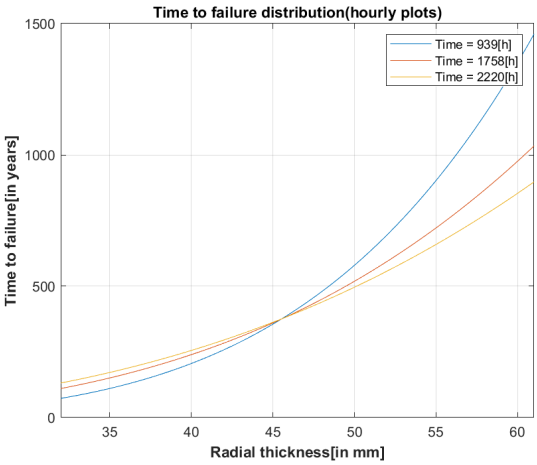

(a) Plot for time to failure of the insulation layer (Case 1)

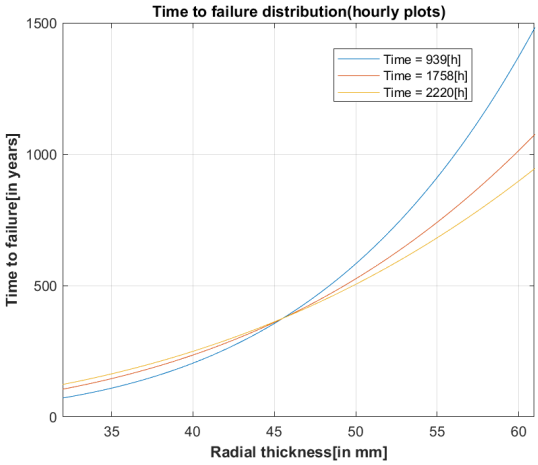

(b) Plot for time to failure data of the insulation layer (Case 2)

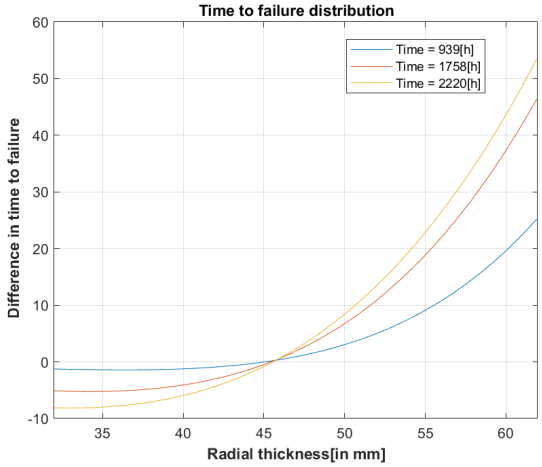

(c) Difference in time to failure for figure 3.4c

Figure 6.3: Variation of time to failure with radial distance[mm] and time interval[h]- (figure 3.4b)

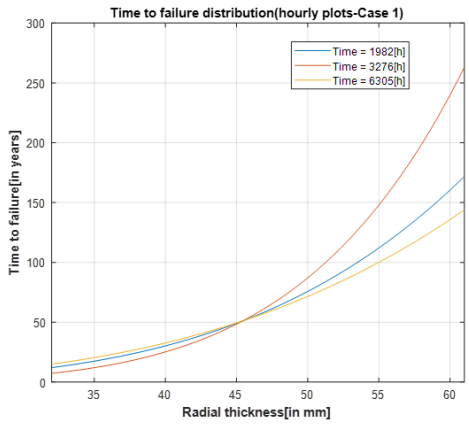

(a) Plot for time to failure of the insulation layer (Case 1)

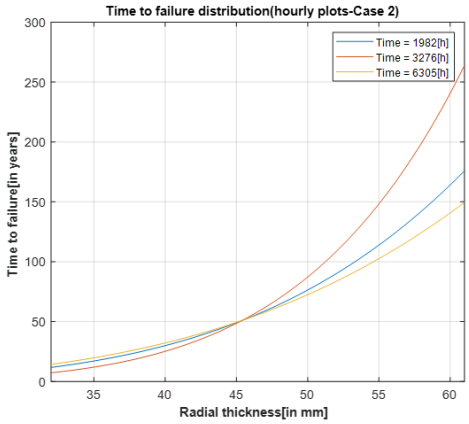

(b) Plot for time to failure data of the insulation layer (Case 2)

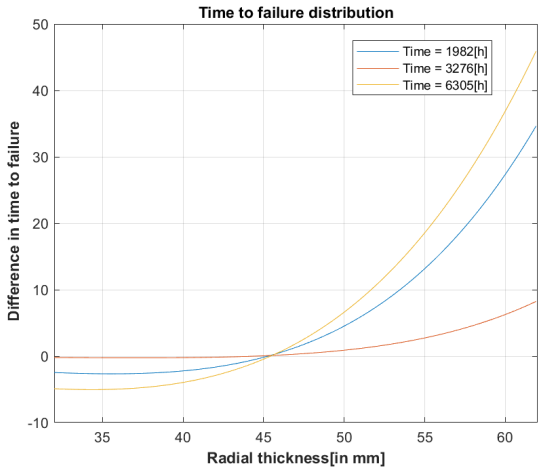

(c) Difference in time to failure for figure 3.4c

Figure 6.4: Variation of time to failure with radial distance[mm] and time interval[h]- (figure 3.4c)

[2]

Minimum[y]		Maximum[y]		Current[A]
Case 1	**Case 2**	**Case 1**	**Case 2**	
225.629	197.128	580.833	647.147	2100.8
113.828	110.873	1012.76	1042.62	1702.4
60.4738	59.9638	1685.1	1713.25	1128.8

Table 6.3: Values for lifetime consumption- (for current vs. time profile -figure 3.4a)

[2]Case 1: L = 1200[mm], thermal conductivity 0.2$[W/mK]$
Case 2: L = 1500[mm], thermal conductivity 0.36$[W/mK]$

Minimum[y]		Maximum[y]		Current[A]
Case 1	**Case 2**	**Case 1**	**Case 2**	
74.1401	71.8287	1448.8	1470.95	1341.2
110.562	106.648	1028.12	1063.33	1689.3
132.761	125.857	892.84	936.138	1806.6

Table 6.4: Values for lifetime consumption- (for current vs. time profile -figure 3.4b)

Minimum[y]		Maximum[y]		Current[A]
Case 1	**Case 2**	**Case 1**	**Case 2**	
87.0753	85.4108	1242.32	1273	1511.7
53.1349	52.928	1899.57	1906.77	949.142
108.77	103.869	1041.8	1076.47	1677.03

Table 6.5: Values for lifetime consumption- (for current vs. time profile -figure 3.4c)

6.3 Conclusions

Results from the lifetime consumption for the AC cable(table 6.2) are a good indicator of the potential degradation of the HVAC cable under long term usage. Usually deterioration in a physical parameter is used as a reference to check the time taken for the insulation breakdown under a certain temperature. Elongation at break is found to be one such parameter. Deterioration by 50% of its original value is used to check the time to breakdown. This value is tested experimentally under certain temperatures and then a multiplicative factor is used along with the time calculated using the Arrhenious equation to get the actual time to breakdown ([49]). Since, experimental results were not available for the cable, the values(mentioned in table 6.2) represent a maximum estimate on the lifetime consumption of the cable under different temperatures.

The Arrhenious equation also assumes first order kinetics for the reaction. Hence, it is concluded that experimental validation is needed to check the accuracy of the results, and a certain numerical factor should be used to multiply the ageing rate so that the result comes out to be accurate ([26]). Based on the results obtained and mentioned in table 6.2, the percentage lifetime consumption is observed to be higher for burial depth of $1200[mm]$ and thermal conductivity $0.2[W/mK]$.

For the HVDC case, equation 6.7 used to calculate the total approximate time to failure does not take into account the effect of space charges in the insulation layer. As it has been observed earlier that substantial degradation of lifetime due to the effect of space charges starts at a field stress values no less than $100[kV/mm]$ ([50]). Therefore, it is necessary to perform accelerated ageing tests for the DC cable to get to a specific formula. Results for the HVDC cable case show that the lifetime is measured as a function of time to failure for the insulation material. The plots for the time to failure for the two different cases are compared for each portion of the actual load profile. Figures 6.2, 6.3 and 6.4 show the result for the time to failure of the cable insulation for different time intervals. The difference plot (figure 6.2c, 6.3c and 6.4c) show that the cable time to failure shows higher values for case with burial depth of $1500[mm]$ and thermal conductivity $0.36[W/mK]$ over the other case with a burial depth of $1200[mm]$ and thermal conductivity $0.2[W/mK]$.
Further, it has been observed that the minimum time to failure observed has a value of 40[y] for the portion of insulation near the conductor screen. Thus showing that if it is assumed that the cable does not have an operation history, then the values obtained correspond to the result from equation 6.7. From the tables 6.3, 6.4 and 6.5 it

has been observed that the minimum time to failure value increases with increasing current value and the maximum time to failure decreases with increasing current value. This trend can be explained based on the effect of the electric field variation. The electric field value decreases with increase in the current value near the conductor screen. Simultaneously, the electric field value increases near the insulation screen with increase in current. Hence, we observe this trend in changing time to failure. These results are obtained under the assumption that the cable failure probability is the same as the design failure probability. Therefore, to get more accurate results, an experimental validation of equation 6.7 needs to be performed before the results can be used for further study.

Chapter 7

Results and Conclusions

In the whole work an effort was made to study the behaviour of both HVAC cable and HVDC cable under dynamic load and understand the significant changes in the cable by quantifying the rate of deterioration inside the cable under two different cases - burial depth and soil thermal conductivity having values (1500[mm],0.36[W/mK]) and (1200[mm],0.2[W/mK]). This chapter gives an overview of the important results which were found in chapters 3, 4, 5and 6 respectively. An attempt has been made to underline the conclusions from the various current vs. time profiles.

7.1 Results from earlier chapters

In the whole work an effort was made to study the behaviour of both HVAC cable and HVDC cable under dynamic load and understand the significant changes in the cable by quantifying the rate of deterioration inside the cable under two different cases - burial depth and soil thermal conductivity having values (1500[mm],0.36[W/mK]) and (1200[mm],0.2[W/mK]).
While accumulating the results for the current variation with time from the wind speed data in chapter 3, it has been assumed that all the wind turbines operate at a specified aggregate capacity factor. In reality, this capacity factor varies with the seasonality and the duration of wind flow through the turbine blades. The power conversion from wind speed to electricity assumes a fixed factor of 57% corresponding to the power flow through the turbines. In reality, this number is a measure of the efficiency of wind power production and is a function of wind speed. Since, the wind speed data is spontaneous, a maximum value of this coefficient has been taken into picture. The code for the wind speed to current vs. time curve can be found in Appendix C.
While studying the simulations of the HVAC cable(Chapter 4), it was found that overloading the cable with a value greater than 310[A] corresponding to 90°C resulted in a temperature increase for the surface of the cable. The cable surface temperature rise was observed to be similar for both the analytical and the numerical models. For a better comparision, the steady state temperature was compared to the transient temperature rise for the cable conductors.It was observed that the temperature of the cable when dynamic rating is used is lesser as compared to the case when static rating is used. Therefore, the dynamic thermal rating has been used to further calculate the ageing of the cables in chapter 6. The cable surface temperature was found to be more for the cable under a burial depth of 1200[mm and soil thermal conductivity of 0.2[W/mK].

For the HVDC cable model simulated with different current vs. time profiles, it has been observed that the variation of electric field inside the cable insulation affects the lifetime consumption of the cable more than the temperature variation. The presence of accumulated space charges also increases the electric field magnitude with time,therefore contributing further to the ageing process. But, in this case the space charge density was observed

to not exceed a value of $1[C/m^3]$. Hence, the effect of space charge on ageing has a very negligible effect on the ageing of the cable under the given maximum field stress of $21[kV/mm]$. Therefore, as suggested in the research conducted on the effect of space charges, this cumulative effect has been ignored. The maximum time to failure observed was found to be around 2700 years which is much larger than the overall design life of 40 years for the XLPE cables. The minimum time to failure was observed to be 39.68 years.

General results show that the cable insulation degrades more rapidly when the burial depth is 1200[mm] and thermal conductivity is $0.2W/mK$. The effect of degradation is more severe as one looks closer to the conductor screen as compared to the insulation screen.

7.2 Conclusions

In this section, answers to the questions posed in the introduction of this chapter have been provided. These conclusions are based on the analytical and numerical simulations which have been performed in this study. To get the complete picture, validation of these results with a suitable experimental setup needs to be done, as the results used here are based on models based on theoretical data and constant ambient values.

1 **How can the power transfer in the cable be increased with the help of dynamic cable rating?**
Both the HVAC and HVDC cable cross sections were subjected to different portions of the load profile. It was observed that the temperature of the conductor rarely exceeded the rated thermal limit. Thus, in order to increase the power capacity through the cable, the only option is to overload the two cables with current values higher than obtained, and check the conductor temperature and the lifetime consumption of the cable under overload. This process was repeated separately for both AC and DC cable cross-sections. The conductor current was increased by 20% of the original value and results were obtained for the respective cable cross-section. The analytical results mentioned here have been accumulated for a burial depth of $1200[mm]$ and soil thermal conductivity of $0.2[W/mK]$. The current profile used for the AC cable cross-section is the one shown in figure 4.5c. The current values for this particular profile have been increased by 20%. The current profile used for the DC case is the one shown in figure 3.4c. Following figures show the original and the new current profiles here.

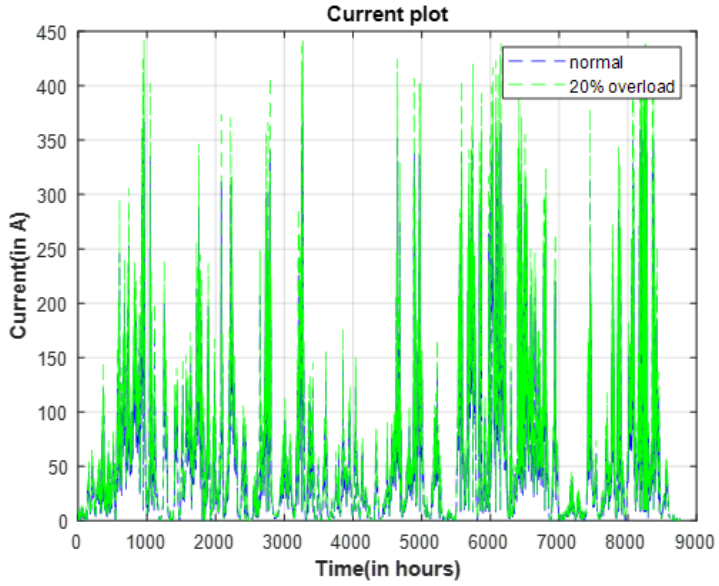

(a) Current vs. time profile(in green) for the AC case

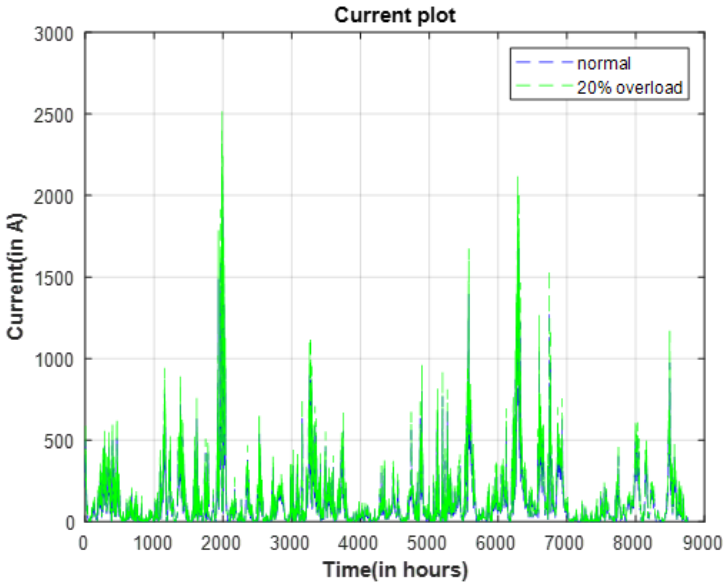

(b) Current vs. time profile(in green) for the DC case

Figure 7.1: new and original current profiles used

The conductor temperature for both the AC and the DC cases are shown-

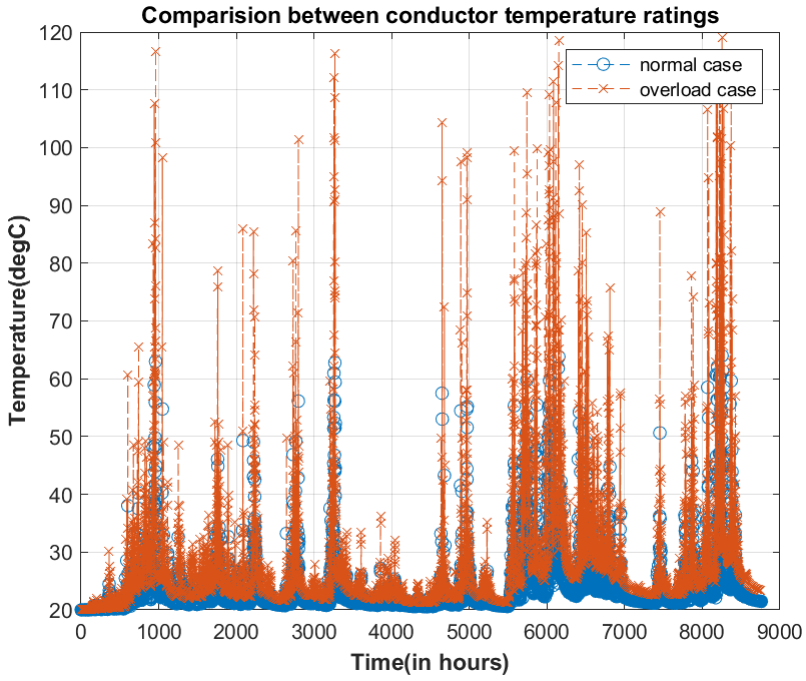

(a) Temperature vs. time plot for AC case

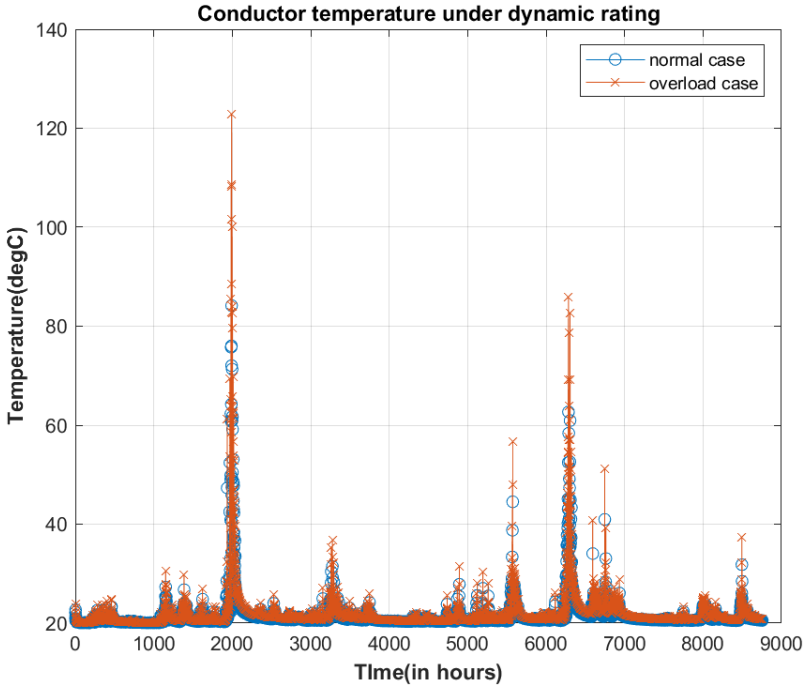

(b) Temperature plot for DC case

Figure 7.2: Temperature plots for both the AC and DC case

As can be observed for the AC case, there is a difference of 53°C when the results for the overloaded current profile(figure 7.2a) are compared to the original result(figure 4.17a). Since, the maximum dynamic current rating has crossed the rated value of 90°C for this case, it is not feasible to operate the cable at currents higher than this value

under continuous operation. Overloading the cable with currents greater than this value will lead to the cable insulation degradation at a faster pace than recorded by the Arrhenious equation. This is due to the resulting chemical degradation not following the first order kinetics. Hence, experimental validation will be necessary for recording further results.

Similar results were observed for the DC cable simulation(figure 7.2b). For this case, it was observed that the maximum temperature for the overloaded case exceeded the normal case current profile temperature rating by 40°C. Overloading beyond this 20% limit was not considered feasible under continuous operation as the cable insulation will degrade at a faster pace than recorded by the Arrhenious equation. Following figure compares the lifetime deterioration of the AC cable under both cases-

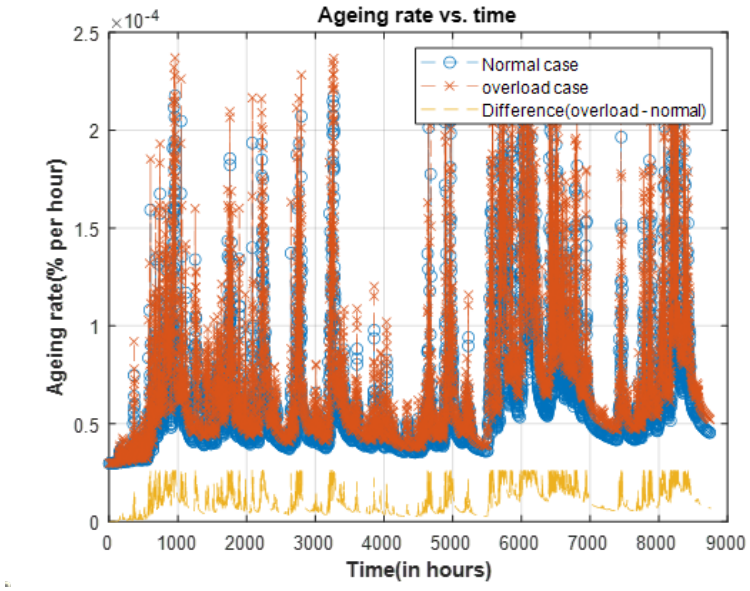

Figure 7.3: Comparision of ageing rate for both the cases

For the overload case, the cumulative percent lifetime consumption under overload was found to be 0.6208% as compared to the original value of 0.5295%. Thus, there is a nominal increase in the lifetime consumption when the current is increased by 20% of the original value.

For the DC case. the maximum temperature rise observed at the relevant hours have been shown here.

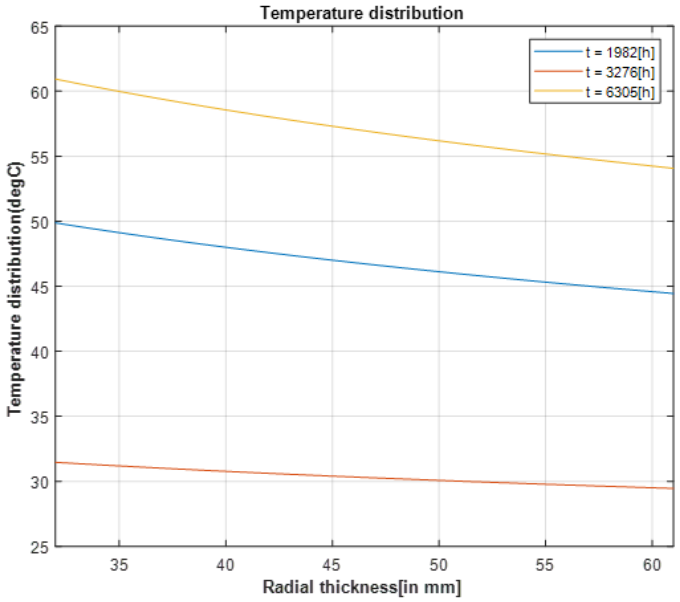

(a) Temperature vs. time plot for normal current case(in blue-figure 7.1b)

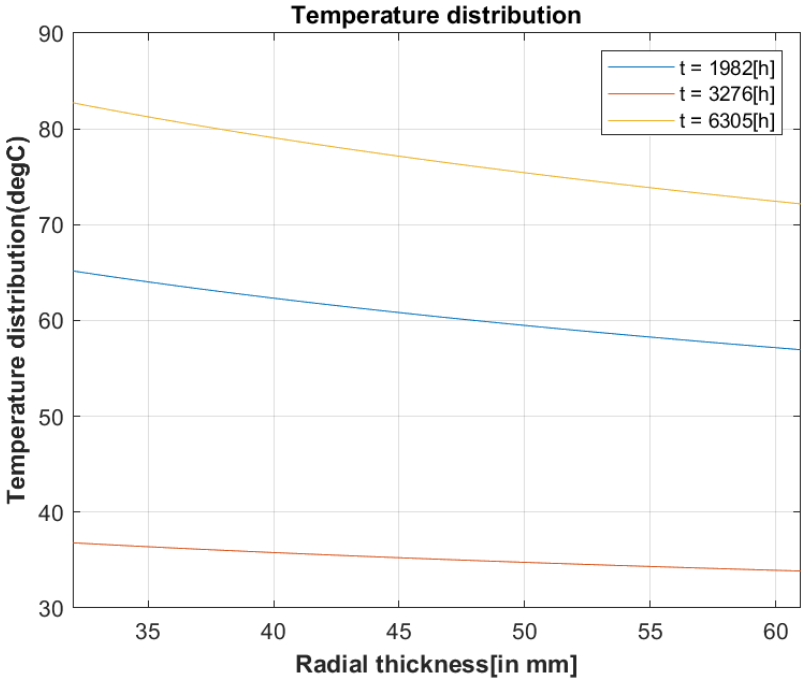

(b) Temperature plot for different hours-DC case(in green-figure 7.1b)

Figure 7.4: Temperature plots for both the AC and DC case

It can be observed by comparing the figures 7.2b and 5.12b. The electric field gradient over the insulation is almost the same as the previous one.A field reversal at 1992[h] has been observed when comparing the electric field stresses.The insulation degradation in this case has more dependence on the electric field stress as compared to the temperature. Following figure shows the electric field stress variation and insulation degradation for specific hours over the insulation

thickness-

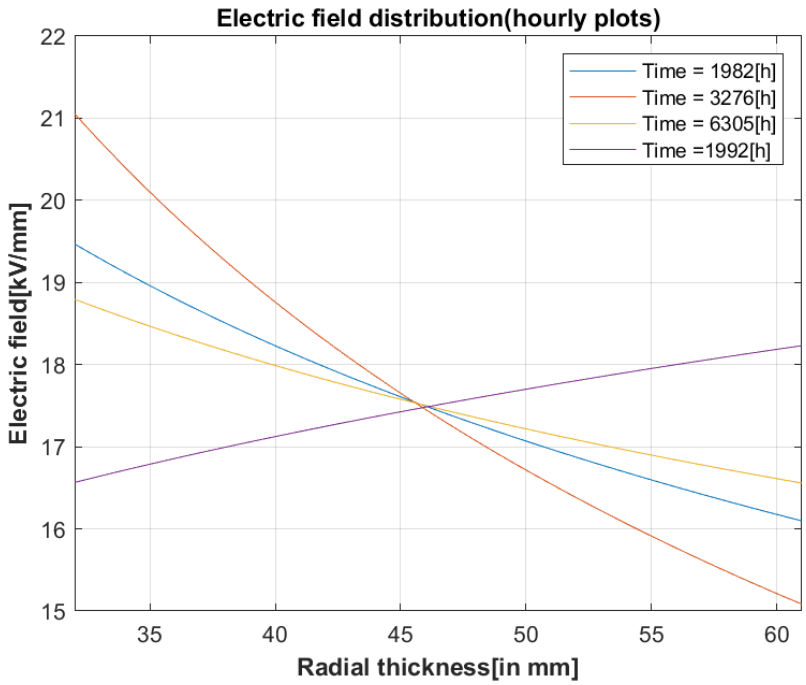

(a) Electric field vs. time plot for DC case with current as shown in green(figure 7.1b)

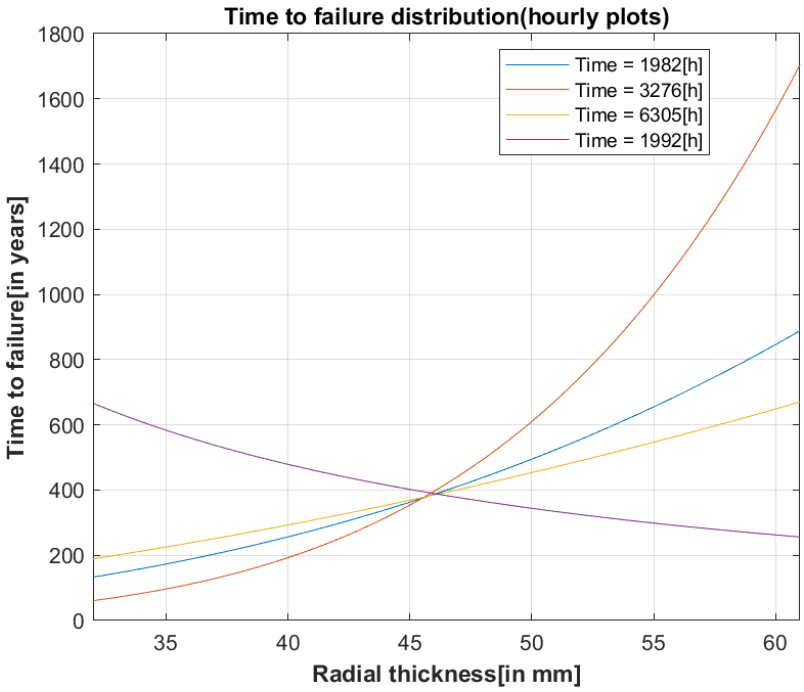

(b) time to failure plot for different hours-DC case(current shown as green(figure 7.1b))

Figure 7.5: Electric field and time to failure plots

It can be observed that the time to failure shows a reversal in the general trend for 1992[h].The effect of field reversal results in a decreasing trend in the time to failure plot as compared to the other hourly plots. This behaviour was not observed for the case with normal current profile(blue curve-figure 7.1b). Therefore, it can be said that both the AC and DC cables can be loaded with currents upto 20% above the rated value. Continuous rating of the cable at current values corresponding to 20% more than the rated values is not suggested due to higher rate of degradation of the cable. However, exceeding this limit may seriously limit the insulation life due to the change in reaction kinetics inside the insulation due to thermal degradation. Therefore, corresponding to a current value increase of 20%, the power flow inside the cables can be increased by a cumulative value of 44%.

2 **How will variations in soil thermal conductivity and burial depth change the operation of the cable?**
In the work, two different cases of soil thermal conductivity and burial depth have been studied. It has been found from the literature study that the soil thermal conductivity increases with increasing burial depth of the cable. This results in relatively lesser soil thermal resistivity at higher depth.Both the AC and DC cable results show lesser thermal transient rating for a burial depth of $1500[mm]$ and soil thermal conductivity of $0.36[W/mK]$. Therefore, the current carrying capacity of the cable improves with increasing burial depth and increasing soil thermal conductivity.

3 **What can be said about the change in lifetime consumption of the cable under changing soil thermal conductivity and burial depth. What can be suggested to mitigate this effect in the future?**
Lifetime deterioration is observed to be scaled according to the nature of the thermal profile (Temperature vs. time).It can be said that the higher the temperature value above the nominal value of temperature, the higher will be the lifetime deterioration of the cable. Therefore, it is important to choose the current limits accordingly to limit the cable degradation upto a certain tolerable limit under continuous operation.The observations made were as follows. For the AC case, when the percentage lifetime consumption was compared for the two cases from table 6.2, case with burial depth of $1500[mm]$ and soil thermal conductivity of $0.36[W/mK]$ shows relatively lower value as compared to the other case.
For the DC case, the time to failure plots at different hours were compared. From comparision of the minimum time to failure values for different hours from tables 6.3, 6.4 and 6.5, the case with burial depth of $1200[mm]$ and soil thermal conductivity $0.2[W/mK]$ shows larger time to failure as compared to the other case. These results show that the HVAC cable shows larger lifetime consumption on decreasing burial depth and soil thermal conductivity. On the other hand, the DC cable shows relatively lesser lifetime consumption on decreasing the burial depth and soil thermal conductivity. Since, this work was done for both the cable systems, the effect on AC cables has been chosen as the final conclusion.

7.3 Future Scope of work

This work concludes the analytical and numerical implementation of dynamic cable rating and related changes in the cable lifetime based on parameter variations. Although, the numerical and analytical models work differently, the primary results indicate similar nature of temperature variation. Both the models assume constant ambient conditions throughout the simulation period. This can be changed with appropriate functions based on the geographical conditions of operation. Results from this work can be used further to study the degradation of the HVDC and HVAC cable systems under accelerated load testing. This is necessary as the cable insulation ages differently under different thermal stress values. For the DC case, space charge buildup will also add to the degradation of the cable. A suitable experimental setup can be used to validate the thermal degradation results and study the changes under different test conditions(like changing probabilities of failure, varying ambient temperature, soil thermal resistivity and burial depth).

To summarise, following are the research areas which can be studied further-

- A suitable function can be used to model the temperature of the external surroundings instead of using a fixed value of 20°C.
- The chemical deterioration of the cable due to thermal effect can be modelled more accurately if a proper numerical equation is derived with the help of accelerated ageing tests on the cable insulation material.
- The effect of space charges can be modelled under a dynamic load experimentally. Cables with different lifetime consumption can be used to start and check the process before the results can be implemented analytically.
- The formula for calculation of HVDC cable time to failure is based on the assumption that the cable design failure probability is the same as the cable failure probability calculated using the weibull distribution. This point can be further investigated with the help of experimental data.
- The analytical model can be improved to take more parameters affecting the temperature distribution into picture. for example-moisture ingress in the cable, effect of chemical degradation due to other factors.

Appendix A

Appendix A

A.1 Matlab code for analytical calculation of the HVAC cable structure.

Following is the code to calculate the steady state and transient temperature variation for two three core cables laid down side by side at a given burial depth.

```
%% Basic values
U0 = 66/(sqrt(3));
f = 50;
theta = 90;
theta_c = 90;
theta_amb = 20;
%delta = 1.61e-7;
%delta = 1.1e-7;
%L2 = 1500; % axial depth of burial of cable(Takes values of 1200[mm] and 1500[mm])
D_e = 183;
%%Cable dimensions for 3 core cable(dimensions in mm) in the pipe
rc3 = 15.95; % radius
ts3 = 1;
tins3 = 10;
tsh3 = 5;
t_ab = 5;
t_a = 12.6;
t_op = 5;
Iss_b = 363; %base value
%% Resultant parameters for 1 core equivalent cable
pho_epr = 5;
pho_cu = 27e-4;
pho_f = 3.5;  % tr of filler material
G = 0.54; %Geometric factor approximate value
%% Thermal resistance and capacitance formulation for 3 core cable(corrected formulae)
lf = 0.8;
```

```
Dx = 61200*(sqrt(delta*24));
De = 2*91.5;
Ds = 63.9;
D_f = 2*68.9;
u = (2*L2)/D_e;
T1_1 = (pho_epr/(2*pi))*log(1 + (2*(tins3)/(2*(rc3+ts3))));
T1 = T1_1/3;%Between Conductor and sheath
pho_st = 1/45;%For steel
pho_pp = 1/0.44;%PP yarn
%pho_s = 1/0.36;% soil % takes the value 5[Km/W] and 2.77[Km/W] respectively
T2 = (pho_f/(2*pi))*G; %between sheath and armor
T3 = ((pho_pp/(2*pi))*log(1+(2*t_ab/(2*68.9))))+((pho_st/(2*pi))*...
...log(1 + (2*t_a/(2*(68.9+t_ab))))) + ((pho_pp/(2*pi))*...
...log(1 + (2*t_op/(2*(68.9+t_ab+t_a))))); %between armor bedding and serving
T4 =  ((pho_s/(2*pi))*log(2*u));%External thermal resistance

% Thermal Capacitances
Qc = (pi*rc3*rc3)*386*(1e-6); %Conductor
Qins = (pi/4)*(((2*(rc3+ts3+tins3))^2) - ((2*(rc3 + ts3))^2))*2000*(1e-6); % insulation
Q_f = ((pi/4)*(((2*68.9)^2)- ((46.18)^2)))*1360*(1e-6); % Filler material
Qs = abs((pi/4)*((2*(rc3+ts3+tins3+ tsh3)^2) - ((2*(rc3 + ts3+tins3))^2))...
...*386*(1e-6)); % sheath
Q_ab = abs(((pi/4)*((2*(68.9 + t_ab))^2 - ((2*68.9)^2)))*(1920)*(1e-6)); % armor bedding
Qa = (pi/4)*((2*(68.9 + t_ab+ t_a))^2 - ((2*(68.9+ t_ab)^2)))*468*(1e-6); %armor
Qse = (pi/4)*((2*(68.9 + t_ab+ t_a+ t_op)^2) - ((2*(68.9+ t_ab+ t_a)^2)))*(1920)*(1e-6); ...
...%outer protection
%% Skin and proximity effect coefficients, sheath loss factor, armor loss factor calculation
eps = 3; %for epr insulation
df = 0.005; %tan delta factor
Di = 53.9; %Dia over insulation
dc = 2*rc3;
C = (eps/(18*log(Di/dc)))*1e-9;
Wd = 2*pi*f*C*U0*U0*df; %Cumulative dielectric losses

s = 63.9; %distance between conductor axes
d = 58.9; %mean sheath diameter
R_ac1 = (1.02e6/800)*(1.7241e-8)*(1+ (3.93e-3*(theta_c - theta_amb)));
Fk = (16*pi*(f^2)/R_ac1)*(1e-7);
ks = 1;
kp = 1;
xs_sq = Fk*ks;
ys = (xs_sq^2)/(192 + 0.8*(xs_sq^2));
xp_sq = Fk*kp;
Fp = (xp_sq^2)/(192 + 0.8*(xp_sq^2));
yp = Fp*((dc/s)^2)*((0.312*((dc/s)^2)+ (1.18/(Fp + 0.27))));
R0 = R_ac1*(1+(1.5*(ys+yp))); %Conductor resistance
theta_sb = theta_c - ((((Iss_b^2)*R0) + (0.5*Wd))*T1);
Rs_b = R_ac1*(1 + (3.93e-3*(theta_sb - theta_amb)));
X = 2*(2*pi*f)*log(2*63.8/d)*(1e-7);
Lsh0 = (Rs_b/R0)*(1.5/(1+((Rs_b/X)^2))); % Sheath loss factor-initial value
theta_arb = theta_c - ((((Iss_b^2)*R0) + (0.5*Wd))*T1 + (((Iss_b^2)*R0*(1+Lsh0))+Wd)*(3*T2));
Ra = (13.8e-8)*(1 + (4.5e-3*(theta_arb - theta_amb)));
```

```
da = (73.7 + 93.7)/2;
La0 = 1.23*(Ra/R0)*(2*55.25/da)*...
...(1/((2.77*Ra*1e6/(2*pi*f)) + 1))*(1 - ((R0/Rs_b)*Lsh0)); %Armor correction factor-initial

%% Calculation for various losses in the cable
%deltheta = theta-theta_amb;
Iss = 64;
%I1 = C3; Current vs. time profile input
Wc0 = (I1(1)^2)*R0; %Conductor loss
Ws0 = Wc0*Lsh0; %Sheath Loss
Wa0 = Wc0*La0; %Armor loss

 delT = zeros([length(I1) 1]);
 for u = 1:1:length(I1) %Steady state temperature calculation
     delT(u) = (I1(u)^2)*((R0*T1)+
     ...(R0*(1+Lsh0)*(3*T2))+(R0*(1+Lsh0+La0)*3*(T3+T4))) + Wd*((0.5*T1)+ 3*(T2+T3+T4));
     delT1(u) = 20 + ...
     ...(3*(I1(u)^2)*R_ac1)*T1 + (3*(I1(u)^2)*R_ac1 + 3*(I1(u)^2)*Rs_b)*T4;
 end
%% Equivalent parameters for 2 step ladder network and transient response of cable.(Model for
syms e2(x1)
e2(x1) = piecewise((abs(x1)<=1),log(abs(x1))-((-0.5772)+ abs(x1) + (-0.2499*(abs(x1)^2))...
...+ (0.0552*abs(x1))+ (-0.0098*abs(x1)) + (0.0011*abs(x1))),...
...(abs(x1)<=8),(1/abs(x1))*(exp(-abs(x1)))*...
...(((abs(x1)^2)+ (2.3347*abs(x1)) + ...
...(0.2506*abs(x1)))/((abs(x1)^2)+ ...
...(3.3307*abs(x1)) + ...
...(1.6915*abs(x1)))),abs(x1)>8,0);
%Van wormer coefficients for capacitances.
p = (1/(2*log(Di/dc))) - (1/((Di/dc)^2-1)); %For insulation
pf = (1/(2*log(D_f/46.18))) - (1/((D_f/46.18)^2-1)); %For filler material
pab = (1/(2*log((D_f + (2*t_ab))/D_f))) - (1/((D_f + (2*t_ab))/D_f)); %For armor bedding
p2 = (1/(2*log(D_e/(D_e - (2*t_op))))) - (1/(D_e/(D_e - (2*t_op)))); %For external serving
Q1 = (Qc*3 + (p*Qins)*3);
Q2 = ((1-p)*Qins*3) + (Q_f*pf) + Qs*3;
Q3 = (1-pf)*Q_f + pab*Q_ab;
Q4 = abs((1-pab)*Q_ab + Qa*(1+La0) + p2*Qse);
Q5 = abs((1-p2)*Qse);

%Ladder network parameters

TA = T1/2;
QA = Q1;
TB0 = (T1/2)+(T2*(1+Lsh0))+(T3*(1+La0))+T4;
QB0 = Q2 + (Q3*((((T2*(1+Lsh0))+...
...(T3*(1+La0))+T4))/TB0)^2) + ...
...(Q4*((((T3*(1+La0))+T4))/TB0)^2) + (Q5*((T4/TB0)^2));

% Transient response calculation-> input current variation, temperature
% variation
```

```
initemp=20;%initil temprature
t1 = 1:1:length(I1); %10 min intervals
dpk = 30;
dpk1 = 45;
L0 = 40;
W = 160e3;
kb = 1.38e-23;
L = zeros([length(t1) 0]);
L(1) = L0;
Q22 = zeros([length(t1) 0]);
Q22(1) = Q2;
Q44 = zeros([length(t1) 0]);
Q44(1) = Q4;
Mo0 = 0.5*((TA*QA)+(TB0*QB0)+(TB0*QA));
No0 = TA*QA*TB0*QB0;
a0 = (Mo0 + sqrt(Mo0^2 - No0))/No0;
b0 = (Mo0 - sqrt(Mo0^2 - No0))/No0;
Ta0 = ((1/QA)- b0*(TA+TB0))*(1/(a0-b0));
Tb0 = TA + TB0 - Ta0;
theta_s =  zeros([length(t1) 0]);
theta_s(1) = theta_sb;
theta_ar = zeros([length(t1) 0]);
theta_ar(1) = theta_arb;
R_s =  zeros([length(t1) 0]);
R_s(1) = Rs_b;
R_a =  zeros([length(t1) 0]);
R_a(1) = Ra;
Lsh = zeros([length(t1) 0]);
Lsh(1) = Lsh0;
La = zeros([length(t1) 0]);
La(1) = abs(La0);
TB = zeros([length(t1) 0]);
TB(1) = TB0;
QB = zeros([length(t1) 0]);
QB(1) = QB0;
Mo = zeros([length(t1) 0]);
Mo(1) = Mo0;
No = zeros([length(t1) 0]);
No(1) = No0;
a = zeros([length(t1) 0]);
a(1) = a0;
b = zeros([length(t1) 0]);
b(1) = b0;
Ta = zeros([length(t1) 0]);
Ta(1) = Ta0;
Tb = zeros([length(t1) 0]);
Tb(1) = Tb0;
Wc = zeros([length(t1) 0]);
Wc(1) = (I1(1)^2)*R_ac1;
Wcc = zeros([length(t1)*60 1]);
Wcc(1) = (I1(1)^2)*R_ac1;
Ws = zeros([length(t1) 0]);
```

```
Ws(1) = Ws0;
Wa = zeros([length(t1) 0]);
Wa(1) = Wa0;
Wt = zeros([length(t1) 0])+ (Wd*ones([length(t1) 0]));
Wt(1) = Wc(1) + Ws(1) + Wa(1) + Wd;
th_c(1) = 90;
%Transient calculation for the different parameters which vary with time
%and the varying losses
W1 = zeros([length(t1) 1]);
 a1 = 1/0.00393;
 %% Dynamic parameter calculations
for t = 2:1:length(t1)
    theta_s(t) = 90 - ((((I1(t)^2)*R0*3) + (0.5*Wd))*T1);
    R_s(t) = R_ac1*(1 + (3.93e-3*(theta_s(t) - theta_amb)));
    Lsh(t) = (R_s(t)/R0)*(1.5/(1+((R_s(t)/X)^2)));
    theta_ar(t) = 90 - ((((I1(t)^2)*R0*3) ...
    ...+ (0.5*Wd))*T1 + (((I1(t)^2)*R0*3*(1+Lsh(t)))+Wd)*(T2));
    R_a(t) = (13.8e-8)*(1 + (4.5e-3*(theta_ar(t) - theta_amb)));
    La(t) =abs(1.23*(R_a(t)/R0)*(2*(55.25)/da)*...
    ...(1/((2.77*R_a(t)*1e6/(2*pi*f)) + 1))*(1 - ((R0/R_s(t)*Lsh(t)))));
    Q22(t) = ((1-p)*Qins*3) + (Q_f*pf) + Qs*3*(1+Lsh(t));
    Q44(t) = (1-pab)*Q_ab + Qa*(1+La(t)) + p2*Qse;
    TB(t) = (T1/2)+(T2*(1+Lsh(t)))+(T3*(1+La(t)))+T4;
    QB(t) = Q22(t) + (Q3*((((T2*(1+Lsh(t)))+(T3*(1+La(t)))+T4)/TB(t))^2))...
    ...+ (Q44(t)*((((T3*(1+La(t)))+T4)/TB(t))^2)) + (Q5*((T4/TB(t))^2));
    Mo(t) = 0.5*((TA*QA)+(TB(t)*QB(t))+(TB(t)*QA));
    No(t) = TA*QA*TB(t)*QB(t);
    a(t) = (Mo(t) + sqrt(Mo(t)^2 - No(t)))/No(t);
    b(t) = (Mo(t) - sqrt(Mo(t)^2 - No(t)))/No(t);
    Ta(t) = ((1/QA)- b(t)*(TA+TB(t)))*(1/(a(t)-b(t)));
    Tb(t) = TA + TB(t) - Ta(t);
    Wc(t) = 3*(I1(t)^2)*R0;
    Ws(t) = Wc(t)*Lsh(t);
    Wa(t) = Wc(t)*La(t);
    Wt(t) = Wc(t) + Ws(t) + Wa(t);

end


time = zeros([length(t1),1]); %Complete duration of profile
thc1 = zeros([length(t1),3]); %conductor temperature
thc2 = zeros([length(t1),3]); %Conductor temperature(with changing conductor resistivity)
ths1 = zeros([length(t1),3]);%Surface temperature
ths2 = zeros([length(t1),3]);%Surface temperature(with changing conductor resistivity)
thc3 = zeros([length(t1),3]);% Final conductor temperature
ths3 = zeros([length(t1),3]);% Final soil temperature

for c = 1:1:length(t1)
    for i = 1:1:length(time)
        thc1(i,2) = 0;
        thc2(i,2) = 0;
        thc3(i,2) = 0;
```

```
ths1(i,2) = 0;
ths2(i,2) = 0;
ths3(i,2) = 0;
ths1(i,3) = 0;
ths2(i,3) = 0;
thc1(i,3) = 0;
thc2(i,3) = 0;

if i>(c-1) %calculate values for one pulse of current
    deltaT = i-(c-1);
    e1_1(i) = expint(((De*(1e-3))^2/(16*delta*(deltaT*3600)))) ...
    ...- expint(((L2*(1e-3))^2/(delta*(deltaT*3600)))); %Cable surface temperature ex
    t = (i-(c-1));
    ct = Wc(c)*((Ta(c)*(1-exp(-a(c)*t*3600)))+ ...
    ...(Tb(c)*(1-exp(-b(c)*t*3600)))); %Conductor transient temperature
    ths1(i,3) = Wt(c)*(pho_s/(4*pi))*e1_1(i); %Cable surface temperature

    if Wc(c)>0
        ths1(i,3) = (ths1(i,3)*ct)/(Wc(c)*(TA + TB(c))); %Cable surface temperature
    end

    thc1(i,3) = ct + ths1(i,3);
end

if c==1
    thc2(i,3) = thc1(i,3)/(1 + (1/(1/(a1 + 0)))...
    ...*(delT1(c) - 0.2 - thc1(i,3))); ...
    ...%Conductor temperature with changing resistivity
    ths2(i,3) = ths1(i,3)/(1 + (1/(1/(a1 + 0)))...
    ...*(delT1(c) - 0.2 - thc1(i,3)));...
    ...%cable surface temperature with changing resistivity
else
    thc2(i,3) = thc1(i,3)/(1 + (1/(1/(a1 + thc1(c,1))))...
    ...*(delT1(c) - 0.2 - thc1(i,3))); ...
    ...%conductor temperature with changing resistivity
    ths2(i,3) = ths1(i,3)/(1 + (1/(1/(a1 + thc1(c,1)))...
    ...*(delT1(c) - 0.2 - thc1(i,3))));...
    ...%cable surface temperature with changin resistivity
end

if i>c
    thc1(i,2) = thc1(i,3)-thc1(i-1,3); %Conductor temperature adjusted value
    ths1(i,2) = ths1(i,3)-ths1(i-1,3); %Cable surface temperature adjusted value

    thc2(i,2) = thc2(i,3)-thc2(i-1,3); %Conductor surface temperature adjusted value
    ths2(i,2) = ths2(i,3)-ths2(i-1,3); %Cable surface temperature adjusted value
else
    thc1(i,2) = thc1(i,3);
    ths1(i,2) = ths1(i,3);

    thc2(i,2) = thc2(i,3);
    ths2(i,2) = ths2(i,3);
```

```
        end

        thc1(i,1) = thc1(i,1) + thc1(i,2);   %Final temperature values for each pulse
        ths1(i,1) = ths1(i,1) + ths1(i,2);
        thc2(i,1) = thc2(i,1) + thc2(i,2);
        ths2(i,1) = ths2(i,1) + ths2(i,2);
    end
end
```

The values for the different computed parameters have been mentioned in Appendix B.

A.2 Matlab Code for Calculation of static and transient cable rating for HVDC cables

Following is the code to calculate the steady state ampacity rating and the Transient electric field rating of the Cable-
This is the portion of the HVDC code used to calculate the steady state temperature and the temperature transient

for the cable surface.

```
    %% Steady state analysis code
% Dimensions of the cable(in mm)
rc = 30; %Radius of conductor
tcs = 2; %Thickness of conductor screen
tii = 30; %Insulation wall
tls = 2; %Lead Sheath
tsa = 11; %Armor thickness
ts = 5; % Serving thickness
%L = 1200; %Burial depth
alpha_cu = 0.00393; %Copper expansion coefficient
%pho_s = 2.77;
T1 = (3.125/(2*pi))*log(1+ ((2*tii)/124));
T2 = (0.02/(2*pi))*log(1+ ((2*tsa)/150));
T3 = ((5.55/(2*pi))*log(1+ ((2*ts)/160)));
T4 = (pho_s/(2*pi))*(log(L/160));

Tc = ((1/398)/(2*pi))*log(32/30); %TR of copper conductor
Tcs = (3.125/(2*pi))*log(1+ ((2*tii)/124)) + ...
...((0.0288/(2*pi))*log(1+ ((2*tls)/128))); %TR of insulation wall and lead sheath
Tsa = (0.02/(2*pi))*log(1+ ((2*tsa)/150)) + ...
...((3.57/(2*pi))*log(1+ ((2*ts)/160))); %TR of armor and serving
Tamb = (pho_s/(2*pi))*(log(L/160)); %TR of ambient soil
Tr =T1+T3+T4;%Total Thermal resistance
theta_amb = 20;
theta_c = 90;
pho_cu = 1.77e-8; %electrical resistivity of copper
R = (pho_cu/(pi*rc*rc*(1e-6)))...
...*(1 + alpha_cu*(70));%Electrical Resistance of cable
%R = (1.732e-8/(pi*900*(1e-6)));
Imax = sqrt((theta_c-theta_amb)/(R*Tr));%Steady state current value
```

```
%Transient parameter variation for current vs. time profiles
%I1 = C4;
%I1 = Ad(2,:)%Test current profile
delT1 = zeros([length(I1) 1]);
for u = 1:1:length(I1)
    delT1(u) = (I1(u)^2)*(R*Tr);
end

%% Parameters for 2 step ladder network equation formulation.
Di = 124; % Inner dia upto insulation
dc = 64; %dia upto conductor screen
Do = 128; %
Ds = 2*(rc + tcs + tii + tls + tsa + ts); %Dia of cable
Qc = pi*(rc^2)*(386)*(1e-6);
Qiw = (pi/4)*(Di^2 - dc^2)*(1360)*(1e-6);
Qa = (pi/4)*((Ds - 2*ts)^2 - Do^2)*(468)*(1e-6);
Qse = (pi/4)*(Ds^2 - (Ds - 2*ts)^2)*(1920)*(1e-6);

p = (1/(2*log(Di/dc))) - (1/((Di/dc)^2 - 1));
p2 = (1/((2*log(Ds/(Ds - 2*ts))))) - (1/((Ds/(Ds - 2*ts))^2 - 1));

Q1 = Qc + p*Qiw;
Q2 = Qiw*(1-p);
Q3 = Qa + p2*Qse;
Q4 = (1 - p2)*Qse;


TA = (T1/2);
TB = (T1/2) + T2 + T3 + T4;
QA = Q1;
QB = Q2 + Q3*((T2 + T3 + T4)/...
...(TB^2)) + Q4*((T3 + T4)/(TB^2));

Wc = R.*(I1.^2);
Mo = 0.5*((TA*QA)+(TB*QB)+(TB*QA));
No = TA*QA*TB*QB;
a = (Mo + sqrt(Mo^2 - No))/No;
b = (Mo - sqrt(Mo^2 - No))/No;
Ta = ((1/QA)- b*(TA+TB))*(1/(a-b));
Tb = TA + TB - Ta;

a1 = 1/alpha_cu;
t1 = 1:1:length(I1);
time = zeros([length(t1),1]);
thc1 = zeros([length(t1),3]);
thc2 = zeros([length(t1),3]);
ths1 = zeros([length(t1),3]);
ths2 = zeros([length(t1),3]);
thc3 = zeros([length(t1),3]);
ths3 = zeros([length(t1),3]);
e1_1 = zeros([length(t1) 1]);
```

```
for c = 1:1:length(t1)
    for i = 1:1:length(time)
        thc1(i,2) = 0;
        thc2(i,2) = 0;
        thc3(i,2) = 0;
        ths1(i,2) = 0;
        ths2(i,2) = 0;
        ths3(i,2) = 0;
        ths1(i,3) = 0;
        ths2(i,3) = 0;
        thc1(i,3) = 0;
        thc2(i,3) = 0;

        if i>(c-1)
            deltaT = i-(c-1);
            e1_1(i) = expint(((Ds*(1e-3))^2/(16*delta*(deltaT*3600)))) ...
            ...- expint(((L*(1e-3))^2/(delta*(deltaT*3600))));
            t = (i-(c-1));
            ct = Wc(c)*((Ta*(1-exp(-a*t*3600)))+...
            ...(Tb*(1-exp(-b*t*3600))));
            ths1(i,3) = Wc(c)*(pho_s/(4*pi))*e1_1(i);

            if Wc(c)>0
                ths1(i,3) = (ths1(i,3)*ct)/(Wc(c)*(TA + TB));
            end

            thc1(i,3) = ct + ths1(i,3);
        end

        if c==1
            thc2(i,3) = thc1(i,3)/(1 + (1/(1/(a1 + 20)))...
            ...*(delT1(c) - 0.2 - thc1(i,3)));
            ths2(i,3) = ths1(i,3)/(1 + (1/(1/(a1 + 20)))...
            ...*(delT1(c) - 0.2 - thc1(i,3)));
        else
            thc2(i,3) = thc1(i,3)/(1 + (1/(1/(a1 + thc1(c,1))))...
            ...*(delT1(c) - 20 - thc1(i,3)));
            ths2(i,3) = ths1(i,3)/(1 + (1/(1/(a1 + thc1(c,1)))...
            ...*(delT1(c) - 20 - thc1(i,3))));
        end

        if i>c
            thc1(i,2) = thc1(i,3)-thc1(i-1,3);
            ths1(i,2) = ths1(i,3)-ths1(i-1,3);

            thc2(i,2) = thc2(i,3)-thc2(i-1,3);
            ths2(i,2) = ths2(i,3)-ths2(i-1,3);
        else
            thc1(i,2) = thc1(i,3);
            ths1(i,2) = ths1(i,3);

            thc2(i,2) = thc2(i,3);
```

```
            ths2(i,2) = ths2(i,3);
        end

        thc1(i,1) = thc1(i,1) + thc1(i,2);
        ths1(i,1) = ths1(i,1) + ths1(i,2);
        thc2(i,1) = thc2(i,1) + thc2(i,2);
        ths2(i,1) = ths2(i,1) + ths2(i,2);
    end
end
```

This is the portion of the code used to calculate the temperature and the electric field transient.

```
Code_DC; %External code to calculate the temperature of the cable surface
%% Code to calculate the temperature gradient for different current values
vc = zeros([length(I1) 1]);
Rc20 = 5.94e-6;
eta = (1- alpha_cu*20)*Rc20;
n = Rc20*alpha_cu;

for i = 1:1:length(I1)
    vc(i) = ((((Tcs + (Tsa + Tamb))*...
    ...eta*(I1(i)^2))+ths1(i,1)+20)/(1 - ((Tcs + (Tsa + Tamb))*n*(I1(i)^2))));
end


%% Temperature Calculation and Electric field analytical calculation
%Preconditiopn-Calculation for theoretical steady state temperature
%variation per hour
rh = 32:0.1:62;
delTd = zeros([length(rh) length(I1)]);

m = 1;
th = 1:1:length(I1);
t = 1:1:3600;
tn = length(t)*length(th); % Total number of time steps taken

T = zeros(length(th),length(rh)); % Temperature function

ra = 32;
rb = 62;

r = ones([tn 1]).*32;
r1 = ones([tn 1]);

%% Temperature calculation

for i = 1:1:tn
    hh = floor(i/3600) + 1;
    r(i) = 32; r1(i) = 1;
    while(r1(i)<= length(rh) && r(i)<= 62 && hh<=length(th))
        delTd(r1(i),hh) = ((Tcs*((pho_cu/(pi*rc*rc*(1e-6)))...
        ...*(1 + alpha_cu*(vc(hh) - (ths1(hh,1)+20))))...
```

```
        ...*(I1(hh)^2))/(2*pi*0.3))*(log(62/r(i)));
        r1(i) = r1(i) +1;
        r(i) = r(i) +0.1;
    end
end


for t2 = 1:1:(tn)
    h = floor(t2/3600) +1;
    r(t2) = 32; r1(t2) = 1;
    while(r1(t2)<= length(rh) && h<=length(th))
        T(h,r1(t2)) = vc(h) + ((delTd(r1(t2),h)/30)...
        ...*(30*h/length(th)));  %Temperature gradient calculation
        r1(t2) = r1(t2) +1;
    end
end


eps0 = 1.6e-19;
epsa = 2.5*eps0;
epsb = 3*eps0;
epsc = 2.3*eps0;
a = 0.0425;
%0.085;
% Insulation material constants a and b
b = 0.032;
%0.0645;

Em = (525)/30; % Maximum magnitude of electrical stress(in kV/mm)
B = (b*Em); %Constant for calculation of Electric field parameter


%Variable initialization for variation of electric field(E,E1,Ed), electrical
%conductivity(sigm), space charge field and space charge electric
%field(pho,phod),current density variation(J)
E1 = zeros(length(rh),length(t));
E_pho = zeros(length(rh),length(t)); E_phod = zeros(length(rh),length(th));
E = zeros(length(rh),length(t)); Ed = zeros(length(rh),length(th));
sigm = zeros(length(rh),length(t));
J = ones(length(rh),length(t));
pho = ones(length(rh),length(t)); phod = zeros(length(rh),length(th));
k = zeros(length(rh) ,length(t));
t1 = 1;
%t2 = 1;
A1 = ones([tn+1 1]); A1d = ones([length(th) 1]);
C = ones([tn+1 1]); C1d = ones([length(th) 1]);
delta = zeros([length(rh) length(th)]);
A = zeros([length(rh) length(th)]);
df = zeros([length(th) 1]);
while t1<=tn
    th1 = floor(t1/3600) + 1;
    r(t1) = 32; r1(t1) = 1;
```

```
    while (r(t1)<=62) && (r1(t1)<=length(rh)) && (th1<=length(I1))
        A(r1(t1),th1) = ((delTd(r1(t1),th1)*a)/log(rb/ra));
        delta(r1(t1),th1) = (A(r1(t1),th1) + B)/(1+B);
        r1(t1) = r1(t1) +1;
        r(t1) = r(t1) + 0.1;
    end
    if th1<=length(I1)
        df(th1) = max(delta(:,th1));
    end
    t1 = t1 +1;
end
t1 = 1;
%Continuous implementation of transient equations as a function of radius
%and time(in s)
while t1<=tn
    if (rem(t1,3600) ~= 0)
        th1 = floor(t1/3600) + 1;
        ts1 = t1 - (th1-1)*3600;


        r(t1) = 32; r1(t1) = 1;
        if (ts1 == 1) && (th1 ==1)
            while (r(t1)<=62) && (r1(t1)<=length(rh))
                if (I1(th1)>=0)
                    E1(r1(t1),ts1) = (1/r(t1))*(525e3/log(rb/ra))*(1e3);
                else
                    E1(r1(t1),ts1) = (1/r(t1))*((-1)*525e3/log(rb/ra))*(1e3);
                end
                E(r1(t1),ts1) = E1(r1(t1),ts1);
                sigm(r1(t1),ts1) = (1e14)*exp(-(1.48*1.6e-19)...
                .../(1.38e-23*(T(th1,r1(t1))+273.15)))...
                ...*(sinh(2e-7*(abs(E(r1(t1),ts1))+0.01))/(abs(E(r1(t1),ts1))+0.01));
                J(r1(t1),ts1) = sigm(r1(t1),ts1)*E(r1(t1),ts1);
                k(r1(t1),ts1) = (-1)*(epsa/(sigm(r1(t1),ts1)));
                pho(r1(t1),ts1+1) = (J(r1(t1),ts1)*...
                ...epsa/(1 - k(r1(t1),ts1)))*(1/sigm(r1(t1),ts1))...
                ...+ pho(r1(t1),ts1)*(k(r1(t1),ts1))/(1 - k(r1(t1),ts1));

                r(t1) = r(t1) + 0.1;
                r1(t1) = r1(t1) + 1;
            end
            r(t1) = 32; r1(t1) = 1;
            while (r(t1)<=62) && (r1(t1)<=length(rh))
                A1(t1+1) = A1(t1+1)...
                ...+ (pho(r1(t1),ts1+1)*(32 + (r1(t1)*0.1))*0.1);
                r(t1) = r(t1) + 0.1;
                r1(t1) = r1(t1) + 1;
            end
%             A1(t1 + 1) = A1(t1+1) + A1(t1);
            r(t1) = 32; r1(t1) = 1;
            while (r(t1)<=62) && (r1(t1)<=length(rh))
                C(t1 + 1) =  C(t1+1) + ...
```

```
            ...(-1/log(rb/ra))*...
            ...((1/(32 + (r1(t1)*0.1)))*A1(t1+1)*0.1);
            r(t1) = r(t1) + 0.1;
            r1(t1) = r1(t1) + 1;
        end
%           C(t1+1) = C(t1+1) + C(t1);
    end
        if (ts1 == 1) && (th1~=1) && (t1< 0.2e5)
            while (r(t1)<=62) && (r1(t1)<=length(rh))
            if (I1(th1)>=0)
                E1(r1(t1),ts1) = (1/r(t1))*(525e3/log(rb/ra))*(1e3);
            else
                E1(r1(t1),ts1) = (1/r(t1))*((-1)*525e3/log(rb/ra))*(1e3);
            end
            E(r1(t1),ts1) = E1(r1(t1),ts1) + ...
            ...E_phod(r1(t1),th1-1)...
            ...+ (1/r(t1))*(A1d(th1-1)+abs(C1d(th1-1)))*(1e3);
            sigm(r1(t1),ts1) = (1e14)*exp(-(1.48*1.6e-19)...
            .../(1.38e-23*(T(th1,r1(t1))+273.15)))...
            ...*(sinh(2e-7*(abs(E(r1(t1),ts1))+0.01))...
            .../(abs(E(r1(t1),ts1))+0.01));
            J(r1(t1),ts1) = sigm(r1(t1),ts1)*E(r1(t1),ts1);
            k(r1(t1),ts1) = (-1)*(epsa/(sigm(r1(t1),ts1)));
            if (r1(t1) == 1)
                pho(r1(t1),ts1+1) = (J(r1(t1),ts1)*epsa/...
                ...(1 - k(r1(t1),ts1)))*...
                ...(1/sigm(r1(t1),ts1)) + ...
                ...pho(r1(t1),ts1)*(k(r1(t1),ts1))/(1 - k(r1(t1),ts1));
            else
                pho(r1(t1),ts1+1) = (J(r1(t1),ts1)*epsa/...
                ...(1 - k(r1(t1),ts1)))*abs(((1/sigm(r1(t1),ts1))...
                ...-(1/sigm(r1(t1)-1,ts1))))...
                ...+ (pho(r1(t1),ts1)*(k(r1(t1),ts1)))...
                .../(1 - k(r1(t1),ts1));
            end
            r(t1) = r(t1) + 0.1;
            r1(t1) = r1(t1) + 1;
            end
        r(t1) = 32; r1(t1) = 1;
        while (r(t1)<=62) && (r1(t1)<=length(rh))
            A1(t1+1) = A1(t1+1) + ...
            ...(pho(r1(t1),ts1+1)*(32 + (r1(t1)*0.1))*0.1);
            r(t1) = r(t1) + 0.1;
            r1(t1) = r1(t1) + 1;
        end
%           A1(t1+1) = A1(t1+1) + A1(t1);
        r(t1) = 32; r1(t1) = 1;
        while (r(t1)<=62) && (r1(t1)<=length(rh))
            C(t1 + 1) =  C(t1+1) + ...
            ...(-1/log(rb/ra))*...
            ...((1/(32 + (r1(t1)*0.1)))*A1(t1+1)*0.1);
            r(t1) = r(t1) + 0.1;
```

```
            r1(t1) = r1(t1) + 1;
        end
%         C(t1+1) = C(t1+1) + C(t1);
        end
    if (ts1 == 1) && (th1~=1) && (t1>= 0.2e5)

        while (r(t1)<=62) && (r1(t1)<=length(rh))

            if (I1(th1)>=0)
                E1(r1(t1),ts1) = ((r(t1)/rb)^(df(th1)-1)...
                ...*(525e3)*(df(th1)/...
                ...(rb*(1 - ((ra/rb)^df(th1))))))*(1e3);
            else
                E1(r1(t1),ts1) = ((r(t1)/rb)^(df(th1)-1)...
                ...*((-1)*525e3)*(df(th1)/...
                ...(rb*(1 - ((ra/rb)^df(th1))))))*(1e3);
            end
            E(r1(t1),ts1) = E1(r1(t1),ts1) + E_phod(r1(t1),th1-1)...
            ...+ (1/r(t1))*(A1d(th1-1)+abs(C1d(th1-1)))*(1e3);
            sigm(r1(t1),ts1) = (1e14)*exp(-(1.48*1.6e-19)...
            .../(1.38e-23*(T(th1,r1(t1))+273.15)))...
            ...*(sinh(2e-7*(abs(E(r1(t1),ts1))+0.01))/...
            ...(abs(E(r1(t1),ts1))+0.01));
            J(r1(t1),ts1) = sigm(r1(t1),ts1)*E(r1(t1),ts1);
            k(r1(t1),ts1) = (-1)*(epsa/(sigm(r1(t1),ts1)));
            if (r1(t1) == 1)
                pho(r1(t1),ts1+1) = (J(r1(t1),ts1)*epsa/(1 - k(r1(t1),ts1)))...
                ...*(1/sigm(r1(t1),ts1)) + pho(r1(t1),ts1)...
                ...(k(r1(t1),ts1))/(1 - k(r1(t1),ts1));
            else
                pho(r1(t1),ts1+1) = (J(r1(t1),ts1)*epsa/(1 - k(r1(t1),ts1)))...
                ...*abs(((1/sigm(r1(t1),ts1))-(1/sigm(r1(t1)-1,ts1))))...
                ...+ pho(r1(t1),ts1)*(k(r1(t1),ts1))/(1 - k(r1(t1),ts1));
            end
            r(t1) = r(t1) + 0.1;
            r1(t1) = r1(t1) + 1;
        end
        r(t1) = 32; r1(t1) = 1;
        while (r(t1)<=62) && (r1(t1)<=length(rh))
            A1(t1+1) = A1(t1+1) + (pho(r1(t1),ts1+1)...
            ...*(32 + (r1(t1)*0.1))*0.1);
            r(t1) = r(t1) + 0.1;
            r1(t1) = r1(t1) + 1;
        end
%         A1(t1+1) = A1(t1+1) + A1(t1);
        r(t1) = 32; r1(t1) = 1;
        while (r(t1)<=62) && (r1(t1)<=length(rh))
            C(t1 + 1) =  C(t1+1) + (-1/log(rb/ra))...
            ...*((1/(32 + (r1(t1)*0.1)))*A1(t1+1)*0.1);
            r(t1) = r(t1) + 0.1;
            r1(t1) = r1(t1) + 1;
        end
```

```
%             C(t1+1) = C(t1+1) + C(t1);
        end
            if (ts1 < 3600) && (t1 < 0.2e5)

                while (r(t1)<=62) && (r1(t1)<=length(rh))
                    if (I1(th1)>=0)
                        E1(r1(t1),ts1) = (1/r(t1))*(525e3/log(rb/ra))*(1e3);
                    else
                        E1(r1(t1),ts1) = (1/r(t1))*((-1)*525e3/log(rb/ra))*(1e3);
                    end
                    E_pho(r1(t1),ts1) = abs((1/r(t1))*(A1(t1)+abs(C(t1))))*(1e3);
                    E(r1(t1),ts1) = E1(r1(t1),ts1) + E_pho(r1(t1),ts1);
                    sigm(r1(t1),ts1) = (1e14)*exp(-(1.48*1.6e-19)...
                    .../(1.38e-23*(T(th1,r1(t1))+273.15)))*...
                    ...(sinh(2e-7*(abs(E(r1(t1),ts1))+0.01))...
                    .../(abs(E(r1(t1),ts1))+0.01));
                    J(r1(t1),ts1) = sigm(r1(t1),ts1)*E(r1(t1),ts1);
                    k(r1(t1),ts1) = (-1)*(epsa/(sigm(r1(t1),ts1)));
                if (r1(t1) == 1)
                     pho(r1(t1),ts1+1) = (J(r1(t1),ts1)*epsa/(1 - k(r1(t1),ts1)))...
                     ...*(1/sigm(r1(t1),ts1)) + pho(r1(t1),ts1)...
                     ...*(k(r1(t1),ts1))/(1 - k(r1(t1),ts1));
                else
                    pho(r1(t1),ts1+1) = pho(r1(t1),ts1)*(-1)*(k(r1(t1),ts1)...
                    .../(1-k(r1(t1),ts1))) + (J(r1(t1),ts1)*epsa...
                    .../(1 - k(r1(t1),ts1)))*...
                    ...abs(((1/sigm(r1(t1),ts1))...
                    ...-(1/sigm(r1(t1)-1,ts1))));
                end

                    r(t1) = r(t1) + 0.1;
                    r1(t1) = r1(t1) + 1;
                end

               r(t1) = 32; r1(t1) = 1;
            while (r(t1)<=62) && (r1(t1)<=length(rh))
                A1(t1+1) = A1(t1+1) + ...
                ...(pho(r1(t1),ts1+1)...
                ...*(32 + (r1(t1)*0.1))*0.1) ;    %Same here needs to be repeated
                r(t1) = r(t1) + 0.1;
                r1(t1) = r1(t1) + 1;
            end
%             A1(t1+1) = A1(t1+1) + A1(t1);
            r(t1) = 32; r1(t1) = 1;
            while (r(t1)<=62) && (r1(t1)<=length(rh))
                C(t1+1) =  C(t1+1) + (-1/log(rb/ra))...
                ...*((1/(32 + (r1(t1)*0.1)))*A1(t1+1)*0.1) ;
                r(t1) = r(t1) + 0.1;
                r1(t1) = r1(t1) + 1;
            end
%             C(t1+1) = C(t1+1) + C(t1);
            end
```

```
if (ts1<3600) && (t1>=0.2e5)

    while (r(t1)<=62) && (r1(t1)<=length(rh))

        if (I1(th1)>=0)
            E1(r1(t1),ts1) = ((r(t1)/rb)^...
            ...(df(th1)-1)*(525e3)*...
            ...(df(th1)/(rb*(1 - ((ra/rb)^df(th1))))))*(1e3);
        else
            E1(r1(t1),ts1) = ((r(t1)/rb)^(df(th1)-1)*...
            ...((-1)*525e3)*(df(th1)/...
            ...(rb*(1 - ((ra/rb)^df(th1))))))*(1e3);
        end
        E_pho(r1(t1),ts1) = abs((1/r(t1))...
        ...*(A1(t1)+abs(C(t1))))*(1e3);
        E(r1(t1),ts1) = E1(r1(t1),ts1) + E_pho(r1(t1),ts1);
        sigm(r1(t1),ts1) = (1e14)*exp(-(1.48*1.6e-19)...
        .../(1.38e-23*(T(th1,r1(t1))+273.15)))...
        ...*(sinh(2e-7*(abs(E(r1(t1),ts1))+0.01))...
        .../(abs(E(r1(t1),ts1))+0.01));
        J(r1(t1),ts1) = sigm(r1(t1),ts1)*E(r1(t1),ts1);
        k(r1(t1),ts1) = (-1)*(epsa/(sigm(r1(t1),ts1)));
    if (r1(t1) == 1)
         pho(r1(t1),ts1+1) = (J(r1(t1),ts1)...
         ...*epsa/(1 - k(r1(t1),ts1)))...
         ...*(1/sigm(r1(t1),ts1))...
         ...+ pho(r1(t1),ts1)*(k(r1(t1),ts1))...
         .../(1 - k(r1(t1),ts1));
    else
        pho(r1(t1),ts1+1) = pho(r1(t1),ts1)...
        ...*(-1)*(k(r1(t1),ts1)/(1-k(r1(t1),ts1)))...
        ...+ (J(r1(t1),ts1)*epsa/(1 - k(r1(t1),ts1)))...
        ...*abs(((1/sigm(r1(t1),ts1))...
        ...-(1/sigm(r1(t1)-1,ts1))));
    end

        r(t1) = r(t1) + 0.1;
        r1(t1) = r1(t1) + 1;
    end

   r(t1) = 32; r1(t1) = 1;
while (r(t1)<=62) && (r1(t1)<=length(rh))
    A1(t1+1) = A1(t1+1) + ...
    ...(pho(r1(t1),ts1+1)...
    ...*(32 + (r1(t1)*0.1))*0.1) ;    %Same here needs to be repeated
    r(t1) = r(t1) + 0.1;
    r1(t1) = r1(t1) + 1;
end
%         A1(t1+1) = A1(t1+1) + A1(t1);
r(t1) = 32; r1(t1) = 1;
while (r(t1)<=62) && (r1(t1)<=length(rh))
    C(t1 + 1) =  C(t1+1) + ...
```

```
                ...(-1/log(rb/ra))...
                ...*((1/(32 + (r1(t1)*0.1)))*A1(t1+1)*0.1) ;
                r(t1) = r(t1) + 0.1;
                r1(t1) = r1(t1) + 1;
            end
%             C(t1+1) = C(t1+1) + C(t1);
            end


    else
        r(t1) = 32; r1(t1) = 1;
        th1 = (t1/3600);
        if th1<=length(I1)
            ts1 = 3600;   %This loop needs to be corected as ts1(3600) is insignificant here.

            if (ts1 == 3600) && (t1<0.2e5)     % 1 instead of 2 if implememntations will do

                while (r(t1)<=62) && (r1(t1)<=length(rh))
                    if (I1(th1)>=0)
                        E1(r1(t1),ts1) = (1/r(t1))...
                        ...*(525e3/log(rb/ra))*(1e3);
                    else
                        E1(r1(t1),ts1) = (1/r(t1))...
                        ...*((-1)*525e3/log(rb/ra))*(1e3);
                    end
                    E_pho(r1(t1),ts1) = abs((1/r(t1))...
                    ...*(A1(t1)+abs(C(t1))))*(1e3);
                    E(r1(t1),ts1) = E1(r1(t1),ts1) + E_pho(r1(t1),ts1);
                    sigm(r1(t1),ts1) = (1e14)*exp(-(1.48*1.6e-19)...
                    .../(1.38e-23*(T(th1,r1(t1))+273.15)))*...
                    ...(sinh(2e-7*(abs(E(r1(t1),ts1))+0.01))...
                    .../(abs(E(r1(t1),ts1))+0.01));
                    E_phod(r1(t1),th1) = E_pho(r1(t1),ts1);
                    Ed(r1(t1),th1) = E(r1(t1),ts1);
                    J(r1(t1),ts1) = sigm(r1(t1),ts1)*E(r1(t1),ts1);
                    k(r1(t1),ts1) = (-1)*(epsa/(sigm(r1(t1),ts1)));
                    if (r1(t1) == 1)
                        pho(r1(t1),ts1+1) = (J(r1(t1),ts1)*epsa...
                        .../(1 - k(r1(t1),ts1)))*(1/sigm(r1(t1),ts1))...
                        ...+ pho(r1(t1),ts1)*(k(r1(t1),ts1))...
                        .../(1 - k(r1(t1),ts1));
                    else
                        pho(r1(t1),ts1+1) = pho(r1(t1),ts1)*(-1)...
                        ...*(k(r1(t1),ts1)/(1-k(r1(t1),ts1)))...
                        ...+ (J(r1(t1),ts1)*epsa/(1 - k(r1(t1),ts1)))...
                        ...*abs((1/sigm(r1(t1),ts1))-...
                        ...(1/sigm(r1(t1)-1,ts1)));
                    end
                    phod(r1(t1),th1) = pho(r1(t1),ts1);

                    r(t1) = r(t1) + 0.1;
                    r1(t1) = r1(t1) + 1;
```

```
        end
       r(t1) = 32; r1(t1) = 1;
    while (r(t1)<=62) && (r1(t1)<=length(rh))
        A1(t1+1) = A1(t1+1) + ...
        ...(pho(r1(t1),ts1+1)*(32 + (r1(t1)*0.1))*0.1);
        r(t1) = r(t1) + 0.1;
        r1(t1) = r1(t1) + 1;
    end
%       A1(t1+1) = A1(t1+1) + A1(t1);
    r(t1) = 32; r1(t1) = 1;
    while (r(t1)<=62) && (r1(t1)<=length(rh))
        C(t1+1) =  C(t1+1) + (-1/log(rb/ra))...
        ...*((1/r(t1))*A1(t1+1)*0.1);
        r(t1) = r(t1) + 0.1;
        r1(t1) = r1(t1) + 1;
    end
%       C(t1+1) = C(t1+1) + C(t1);
    A1d(th1) = A1(t1);
    C1d(th1) = C(t1);
    end
if (ts1 == 3600) && (t1>=0.2e5)

    while (r(t1)<=62) && (r1(t1)<=length(rh))

        if (I1(th1)>=0)
            E1(r1(t1),ts1) = ((r(t1)/rb)^(df(th1)-1)*...
            ...(525e3)*(df(th1)/(rb*(1 - ((ra/rb)...
            ...^df(th1))))))*(1e3);
        else
            E1(r1(t1),ts1) = ((r(t1)/rb)^(df(th1)-1)...
            ...*((-1)*525e3)*(df(th1)/...
            ...(rb*(1 - ((ra/rb)^df(th1))))))*(1e3);
        end
        E_pho(r1(t1),ts1) = abs((1/r(t1))...
        ...*(A1(t1)+abs(C(t1))))*(1e3);
        E(r1(t1),ts1) = E1(r1(t1),ts1) + E_pho(r1(t1),ts1);
        sigm(r1(t1),ts1) = (1e14)*...
        ...exp(-(1.48*1.6e-19)/(1.38e-23*...
        ...(T(th1,r1(t1))+273.15)))*...
        ...(sinh(2e-7*(abs(E(r1(t1),ts1))+0.01))...
        .../(abs(E(r1(t1),ts1))+0.01));
        E_phod(r1(t1),th1) = E_pho(r1(t1),ts1);
        Ed(r1(t1),th1) = E(r1(t1),ts1);
        J(r1(t1),ts1) = sigm(r1(t1),ts1)*E(r1(t1),ts1);
        k(r1(t1),ts1) = (-1)*(epsa/(sigm(r1(t1),ts1)));
        if (r1(t1) == 1)
            pho(r1(t1),ts1+1) = (J(r1(t1),ts1)*epsa...
            .../(1 - k(r1(t1),ts1)))...
            ...*(1/sigm(r1(t1),ts1)) + ...
            ...pho(r1(t1),ts1)*(k(r1(t1),ts1))...
            .../(1 - k(r1(t1),ts1));
        else
```

```
                    pho(r1(t1),ts1+1) = pho(r1(t1),ts1)*(-1)*...
                    ...(k(r1(t1),ts1)/(1-k(r1(t1),ts1)))...
                    ...+ (J(r1(t1),ts1)*epsa/(1 - k(r1(t1),ts1)))...
                    ...*((1/sigm(r1(t1),ts1))-...
                    ...(1/sigm(r1(t1)-1,ts1)));
                end
                phod(r1(t1),th1) = pho(r1(t1),ts1);

                r(t1) = r(t1) + 0.1;
                r1(t1) = r1(t1) + 1;
            end
           r(t1) = 32; r1(t1) = 1;
        while (r(t1)<=62) && (r1(t1)<=length(rh))
            A1(t1+1) = A1(t1+1) + (pho(r1(t1),ts1+1)...
            ...*(32 + (r1(t1)*0.1))*0.1);
            r(t1) = r(t1) + 0.1;
            r1(t1) = r1(t1) + 1;
        end
%           A1(t1+1) = A1(t1+1) + A1(t1);
        r(t1) = 32; r1(t1) = 1;
        while (r(t1)<=62) && (r1(t1)<=length(rh))
            C(t1+1) =  C(t1+1) + (-1/log(rb/ra))...
            ...*((1/r(t1))*A1(t1+1)*0.1);
            r(t1) = r(t1) + 0.1;
            r1(t1) = r1(t1) + 1;
        end
%           C(t1+1) = C(t1+1) + C(t1);
        A1d(th1) = A1(t1);
        C1d(th1) = C(t1);
        end

    end
    end
   t1 = t1 +1;
end


S = sum((phod.*(1e9))./(8.61e-4),1);


%% Reliability function implementation
t_df = zeros(length(rh), length(th));
r = ones([tn 1]).*32;
r1 = ones([tn 1]);
t2 = 1;
while t2<=tn
    th2 = floor(t2/3600) + 1;
    ts2 = t2 - (th2-1)*3600;
        while (r(t2)<=64) && (r1(t2)<=301)...
        ...&& (rem(t2,3600)==0) && (th2<=length(I1))
            t_df(r1(t2),th2) = 40*((Ed(r1(t2),th2)/...
            ...(18e6))^(10 - 0.5*((1/90) - (1/T(th2,r1(t2))))...
```

```
                ...*(3^(0.5*((1/90) - (1/T(th2,r1(t2))))))...
                ...*exp(12430*((1/90) - (1/T(th2,r1(t2))))));
%                 t_df(r1(t2),th2) = 40*(abs(Ed(r1(t2),th2))/...
...(18e6*(2*pi*46*(1e-6)))^(-10)*...
...(exp(-12430*(-(1/(90))+(1/(T(2000,r1(t2))))));
                r(t2) = r(t2) + 0.01;
                r1(t2) = r1(t2) + 1;
            end
            t2 = t2 +1;
end


%Space charge density in nC/m^3.

%T1 = T + (273.15).*ones(length(t),length(rh)); %Temperature distribution in K
Ekv = E.*(1e-6); % Electric field value in kV/mm(intrinsic value)
E1kv = E1.*(1e-6); %Electric field in kV/mm(including the effect of space charges)
```

The details of the values used in all of these model implementations can be found in Appendix B.

Appendix B

Appendix B

B.1 Description of values used in the HVAC cable

Serial Number	Parameter	Description	Value
1	Uo	Voltage level	38.105kV
2	lf	Load factor	0.8
3	$theta_c$	Conductor temperature	90°C
4	$theta_{amb}$	ambient temperature	20°C
5	G	geometric factor	0.514
6	δ	Soil diffusivity	0.6e-7$[m^2/s]$-Case 1,1.1e-7$[m^2/s]$-Case 2
7	ρ_{epr}	Thermal resistivity of ethylene polypropylene	3.5$[KmW^{-1}]$
8	ρ_f	Thermal resistivity of filler	5$[KmW^-1]$
9	ρ_{st}	Thermal resistivity of steel	0.02$[KmW^-1]]$
10	ρ_{pp}	Thermal resistivity of polypropylene	2.2727$[KmW^-1]$
11	ρ_s	Thermal resistivity of soil	5$[KmW^-1]$-Case 1,2.77$[KmW^-1]$-Case 2
12	p	VW coefficient for insulation	0.4141
13	p_f	VW coefficient for filler material	0.3308

Serial Number	Parameter	Description	Value
14	p_{ab}	VW coefficient for armor bedding	6.2047
15	p_2	VW coefficient for external serving	7.9523
16	s	Distance between conductor axes	63.9[mm]
17	d	Mean sheath diameter	58.9[mm]

Transient parameter description

Serial number	Parameter	Description
1	L_{sh}	Sheath loss factor
2	L_a	Armor loss factor
3	$W_c(t)$	Conductor losses
4	$W_s(t)$	Sheath losses
5	$W_a(t)$	Armor losses
6	$W_I(t)$	Total loses
7	$\theta_c(t)$	Conductor temperature
8	$\theta_e(t)$	influence of soil
9	$\alpha(t)$	Attainment factor
10	$\theta_{pk}(t)$	Temperature rise due to other cable
11	Wd	Dielectric losses - 7.2472e-7[W]

1 2

[1]VW - Van wormer coefficient
[2]Case 1- L = 1200$[mm]$,TC = 0.2$[W/mK]$;Case 2- L = 1500$[mm]$,TC = 0.36$[W/mK]$

B.2 Description of values used for ampacity calculation of HVDC cable

Serial Number	Parameter	Description	Value
1	R_o	Electrical Resistance at 20°C	0.0626[Ω]
2	R	DC resistance at a value of 90°C	32 mm
3	U_o	Maximum value of DC voltage level	525[kV]
4	T_c	Conductor thermal resistance	2.58e-5[K/W]
5	T_{cs}	Thermal resistance for insulation and sheath	0.1964[K/W]
6	T_{sa}	Thermal resistance of armor and serving	11[K/W]
7	T_{amb}	Thermal resistance of ambient soil	0.1964[K/W]
8	ρ_T	Thermal resistivity of copper	0.0025[Km/W]
9	ρ_i	Thermal resistivity of insulation	3.125[Km/W]
10	ρ_a	Thermal resistivity of armor	0.02[Km/W]
11	ρ_{ls}	Thermal resistivity of lead sheath	0.0288[Km/W]
12	ρ_{se}	Thermal resistivity of external serving	3.57[Km/W]
13	ρ_s	Thermal resistivity of soil	2.77[Km/W]
14	D_o	Outer diameter of conductor(upto conductor screen)	64[mm]
15	D_i	Inner dia of conductor	60[mm]
16	t_{ii}	thickness of insulation wall	30[mm]
17	D_{cs}	Diameter upto insulation	124[mm]
18	t_{ls}	thickness of lead sheath	2[mm]
19	D_{ls}	Dia upto lead sheath	128[mm]

Serial Number	Parameter	Description	Value
20	t_s	thickness of external serving	5[mm]
21	D_{se}	Dia upto external serving 160[mm]	
22	L	Burial depth	1200[mm]
23	D_e	Dia of the structure	160[mm]
24	r_b, r_o	radius upto the conductor screen	32[mm]
25	r_a, r_i	radius of the conductor	30[mm]
26	c	specific heat capacity of Copper	385[J/kg.K]
27	δ	Density of copper material	8900[kg/m^3]
28	I_d	Steady state current value	2186[A]
29	a	temperature coefficient	0.00425[K^{-1}]
30	b	Electric field coefficient	0.032[mm/kV]
31	t_{sa}	thickness of armor	11[mm]
32	D_a	Dia upto armor	150[mm]

Appendix C

Appendix C

C.1 Input load profiles for the wind power models

This section focuses on the different load profiles which are used in implementing the different cable models. For this case, time series forecasting techniques have been used to predict the wind speed and then a particular load profile has been developed for this case. Following sections elaborate the different load profiles which will be used here.

C.1.1 Code for wind speed to current vs. time profile

Following is the Code which explains the development of the load profiles-

```
import numpy as np
import pandas as pd
import seaborn as sns
import matplotlib.pyplot as plt
plt.style.use('ggplot')
path = r'C:/Users/akshajsrivasta/Downloads/wspeed_1.xlsx'

data = pd.read_excel(path)
D_ind = data.set_index(['S.no'])
D_ind = D_ind.dropna()
print(D_ind)


plt.xlabel = ['intervals']
plt.ylabel = ['wind_speed']
plt.plot(D_ind)


pho = 1.293;
C_p = 0.5;
R = 64.5;
N = 80.0;
```

```
v = data["Wind Speed"].tolist();
P = np.zeros(len(v))
for i in range(len(v)):
    if v[i]<=3.0:
        P[i] = 0;
    elif v[i]>=25.0:
        P[i] = 19;
    else:
        P[i] = 0.5*pho*C_p*N*3.14*(pow(R,2.0))*(pow(v[i],3.0))*(1.0/6)*(1e-6);

for x in range(len(P)):
    if P[x]<= 9.9:
        P[x] = 9.9;
    elif P[x]>=19.05:
        P[x] = 19.05;

I = np.zeros(len(P));

for a in range(len(P)):
    I[a] = (P[a]/(pow(3.0,0.5)*66.0*0.8))*(1e3);

for s in range(len(I)):
    if (I[s]<=625.0):
        I[s] = 625.0;
    elif (I[s]>=1250):
        I[s] = 1250.0;

P_wnan = P[np.logical_not(np.isnan(P))]
I_wnan = I[np.logical_not(np.isnan(I))]
print(I)
plt.plot(I_wnan[0:600])



path_xl =  r'C:/Users/akshajsrivasta/Downloads/Book1.xlsx'
df = pd.DataFrame(I_wnan)
df.to_excel(path_xl,sheet_name='Sheet2',index=False,header=False,startrow=1,startcol=0);
```

Appendix D

Appendix D

D.1 Nomograms used for approximation of exponential integral

Following section describes the approximation of the exponential integral which has been used in the code for transient variation of HVAC cable temperature and influence on the soil temperature rise.
The exponential integral is defined as-
For $0 \leq x \leq 1$:

$$-Ei(-x) = -\ln(x) + \sum_{i=0}^{5} a_i x^i \tag{D.1}$$

Here,the coefficients a_0 to a_5 are defined as-

a_0	-0.5772
a_1	1.0000
a_2	-0.2499
a_3	0.0552
a_4	-0.0098
a_5	0.0011

For $0 \leq x \leq 8$:

$$-Ei(-x) = \frac{1}{x\exp^x}[\frac{x^2 + a_1 x + a_2}{x^2 + b_1 x + b_2}] \tag{D.2}$$

a_1	2.3347
a_2	0.2506
b_1	3.3307
b_2	1.6915

For $x \geq 8$, the value of the integral is set to 0. These nomograms can be found in IEC 60853([51]) and Appendix B of Heggas ([52]).

References

[1] N. Olijve, "2 GW HVDC Grid Design and Reliability & Availability", en, 2019.

[2] R. Huang, J. A. Pilgrim, P. L. Lewin, and D. Payne, "Dynamic cable ratings for smarter grids", en, in *IEEE PES ISGT Europe 2013*, Lyngby, Denmark: IEEE, Oct. 2013, pp. 1–5, ISBN: 978-1-4799-2984-9. DOI: 10.1109/ISGTEurope.2013.6695230. [Online]. Available: http://ieeexplore.ieee.org/document/6695230/ (visited on 12/03/2022).

[3] EWEA, *Transmission system operation with a large penetration of wind and other renewable electricity sources in electricity networks using innovative tools and integrated energy solutions (TWENTIES)*. [Online]. Available: https://www.ewea.org/fileadmin/files/library/publications/reports/Twenties.pdf (visited on 09/07/2023).

[4] S. H. Alwan and J. Jasni, "Factors Affecting Current Ratings for Underground and Air Cables", en, *International Journal of Energy and Power Engineering*, vol. 10, no. 11, p. 7, 2016.

[5] *IEC 60287-1-1:Calculation of Current rating-Part 1*.

[6] *Cable ampacity Calculation using the Neher-McGrath method*.

[7] P.-Y. Wang, H. Ma, G. Liu, *et al.*, "Dynamic Thermal Analysis of High-Voltage Power Cable Insulation for Cable Dynamic Thermal Rating", *IEEE Access*, vol. 7, pp. 56 095–56 106, 2019, Conference Name: IEEE Access, ISSN: 2169-3536. DOI: 10.1109/ACCESS.2019.2913704.

[8] E. C. Rusty Bascom and B. Clairmont, "Considerations for advanced temperature monitoring of underground power cables", in *2014 IEEE PES T&D Conference and Exposition*, ISSN: 2160-8563, Apr. 2014, pp. 1–5. DOI: 10.1109/TDC.2014.6863155.

[9] J. Heckenbergerová and J. Hošek, "Dynamic thermal rating of power transmission lines related to wind energy integration", in *2012 11th International Conference on Environment and Electrical Engineering*, May 2012, pp. 798–801. DOI: 10.1109/EEEIC.2012.6221484.

[10] M. Baù, N. Viafora, C. S. Hansen, L. M. Bergholdt Dall, T. Ebdrup, and F. Faria da Silva, "Steady state modelling of three-core wire armoured submarine cables: Power losses and ampacity estimation based on FEM and IEC", in *2016 51st International Universities Power Engineering Conference (UPEC)*, Sep. 2016, pp. 1–6. DOI: 10.1109/UPEC.2016.8114078.

[11] H. Brakelmann and G. J. Anders, "Current Rating Considerations in Designing HVDC Cable Installations", *IEEE Transactions on Power Delivery*, vol. 33, no. 5, pp. 2315–2323, Oct. 2018, Conference Name: IEEE Transactions on Power Delivery, ISSN: 1937-4208. DOI: 10.1109/TPWRD.2018.2803279.

[12] H. Sugihara and T. Funaki, "Analysis on Temperature Dependency of Effective AC Conductor Resistance of Underground Cables for Dynamic Line Ratings in Smart Grids", in *2019 IEEE 21st International Conference on High Performance Computing and Communications; IEEE 17th International Conference on Smart City; IEEE 5th International Conference on Data Science and Systems (HPCC/SmartCity/DSS)*, Aug. 2019, pp. 2637–2643. DOI: 10.1109/HPCC/SmartCity/DSS.2019.00370.

[13] S. J. M. Balla, J. J. Walker, and I. K. Kyere, "Application of finite element method to compare the installation requirements in a buried cable according to IEC60287 standards", in *22nd International Symposium on High Voltage Engineering (ISH 2021)*, vol. 2021, Nov. 2021, pp. 907–911. DOI: 10.1049/icp.2022.0506.

[14] O. E.-S. Gouda, G. F. A. Osman, W. A. A. Salem, and S. H. Arafa, "Cyclic Loading of Underground Cables Including the Variations of Backfill Soil Thermal Resistivity and Specific Heat With Temperature Variation", *IEEE Transactions on Power Delivery*, vol. 33, no. 6, pp. 3122–3129, Dec. 2018, Conference Name: IEEE Transactions on Power Delivery, ISSN: 1937-4208. DOI: 10.1109/TPWRD.2018.2849017.

[15] "Rating of PipeType Cables with Slow Oil Circulation of Dielectric Fluid", en, in *Rating of Electric Power Cables in Unfavorable Thermal Environment*, IEEE, 2010, ISBN: 978-0-471-71874-1. DOI: 10.1109/9780471718741.ch7. [Online]. Available: http://ieeexplore.ieee.org/search/srchabstract.jsp?arnumber=5444118 (visited on 12/06/2022).

[16] Y. Wang, S. Liu, W. Zhu, L. Zhao, and Y. Tian, "Study on ± 500 kV VSC-HVDC Submarine Cable Transmission Bottlenecks Under Different Laying Methods", en, in *Advances in Transdisciplinary Engineering*, J. Xu, Ed., IOS Press, Dec. 2022, ISBN: 978-1-64368-366-9 978-1-64368-367-6. DOI: 10.3233/ATDE221197. [Online]. Available: https://ebooks.iospress.nl/doi/10.3233/ATDE221197 (visited on 03/02/2023).

[17] J.-R. Riba and J. Llauradó, "A Model to Calculate the Current–Temperature Relationship of Insulated and Jacketed Cables", en, *Materials*, vol. 15, no. 19, p. 6814, Sep. 2022, ISSN: 1996-1944. DOI: 10.3390/ma15196814. [Online]. Available: https://www.mdpi.com/1996-1944/15/19/6814 (visited on 02/19/2023).

[18] S. Liu and K. Kopsidas, "Risk-Based Underground Cable Circuit Ratings for Flexible Wind Power Integration", *IEEE Transactions on Power Delivery*, vol. 36, no. 1, pp. 145–155, Feb. 2021, Conference Name: IEEE Transactions on Power Delivery, ISSN: 1937-4208. DOI: 10.1109/TPWRD.2020.2980437.

[19] S. Dubitsky, G. Greshnyakov, and N. Korovkin, "Comparison of finite element analysis to IEC-60287 for predicting underground cable ampacity", en, in *2016 IEEE International Energy Conference (ENERGYCON)*, Leuven, Belgium: IEEE, Apr. 2016, pp. 1–6, ISBN: 978-1-4673-8463-6. DOI: 10.1109/ENERGYCON.2016.7514107. [Online]. Available: http://ieeexplore.ieee.org/document/7514107/ (visited on 12/01/2022).

[20] G. Mazzanti and M. Marzinotto, Eds., *Extruded Cables For High-Voltage Direct-Current Transmission*, en, 1st ed. Wiley, Jul. 2013, ISBN: 978-1-118-09666-6 978-1-118-59042-3. DOI: 10.1002/9781118590423. [Online]. Available: https://onlinelibrary.wiley.com/doi/book/10.1002/9781118590423 (visited on 02/27/2023).

[21] B. Diban, G. Mazzanti, L. Mazzocchetti, and P. Seri, "Experimental Investigation of the Effect of Transient Overvoltages on XLPE-insulated HVDC Cables", en, preprint, Dec. 2022. DOI: 10.36227/techrxiv.21641504.v2. [Online]. Available: https://www.techrxiv.org/articles/preprint/Experimental_Investigation_of_the_Effect_of_Transient_Overvoltages_on_XLPE-insulated_HVDC_Cables/21641504/2 (visited on 02/19/2023).

[22] J. C. Fothergill, "Ageing, Space Charge and Nanodielectrics: Ten Things We Don't Know About Dielectrics", in *2007 IEEE International Conference on Solid Dielectrics*, ISSN: 2159-1687, Jul. 2007, pp. 1–10. DOI: 10.1109/ICSD.2007.4290739.

[23] J. Densley, "Ageing mechanisms and diagnostics for power cables - an overview", *IEEE Electrical Insulation Magazine*, vol. 17, no. 1, pp. 14–22, Jan. 2001, Conference Name: IEEE Electrical Insulation Magazine, ISSN: 1558-4402. DOI: 10.1109/57.901613.

[24] G. Mazzanti, G. Montanari, and L. Simoni, "Insulation characterization in multistress conditions by accelerated life tests: An application to XLPE and EPR for high voltage cables", *IEEE Electrical Insulation Magazine*, vol. 13, no. 6, pp. 24–34, Nov. 1997, Conference Name: IEEE Electrical Insulation Magazine, ISSN: 1558-4402. DOI: 10.1109/57.637151.

[25] T. Slinde, M. Heggås, and R. Bakken, "A review of condition assessment methods for high voltage subsea power cables", en,

[26] M. M. Jensen, "Overload Capacity of Polymer Insulated Medium Voltage Ca- bles", en, 2011.

[27] L. Deschamps, "High temperature use of polymer insulated high voltage cables", en,

[28] M. Shwehdi, M. Morsy, and A. Abugurain, "Thermal aging tests on XLPE and PVC cable insulation materials of Saudi Arabia", en, in *2003 Annual Report Conference on Electrical Insulation and Dielectric Phenomena*, Albuquerque, NM, USA: IEEE, 2003, pp. 176–180, ISBN: 978-0-7803-7910-7. DOI: 10.1109/CEIDP.2003.1254822. [Online]. Available: http://ieeexplore.ieee.org/document/1254822/ (visited on 09/07/2023).

[29] G. C. Montanari and G. Mazzanti, "From thermodynamic to phenomenological multi-stress models for insulating materials without or with evidence of threshold (XLPE cables)", en, *Journal of Physics D: Applied Physics*, vol. 27, no. 8, pp. 1691–1702, Aug. 1994, ISSN: 0022-3727, 1361-6463. DOI: 10.1088/0022-3727/27/8/017. [Online]. Available: https://iopscience.iop.org/article/10.1088/0022-3727/27/8/017 (visited on 08/09/2023).

[30] G. Montanari, G. Mazzanti, and L. Simoni, "Progress in electrothermal life modeling of electrical insulation during the last decades", *IEEE Transactions on Dielectrics and Electrical Insulation*, vol. 9, no. 5, pp. 730–745, Oct. 2002, Conference Name: IEEE Transactions on Dielectrics and Electrical Insulation, ISSN: 1558-4135. DOI: 10.1109/TDEI.2002.1038660.

[31] W. Zenger, "Cable System Technology Review of XLPE EHV Cables, 220kV to 500kV", en,

[32] b. Gov., *Offshore Wind Submarine Cable Spacing Guidance*. [Online]. Available: https://www.boem.gov/sites/default/files/renewable-energy-program/Studies/TAP/722AA.pdf (visited on 07/09/2023).

[33] *V150-6.0 MW™*, en, Jul. 2023. [Online]. Available: https://www.vestas.com/en/products/enventus-platform/v150-6-0 (visited on 07/10/2023).

[34] T. consultancy, *J-tubes_and_number_of_bays_v3.0.pdf*. [Online]. Available: https://offshore-documents.tennet.eu/fileadmin/offshore_document_uploads/Consultation_documents/12._J-tubes_and_Number_of_Bays/ONL_TTB-05419_T11_J-tubes_and_Number_of_Bays_V3.0.pdf (visited on 07/09/2023).

[35] O. C. Castillo, V. R. Andrade, J. J. R. Rivas, and R. O. González, "Comparison of Power Coefficients in Wind Turbines Considering the Tip Speed Ratio and Blade Pitch Angle", en, *Energies*, vol. 16, no. 6, p. 2774, Mar. 2023, ISSN: 1996-1073. DOI: 10.3390/en16062774. [Online]. Available: https://www.mdpi.com/1996-1073/16/6/2774 (visited on 01/21/2024).

[36] H. Holtinnnen, *VTT research*. [Online]. Available: https://www.vttresearch.com/sites/default/files/pdf/publications/2004/P554.pdf (visited on 11/08/2023).

[37] *WINS50 - wind at 10-600 meter height for the Netherlands from HARMONIE-AROME with wind farm parameterization as time series per grid point - KNMI Data Platform*, en. [Online]. Available: https://dataplatform.knmi.nl/dataset/access/wins50-wfp-nl-ts-singlepoint-3 (visited on 09/28/2023).

[38] T. offshore consultancy, *ONL_ttb-05579_t16_cable_laying_configurations_and_availability_v3.0.pdf*. [Online]. Available: https://offshore-documents.tennet.eu/fileadmin/offshore_document_uploads/Consultation_documents/17._Cable_laying_configurations_and_availability/ONL_TTB-05579_T16_Cable_laying_configurations_and_availability_V3.0.pdf (visited on 07/08/2023).

[39] P. Prysmian, *66 kV Submarine Cable Systems*. [Online]. Available: https://www.prysmiangroup.com/sites/default/files/business_markets/markets/downloads/datasheets/leaflet_submarine_epr_66%20Kv_%20final.pdf (visited on 07/11/2023).

[40] G. J. Anders, *Rating of electric power cables in unfavorable thermal environment* (IEEE Press series on power engineering), en. Hoboken, N.J: Wiley, 2005, OCLC: ocm57527543, ISBN: 978-0-471-67909-7.

[41] *Thermal environment design considerations for ampacity of buried power cables — Connected Papers*. [Online]. Available: https://www.connectedpapers.com/main/720755d55d180a29773b72d06a54e6e3080729c6/Thermal-environment-design-considerations-for-ampacity-of-buried-power-cables/graph (visited on 11/25/2022).

[42] I. E. Kommission and B. S. Institution, Eds., *Electric cables - calculation of the current rating. Part 2 1: Thermal resistance Calculation of thermal resistance* (BSI standards publication BS IEC 60287-2-1), en. London: bsi, 2015, ISBN: 978-2-8322-2583-7 978-0-580-80953-8.

[43] *The 2GW Program — TenneT*. [Online]. Available: https://www.tennet.eu/about-tennet/innovations/2gw-program (visited on 07/18/2023).

[44] Prysmian, *525kV XLPE cable Datasheet*. [Online]. Available: https://www.prysmiangroup.com/staticres/525-kv-hvdc-new-cable-systems/documents/XLPE-DATASHEET---Submarine.pdf (visited on 07/18/2023).

[45] S. Kumara, Y. V. Serdyuk, and M. Jeroense, "Calculation of Electric Fields in HVDC Cables: Comparison of Different Models", *IEEE Transactions on Dielectrics and Electrical Insulation*, vol. 28, no. 3, pp. 1070–1078, Jun. 2021, Conference Name: IEEE Transactions on Dielectrics and Electrical Insulation, ISSN: 1558-4135. DOI: 10.1109/TDEI.2021.009371.

[46] R. Bodega, *Space charge measurements in polymeric high voltage DC cable systems*.

[47] T. W. Dakin, "Electrical Insulation Deterioration Treated as a Chemical Rate Phenomenon", *Transactions of the American Institute of Electrical Engineers*, vol. 67, no. 1, pp. 113–122, Jan. 1948, Conference Name: Transactions of the American Institute of Electrical Engineers, ISSN: 2330-9431. DOI: 10.1109/T-AIEE.1948.5059649.

[48] B. Diban, *LIFE ESTIMATION OF HVDC CABLES SUBJECTED TO QUALIFICATION TEST CONDITIONS*. [Online]. Available: https://amslaurea.unibo.it/18955/1/Thesis%20Final_Bassel%20Diban.pdf (visited on 02/19/2023).

[49] B. Shan, C. Du, J. Cheng, W. Wang, and C. Li, "Residual Life Prediction of XLPE Distribution Cables Based on Time-Temperature Superposition Principle by Non-Destructive BIS Measuring on Site", en, *Polymers*, vol. 14, no. 24, p. 5478, Dec. 2022, ISSN: 2073-4360. DOI: 10.3390/polym14245478. [Online]. Available: https://www.mdpi.com/2073-4360/14/24/5478 (visited on 01/02/2024).

[50] G. Mazzanti, G. Montanari, and L. Dissado, "Electrical aging and life models: The role of space charge", en, *IEEE Transactions on Dielectrics and Electrical Insulation*, vol. 12, no. 5, pp. 876–890, Oct. 2005, ISSN: 1070-9878. DOI: 10.1109/TDEI.2005.1522183. [Online]. Available: http://ieeexplore.ieee.org/document/1522183/ (visited on 08/05/2023).

[51] *Cableizer - Blog post about "Validation of emergency rating calculations acc. IEC 60853-2"*. [Online]. Available: https://www.cableizer.com/blog/post/validation-emergency-rating-calculations-iec-60853-2/ (visited on 04/18/2023).

[52] M. Heggås, *Dynamic Rating of Power Cables Based upon Transient Temperature Calculations*.